2-P

ATS-16560

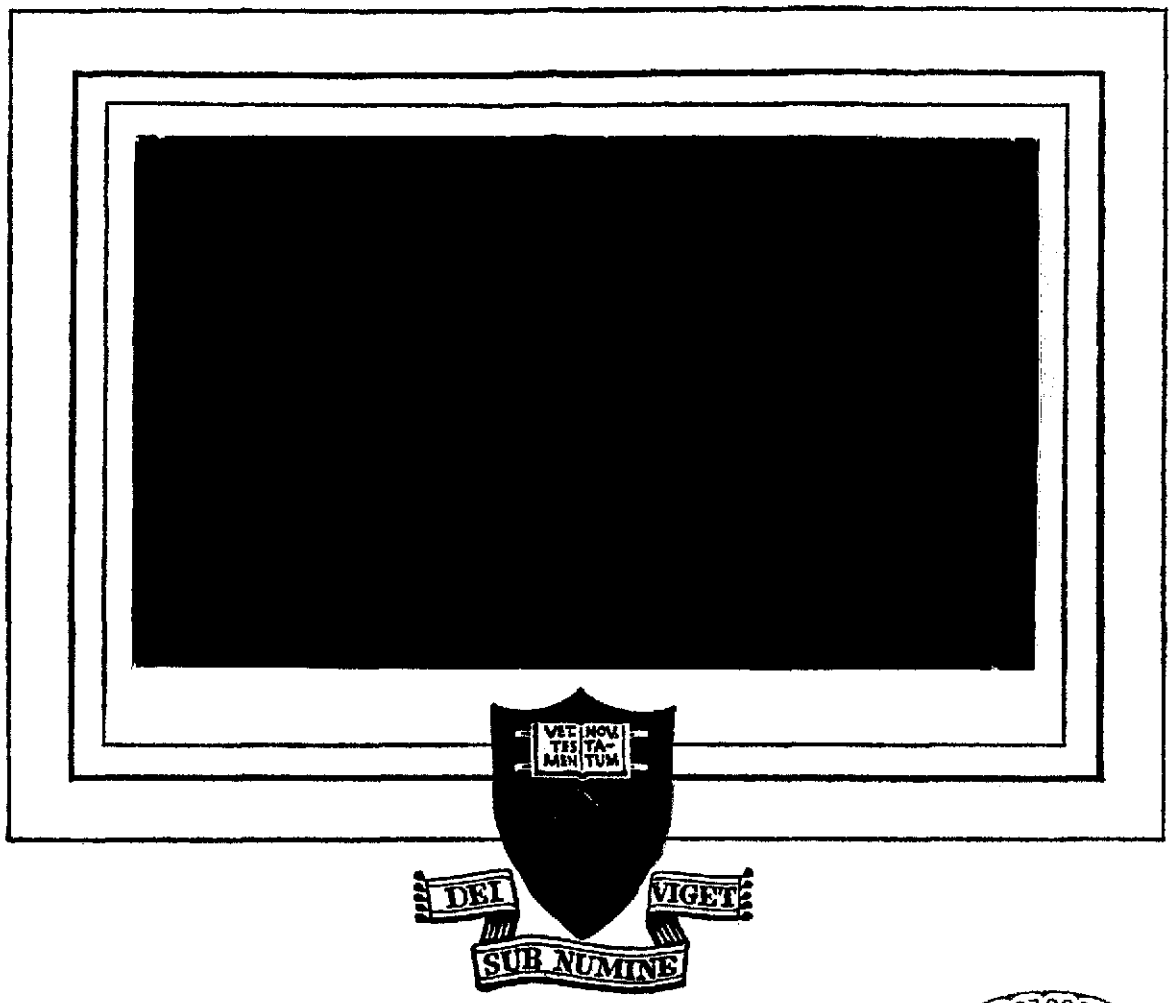

PRINCETON UNIVERSITY

DEPARTMENT OF
AEROSPACE AND MECHANICAL SCIENCES

National Aeronautics and Space Administration
NGL 31-001-005

PULSED ELECTROMAGNETIC GAS ACCELERATION

1 January 1973 to 30 June 1973

Semi-annual Report 634u

Prepared by: Robert G. Jahn
Robert G. Jahn
Dean, School of Engineering and
Principal Investigator

W. von Jaskowsky
Woldemar F. von Jaskowsky
Sr. Research Engineer and
Lecturer

Kenn E. Clark
Kenn E. Clark
Research Engineer

July 1973

School of Engineering and Applied Science
Department of Aerospace and Mechanical Sciences
Guggenheim Aerospace Propulsion Laboratories
Princeton University
Princeton, N.J.08540

ABSTRACT

Direct measurement with thermocouples of the power deposited in the anode of a multi-megawatt magnetoplasma-dynamic discharge has shown the fractional anode power to decrease from 50% at 200 kW to 10% at 20 MW. Using local measurements of current density, electric potential, and electron temperature, the traditional model for heat conduction to the anode is found to be inadequate. Other experiments in which the voltage-current characteristics and exhaust velocities of MPD arcs using Plexiglas and boron nitride chamber insulators and various mass injection configurations show that ablation can affect nominal accelerator operation in several distinct ways.

The incorporation of a hollow cathode in a 7 kA plasma discharge has shown that a stable current attachment can be realized in the cavity without the aid of cathode heaters, keeper electrodes, or emissive coatings. Measured current and potential distributions within the cathode cavity reveal that the bulk of the current attaches in a region of weak axial potential gradient. Infrared spectra reveal an electron number density of several times 10^{17} cm^{-3} inside the cavity, more than an order of magnitude greater than previously observed in solid cathode MPD discharges at twice the arc current level.

To determine the suitability of the MPD discharge as a plasmadynamic laser source, the optical depth of several ionized argon spectral lines has been determined. Preliminary data, which can be related to the gain characteristics of the expanding exhaust flow, have as yet revealed no evidence of inverted population distributions. In a complimentary experiment, significant vacuum ultraviolet radiance has been detected in the exhaust flow indicating the possible generation of inversions in the recombination process.

TABLE OF CONTENTS

LIST OF ILLUSTRATIONS

LIST OF ILLUSTRATIONS

CURRENT STUDENT PARTICIPATION

Student	Period	Degree	Thesis Topic
BOYLE, Michael J.	1968-1969 1971-	B.S.E. Ph.D. Cand.	Velocity and Acceleration Patterns in the MPD Exhaust
CAMPBELL, Edward M.	1972-		Plasmadynamic Laser Studies
DUTT, Gautam S.	1971-	Ph.D. Cand.	Stimulated Emission of Argon Ion Lines in High Current Discharges
KRISHNAN, Mahadevan	1972-	Ph.D. Cand.	Hollow Cathode Discharges
RUDOLPH, L. Kevin	1973-		Hollow Cathode MPD Discharges
SABER, Aaron J.	1969-	Ph.D. Cand.	Anode Power Deposition in a Quasi-Steady MPD Accelerator
VILLANI, Daniel D.	1969-	Ph.D. Cand.	Effect of Distribution of Injected Propellant on MPD Discharges

I. INTRODUCTION

The plasma research program at Princeton recently was expanded from one which concentrated solely on plasma propulsion to one which now incorporates substantial efforts in the areas of hollow cathode physics and plasmadynamic lasers. The present division of effort within the laboratory reflects this new emphasis with three graduate students in the terminal phases of their Ph.D. programs involving magnetoplasmadynamic acceleration processes, two students exploring various aspects of plasmadynamic lasers and one making rapid strides in the hollow cathode area. In addition, the two research staff members have been concentrating their effort mainly on the two new research topics.

In the MPD accelerator program, the work of two of the students, A. J. Saber and M. J. Boyle, will be presented as papers at the AIAA 10th Electric Propulsion Conference to be held at Lake Tahoe, Nevada, October 31 through November 2, 1973. These two papers appear in a slightly modified form in this report. The first details the decrease in the fractional anode power loss as total arc power increases, while the second concentrates on the several effects of insulator ablation on MPD accelerator operation. In a separate study, the effects of the injected propellant distribution on both terminal and internal properties of the MPD discharge are presented.

Significant progress has been made in the hollow cathode area. Most important has been the attainment of pulsed, high current hollow cathode operation with all of the current attaching inside the cavity. In this mode, the current and potential distributions have been mapped for the first time, allowing models for the emission process to be discussed.

This material will also be presented at the forthcoming Electric Propulsion Conference.

Although the plasmadynamic laser program is still in its early phases, a preliminary experiment has been initiated to determine the gain or absorption of selected transitions within the argon ion in the expanding MPD exhaust flow. An additional new experiment has identified the ultraviolet radiance characteristics of the discharge, which can be related to the possible generation of inversions in the recombination process.

II. QUASI-STEADY MPD DISCHARGE

II-A. Anode Power Deposition (Saber)

The power deposited in the anode of steady-state arcjets operating at arc powers up to several hundreds of kilowatts can be as large as 50% of the total input power.[A-1] The anode therefore is the major power consumer in these discharges. However, recent indications of anode heat flux in a quasi-steady MPD accelerator, as determined from local measurement of the plasma properties near the anode, indicated that the fraction of the total power delivered to the anode decreased steadily as arc power was increased into the multimegawatt range.[132] This result suggests that as the total power is increased, a fractionally larger power appears in the plasma and is available for subsequent conversion to thrust, i.e. the thrust efficiency will increase. To investigate that significant trend in more detail, the local anode heat flux has been measured directly with thermocouples over the entire anode surface of a quasi-steady MPD accelerator. This direct measurement of anode power covers the range from 200 kW, the level of the high-power steady D.C. arcjet,[A-2] to 20 MW, and verifies the previously inferred drop in fractional anode power as total power is increased. The anode power measurement has recently been augmented by diagnostic determinations of the local plasma properties at the anode, which allow the heat flux into the anode to be compared with the model commonly employed for this process.

Direct Measurement of Anode Power

The direct measurement with thermocouples of the power deposited in the anode has been described in detail previously.[143,146] Briefly, the local anode temperature rise was monitored by 12 thermocouples attached to the inside of a

1-mm-thick shell anode, shown schematically in Fig. 1. Applying the model for heat conduction through a plane parallel slab to the shell, the thermocouple response to the quasi-steady discharge was converted into local heat flux values, and thence to anode power via integration of the heat flux over the anode surface. This technique has been applied over a range of arc currents from 5.5 to 44 kA and argon mass flows from 1 to 48 g/sec. The results, plotted as fractional anode power against total arc power, are repeated in Fig. 2 for subsequent comparison with fractional anode powers calculated from probe data. These direct measurements verify the remarkable decrease in anode power fraction as arc power increases, and encourage further examination of the processes responsible for this dependence.

Indirect Measurement of Anode Power

The heat flux to an arc anode has commonly been accounted for in terms of the flow of electrons of temperature T_e at a current density j_a, through an anode fall V_a, to an absorbing anode of work function ϕ .[A-1] This energy balance can be written:

$$q_a = j_a(V_a + \frac{5}{2}\frac{kT_e}{e} + \phi) + q_{conv} + q_{rad} \qquad (1)$$

where k is Boltzmann's constant, e is the charge on an electron, and q_{conv} and q_{rad} are convective and radiative contributions which are neglected here. In an effort to check the validity of this model, local values, of j_a, V_a and T_e in the anode adjacent plasma were obtained from measurements with magnetic probes, floating Langmuir probes and double probes. These measurements provide an independent calculation of the anode heat flux for comparison with the measured values. Probing was carried out for arc currents from 8 to 22 kA with

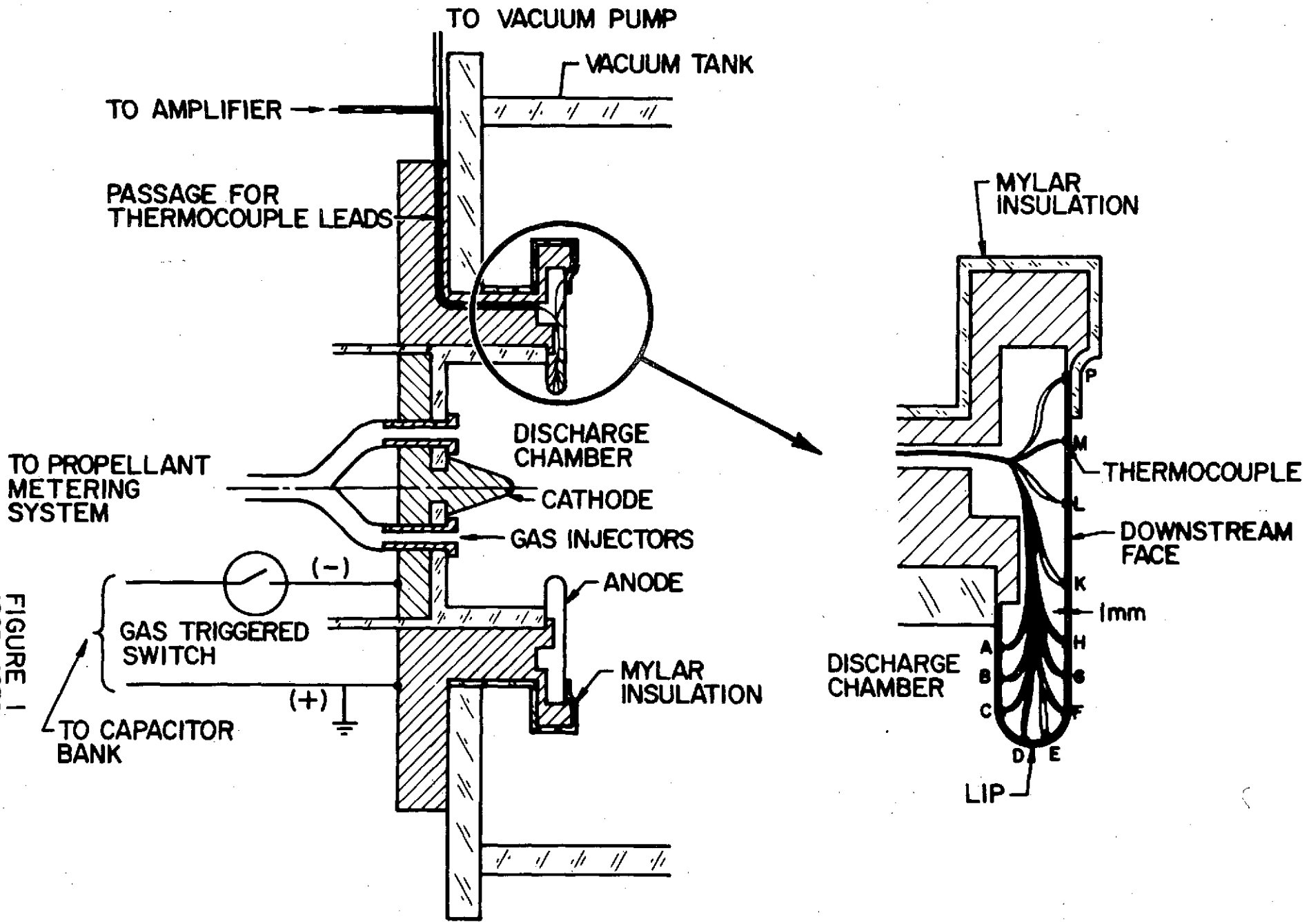

FIGURE 1
AP25-4870

MPD ARC WITH SHELL ANODE, SCHEMATIC

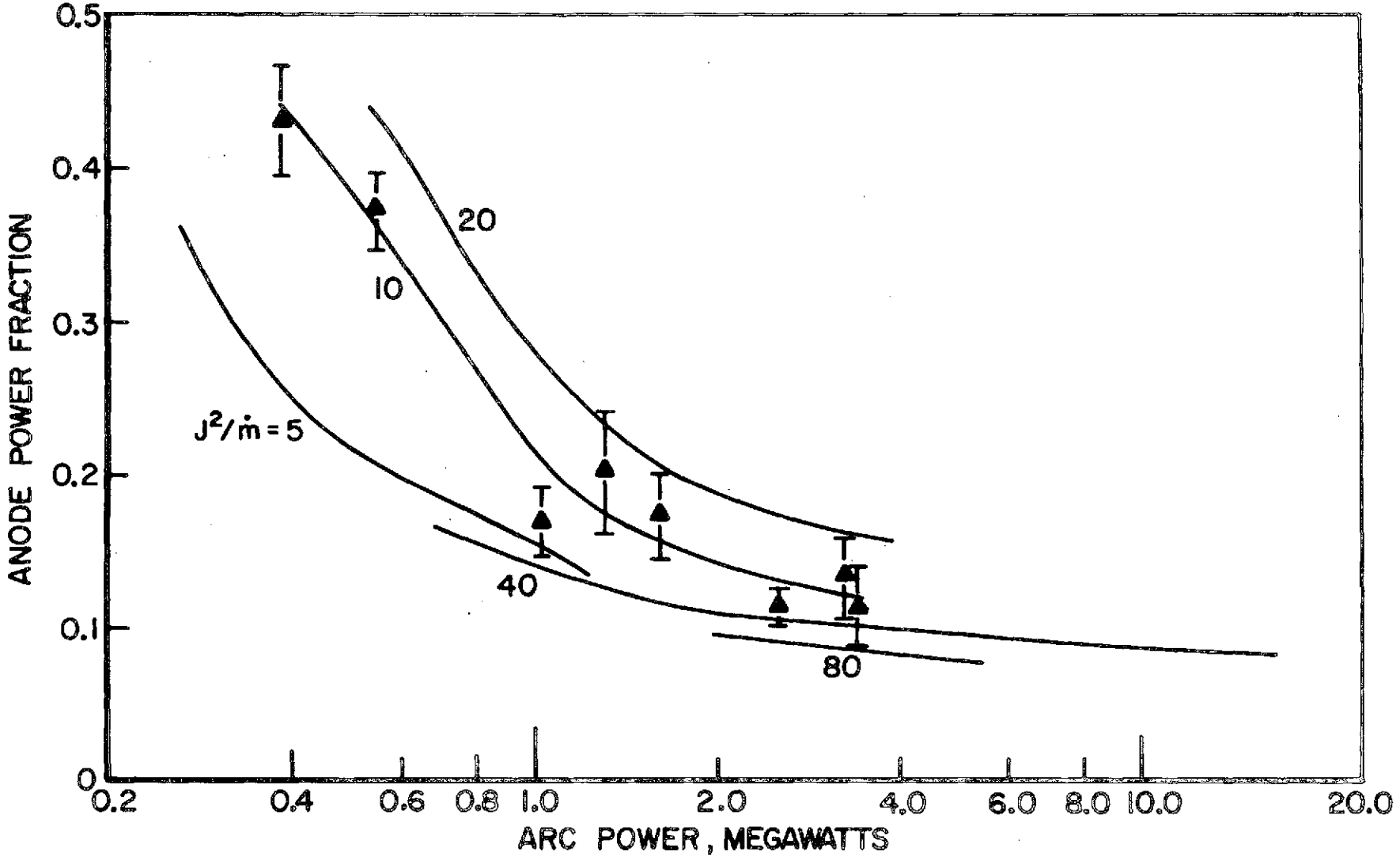

FIGURE 2
AP 25-4956

ANODE POWER FRACTION vs
TOTAL POWER

an argon mass flow of 24 g/sec, for mass flows from 6 to 48 g/sec with a current of 16 kA, and for five combinations of current and mass flow which produce a fixed $J^2/\dot{m}$ = 10 kA^2-sec/g at an arc power increasing from 0.6 to 3.4 MW.

Anode Current

The enclosed current contours were obtained from the integrated signals from magnetic field probes with 0.3-cm-diameter, 120-turn coils in 0.4-cm-diameter glass tubing. Figure 3 shows typical enclosed current contours for operation at 16 kA and 24 g/sec. The 1-cm-wide anode shell and discharge chamber insulating ring are shown. Probing was carried out to about 2 mm from the anode surface and the contours extrapolated to the anode. The indicated currents on the contours show the total current downstream of the given line. The current contours were used to calculate the anode current density shown in Fig. 4 for the same 16 kA x 24 g/sec arc operation. Like the heat flux profile shown previously,[146] the current density peaks in the lip region at about 300 A/cm^2. The current density drops in the chamber to 80 A/cm^2 and to 10 A/cm^2 on the face.

It has been observed that the current conduction pattern at the anode is maintained for other operating conditions for the same $J^2/\dot{m}$ = 10. However, a larger portion of the total current attaches on the downstream face of the anode as $J^2/\dot{m}$ is increased.

Electron Temperature

The electron temperature was determined from the measured characteristic of a double probe with 0.7-cm-long by 0.007-cm-diameter electrodes.[A-3] The electron temperature at 24 g/sec and total currents increasing from 8 to 22 kA is shown in Fig. 5a for a location in the anode midplane, 0.2 cm radially

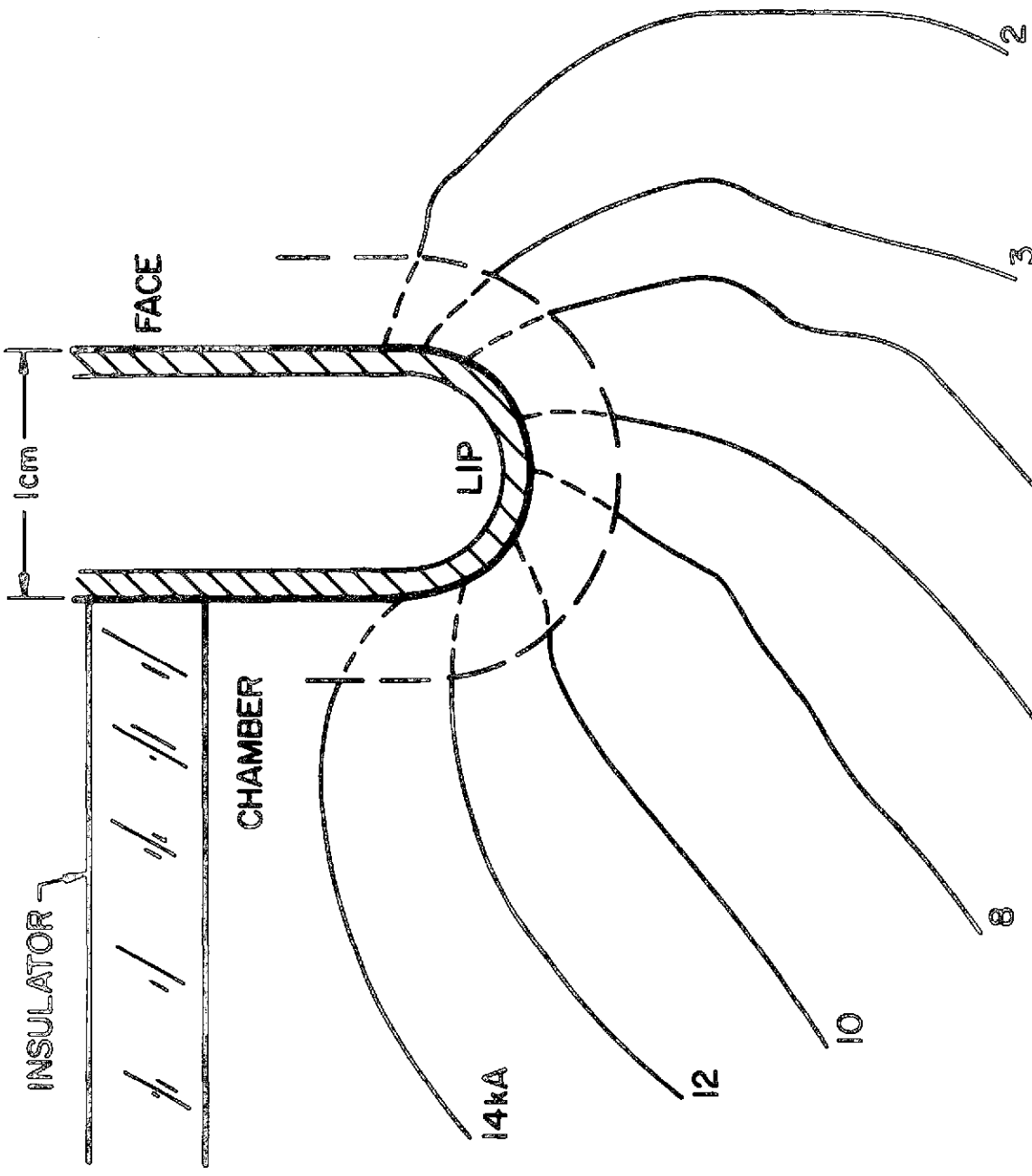

FIGURE 3
AP25·4957

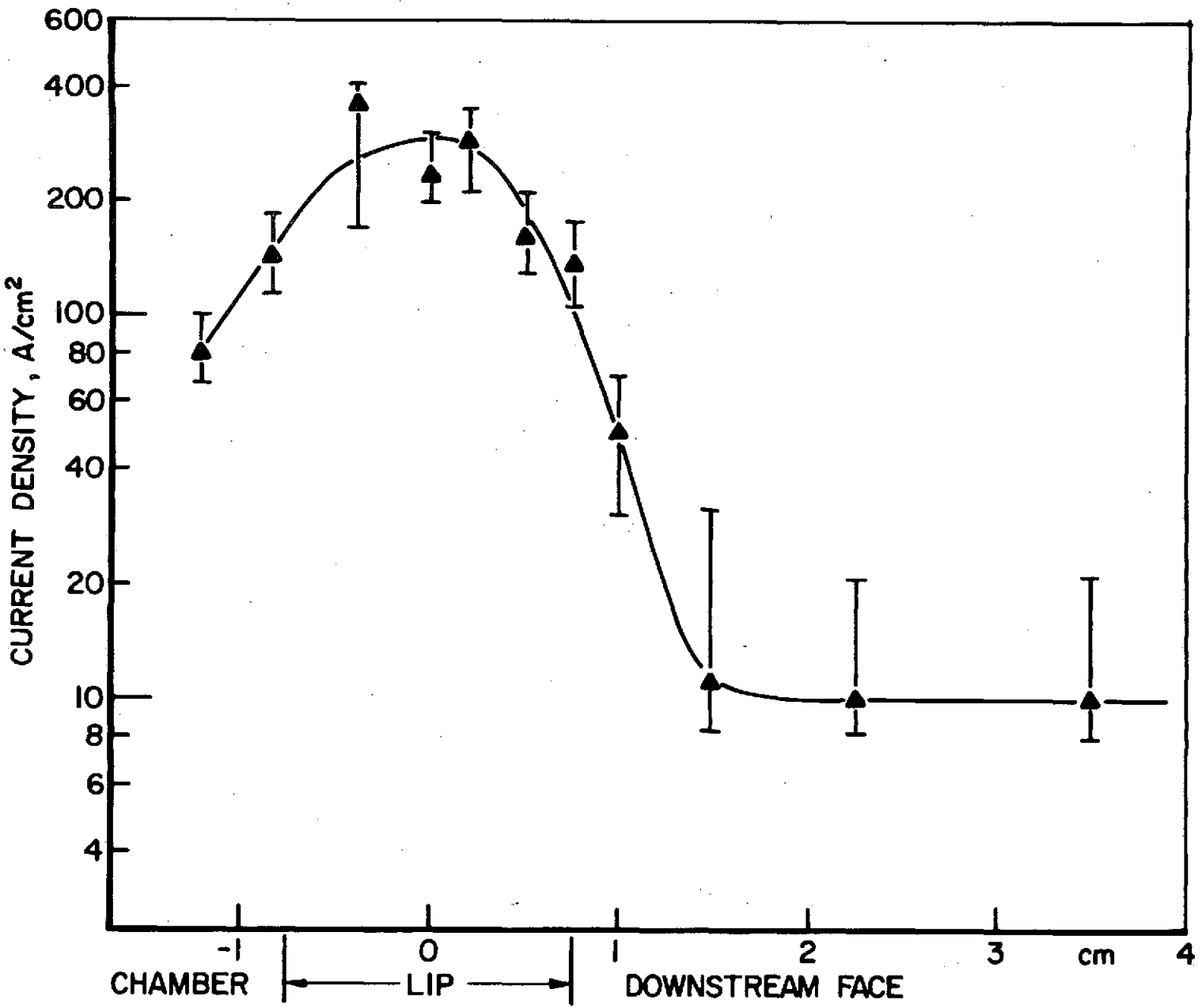

ANODE CURRENT DENSITY
16 kA, 24g/sec

FIGURE 4
AP25-4958

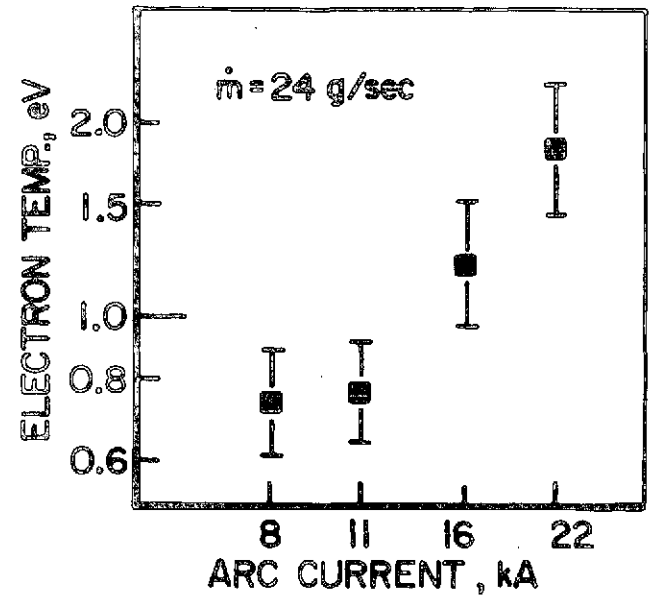

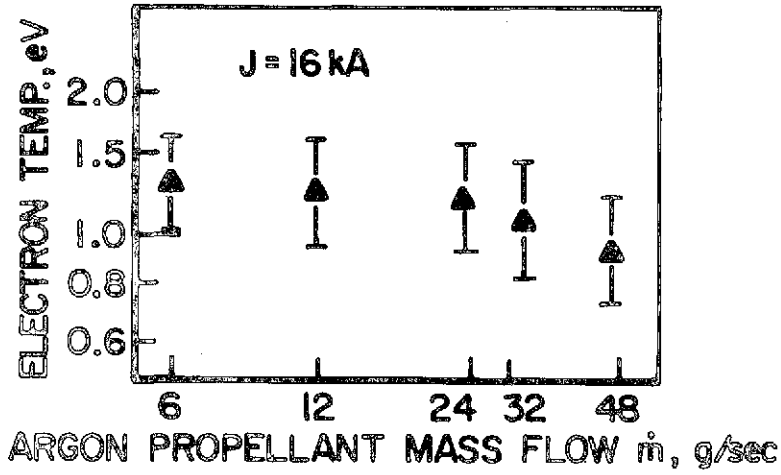

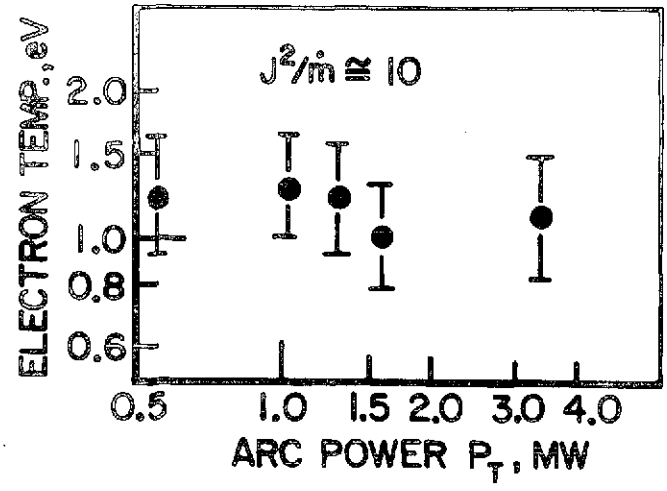

ELECTRON TEMPERATURE AT THE ANODE LIP

FIGURE 5
AP25-4959

inward from the lip. The increase from 0.7 eV to about 2 eV, nearly a factor of 3, indicates an approximately linear dependence of electron temperature on arc current. The much weaker dependences of the electron temperature on mass flow and on arc power are shown in Fig. 5b and 5c. For the same range of discharge currents and mass flows, the electron temperature 0.2 cm upstream of the anode, 0.2 cm from the chamber insulator, was approximately 20% lower than at the lip and about 10% lower at a corresponding position near the downstream face of the anode. The accuracy of the electron temperature measurement was estimated at approximately ± 20% since the reduction of the data is very sensitive to the small superimposed fluctuations on the probe current, which may have been caused by ion density fluctuations in the plasma.

Anode Fall Voltage

The anode fall voltage was derived from the measurement of the floating potential distribution obtained with a radially orientated Langmuir probe with a 0.1-cm-long by 0.007-cm-diameter tungsten tip. The floating potential pattern for the 16 kA x 24 g/sec operating point is shown in Fig. 6. The anode lip, discharge chamber insulator and enclosed current contours are shown for reference. The separation of the equipotentials gives an indication of the electric field over the anode. The electric field is highest on the upstream lip where the equipotentials are most closely spaced.

The floating potential measurements were reduced to plasma potentials by the addition of a term approximately four to five times the electron temperature in electron volts. This correction term includes the contribution from the flow of ions impinging on the probe[A-4,A-5] in addition to the usual ion and electron current terms.[A-6,A-7] The accuracy of the anode fall voltage, which is defined here as the plasma potential 0.1 cm

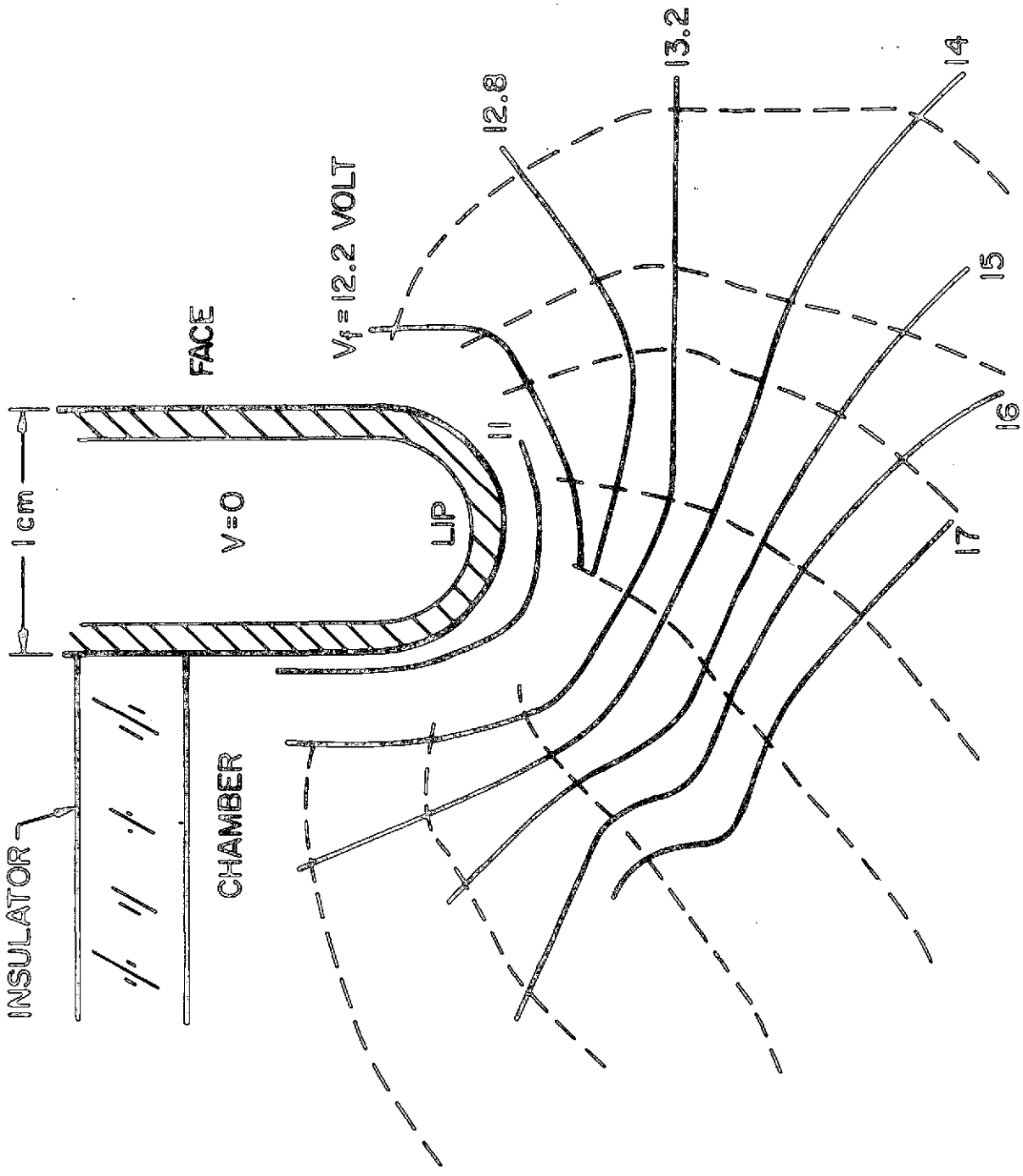

FLOATING POTENTIAL PROFILES
16 kA , 24 g/sec

FIGURE 6
AP25-4960

from the anode surface, is therefore dominated by this correction term which contains the electron temperature and is subject to its inaccuracies.

The anode fall voltage is shown in Fig. 7 for constant mass flow, current and $J^2/\dot{m}$ parameter. Examining the operation at low currents for a constant mass flow of 24 g/sec (Fig. 7a), the anode fall voltage is nearly constant at 2 volts in the chamber and on the downstream face, dipping about 1½ volts on the lip. As the current is increased, the anode fall voltage increases strongly. Figure 7c exhibits the anode fall voltage profiles for constant $J^2/\dot{m} = 10$ as the arc power is increased from 0.6 MW to 3.4 MW. The 0.6 MW profile is at an approximately 5 volt level inside the chamber and rises to 8 volts on the downstream anode face while the 3.4 MW profile is 5.5 volts in the chamber and rises to 12 volts on the downstream side, only 50% higher than the 0.6 MW profile.

Anode Power from Probe Measurements

Using the measured local values of current density, electron temperature and anode fall voltage, each of the terms in Eq.(1) can be calculated and integrated over the anode to yield a theoretical anode power fraction. The individual anode power components, due to anode fall, work function and electron temperature, are shown in Fig. 8, along with their sum, in comparison with the anode power fraction measured with thermocouples. The anode power calculated from Eq. (1) is seen to lie consistently below the power measured by the thermocouples, with the discrepancy increasing at the lower total powers.

The source of this discrepancy is not yet firmly established, but appears to be related to the ability of the conduction electrons to acquire kinetic energy from a larger portion of the inner-electrode potential than simply the anode fall. That is,

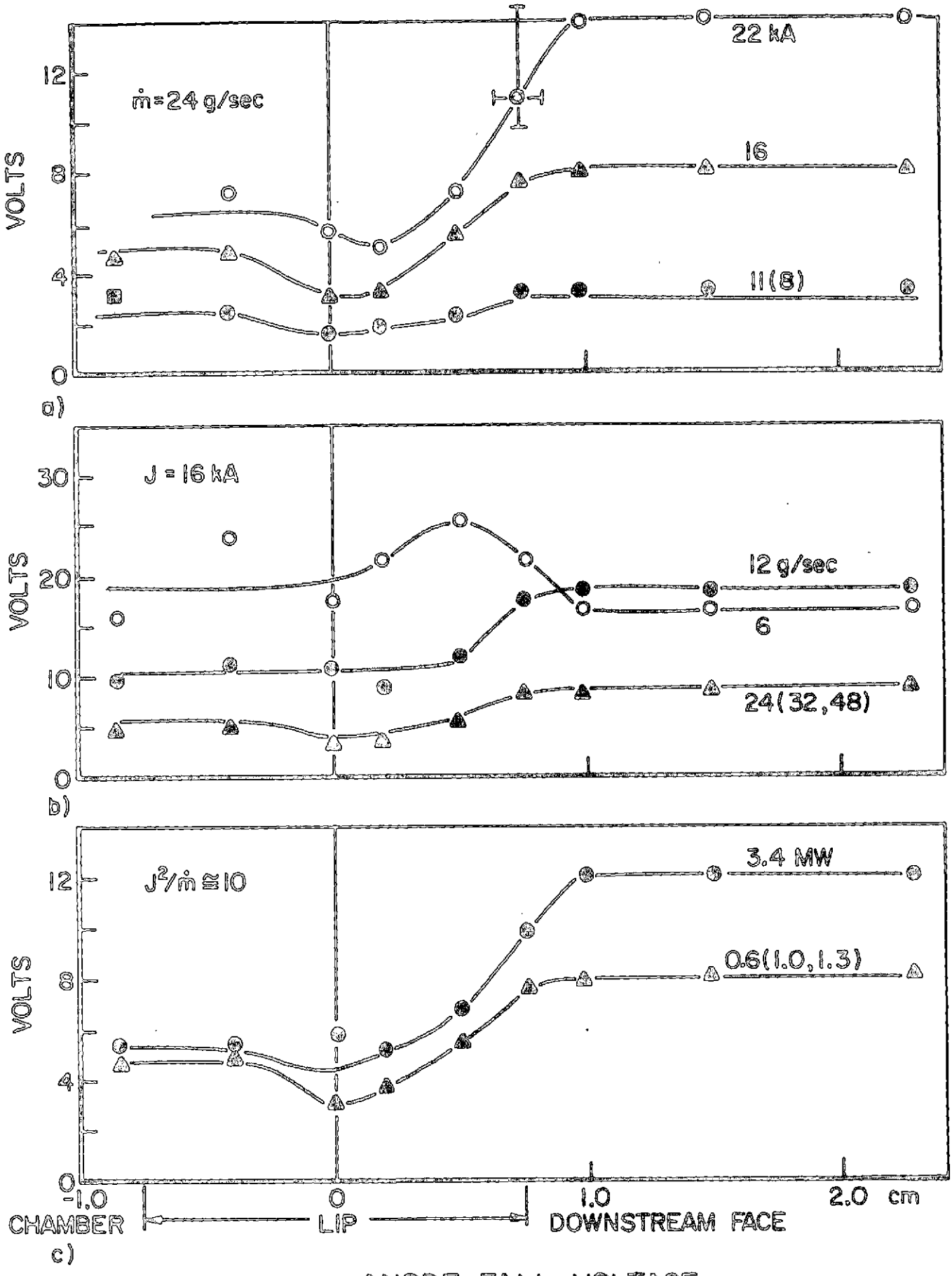

ANODE FALL VOLTAGE

FIGURE 7

AP25·4961

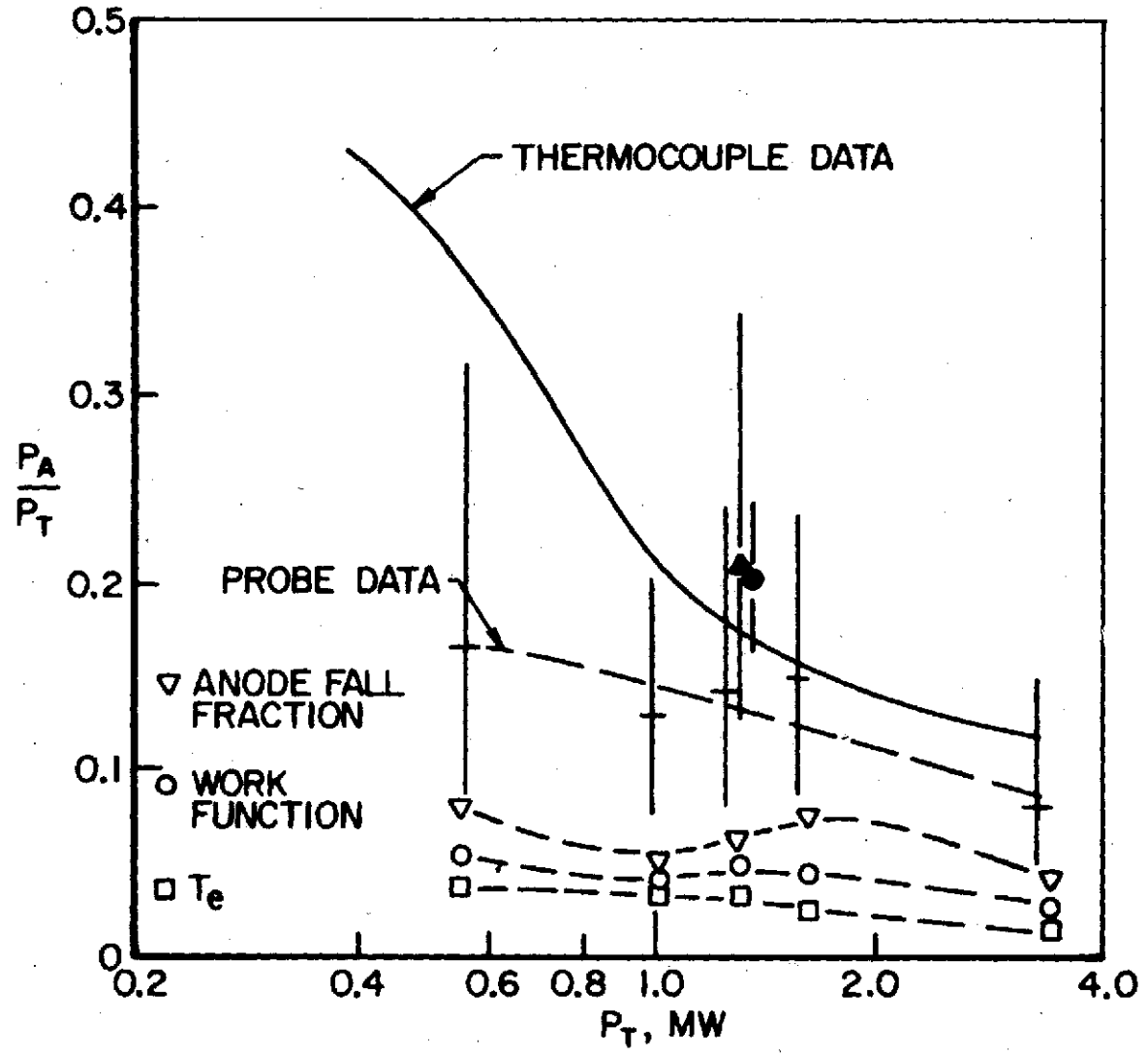

COMPARISON OF FRACTIONAL ANODE POWERS

FIGURE 8
AP25-4962

the effective electron mean free path for energy transfer in the prevailing discharge environment considerably exceeds the dimension of the anode sheath. Based on the measurements of electron number density and temperature available, we have estimated this effective mean free path to be some 2 cm at the 16 kA x 24 g/sec condition, which, in view of the prevailing inter-electrode potential distribution implies that a typical electron falls through some 10 volts, rather than only the 5 volts of the anode fall on its way to the anode surface. This, in turn, increases the fractional anode power from this component from .07 to .14 and thence the composite power from 0.14 to 0.21 as shown by the solid triangle in Fig. 8 (the solid circle represents thermocouple results for the same condition). Preliminary examination of available data indicate that this effective potential drop experienced by the electrons reaching the anode deviates less from the standard anode fall as the power density of the discharge increases. Thus the trend is to bring the computed curve into better agreement with the measured behavior over the range of arc powers studied.

II-B. Effect of Insulator Ablation on the MPD Discharge (Boyle)

High power, quasi-steady operation of the MPD accelerator is known to increase its attractiveness as a primary propulsion device. Specific impulses of several thousand seconds have been measured,[A-8] and thrust has been verified to scale as the square of the current in this operating mode.[A-9] In addition, as shown in the previous section, the power loss to the anode becomes fractionally less important as the total input power is increased. Countervening these benefits, multimegawatt quasi-steady arcjet operation tends to produce serious insulator ablation, which must be properly accounted for in evaluating the arcjet's high power performance characteristics, and must be virtually eliminated before long-term thruster operation can be contemplated.

This section describes the manner in which arc voltage and exhaust velocity of a quasi-steady MPD arc are affected by the introduction of ablation products into the discharge and exhaust stream, and discusses techniques for eliminating such effects. Actually, several categories of ablation need be distinguished, according to the effects produced relative to nominal MPD arc operation. Ranked in descending degrees of ablation, we define: (1) "significant ablation" to imply ablation-dominated terminal voltages and ablation-dependent velocities; (2) "reduced ablation" where only the exhaust velocities are affected; (3) "minimal ablation" where the quasi-steady arc characteristics are independent of insulator material, but the presence of ablated species in the discharge is detected spectroscopically; and (4) "no ablation" detectable in any fashion. Examples of the first three categories and the steps taken to alleviate their perturbing

effects are discussed. Category (4) has not yet been realized except under low current, high mass flow rate operating conditions far outside the range of space thruster interest.

The discharge configuration used for these experiments is identical to that shown in Fig. 1 with the exception that the shell anode has been replaced with a solid anode of equal dimensions. The anode is electrically insulated from the cathode by a cylindrical pyrex wall insert and a circular rear end plate. Insulator ablation in the present context refers to the ablation of this end plate, which is constructed of either Plexiglas or boron nitride. In addition to acting as an insulator, the end plate contains the injection orifices through which argon propellant is supplied to the discharge chamber. Changes in mass injection geometry refer to the use of end plates which distribute the injected propellant to different locations within the discharge chamber.

Effects of Insulator Ablation on the Voltage-Current Characteristic

For a given accelerator geometry, current level, and input mass flow rate and distribution, the voltage-current characteristic of the MPD arc indicates the electric potential required to drive that current between the anode and cathode in the presence of plasma resistivity, plasma flow, magnetic fields and electrode sheaths. The terminal arc voltage may be expressed as the sum of an ohmic, motional emf, Hall and electrode fall term:

$$V = \int_C^A \frac{\bar{j}\cdot\bar{dl}}{\sigma} - \int_C^A (\bar{u}\times\bar{B})\cdot\bar{dl} + \int_C^A \frac{(\bar{j}\times\bar{B})\cdot\bar{dl}}{n_e e} + V_F \qquad (2)$$

where $\int_C^A \bar{dl}$ implies integration along any convenient contour

from the cathode to anode sheath surfaces, and V_F equals the sum of the anode and cathode falls. Order of magnitude estimates for the plasma environment of this study imply that additional contributions to the voltage due to electron pressure gradients and ion slip are negligible.

The voltage-current (V-J) characteristic of the arc for a given mass flow rate and injection geometry is obtained on a shot to shot basis. Arc voltages are measured with respect to anode ground by a 1000:1 Tektronix high voltage probe attached to the cathode, while the arc current is recorded by a Rogowski loop embedded about the cathode. The total electrode fall voltage in each case is determined by extrapolating the terminal voltage back to its zero current value. $(V-V_F)$ is then plotted against the current.

The V-J characteristic for a six-hole Plexiglas insulator end plate and a total mass flow rate of 6 g/sec is presented on a log-log scale in Fig. 9. The argon propellant is injected axially into the discharge chamber through six 0.48 cm orifices symmetrically distributed about the 2.54 cm radius as illustrated in Fig. 10a. The Plexiglas characteristic may be divided into three separate regions shown in Fig. 9: (I) a low current region where the arc voltage is proportional to the current, (II) an intermediate current region characterized by a voltage proportional to the cube of the current, and (III) a high current region where the arc voltage scales linearly with the current. The functional behavior of the voltage with current within the three regions of the Plexiglas V-J characteristic may indicate respectively, electrothermal, electromagnetic, and ablation-dominated modes of operation.

The voltages in region I exhibit a linear dependence with current suggestive of electrothermal arcjet operation. Electrothermal plasma acceleration is characterized by the creation

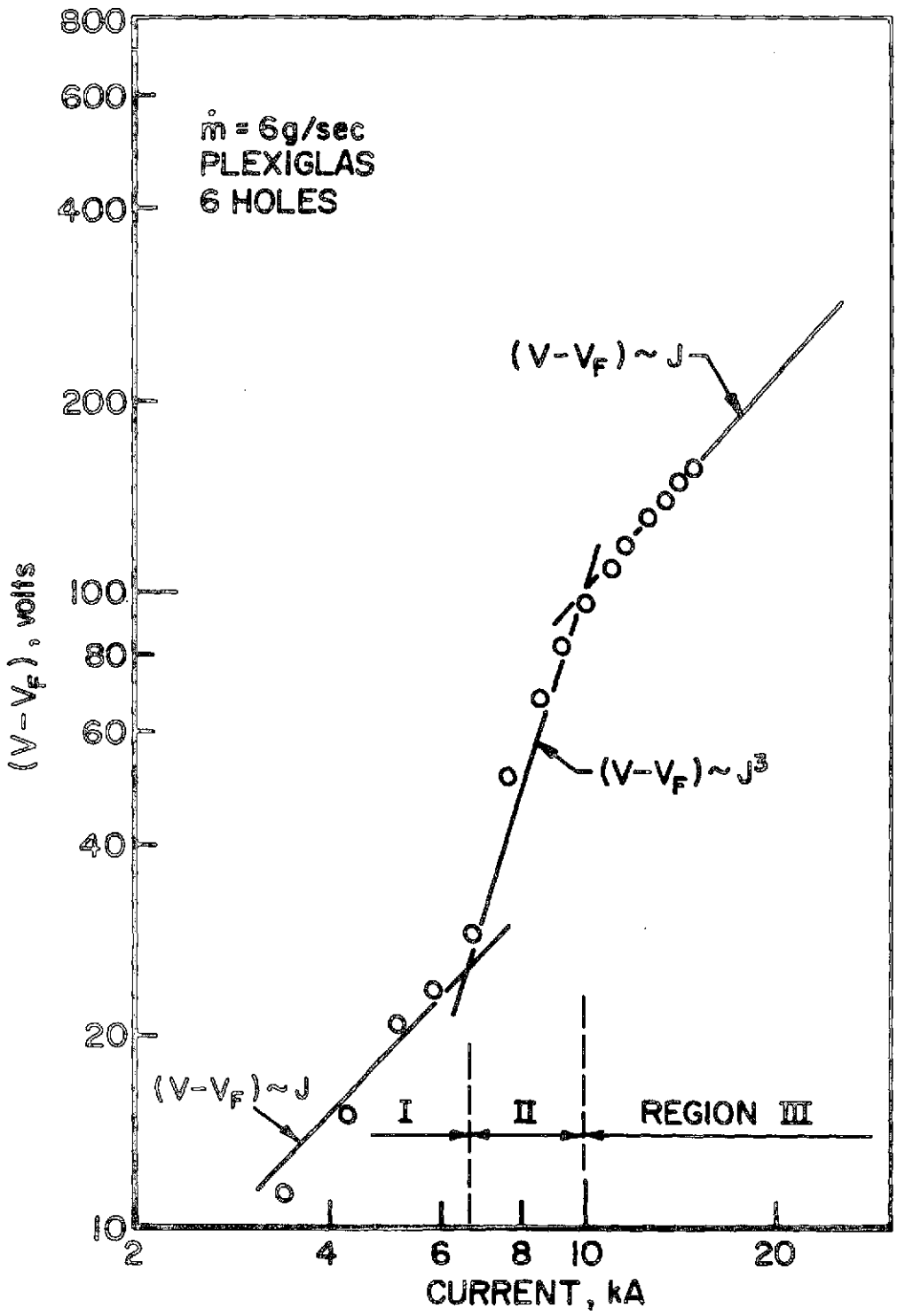

V-J CHARACTERISTIC, SIX-HOLE, PLEXIGLAS

FIGURE 9
AP25-4963

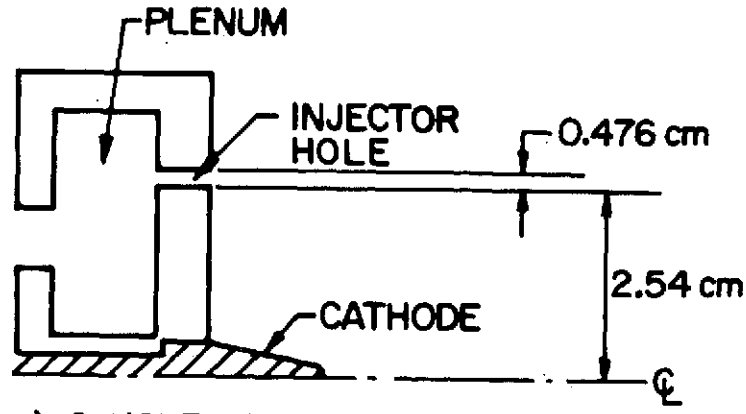

a) 6 HOLE GEOMETRY

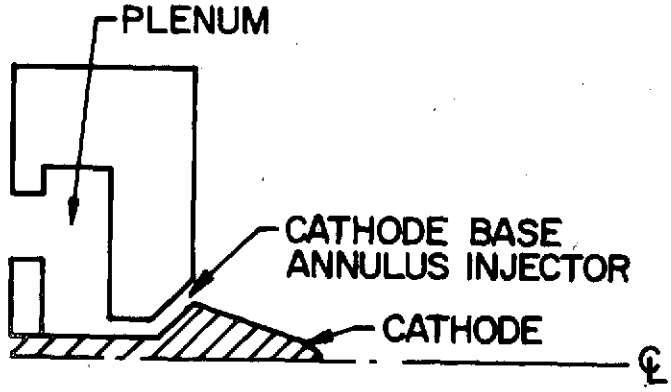

b) ANNULAR CATHODE BASE GEOMETRY

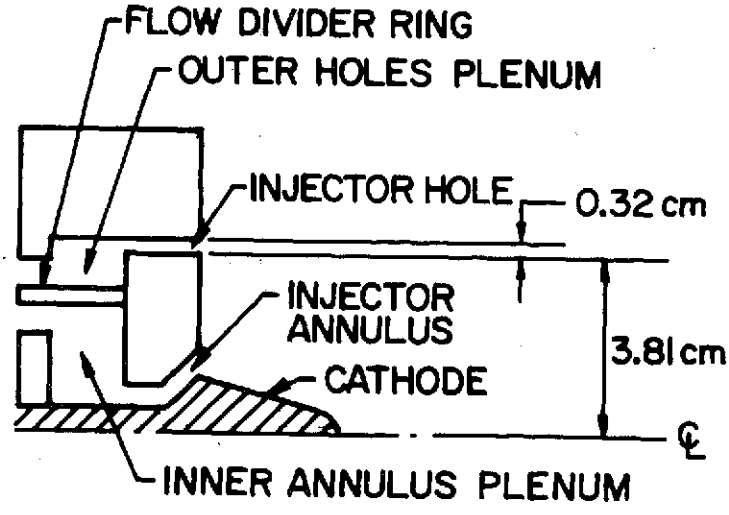

c) 12 HOLE CATHODE ANNULUS GEOMETRY

MASS INJECTION CONFIGURATIONS

FIGURE 10
AP25-4964

and subsequent expansion of a resistively heated, high enthalpy plasma at sufficiently low current that the $\bar{j} \times \bar{B}$ body forces within the discharge are negligible. Because resistive heating phenomena dominate the electrothermal mode, electrothermal terminal voltages should accordingly scale as the ohmic integral $\int_C^A \frac{\bar{j} \cdot d\bar{\ell}}{\sigma}$. Since the plasma conductivity in this regime of arc operation is only weakly sensitive to current density, the complete integral scales nearly linearly with current.

Similarly, region II may be associated with an electromagnetic mode of arcjet operation. In the Ohm's law formulation of the V-J characteristic, equation (2), the electromagnetic mode of arcjet operation appears as the motional emf integral $\int_C^A (\bar{u} \times \bar{B}) \cdot d\bar{\ell}$. Since the self magnetic field, B, is proportional to the current, J, the back emf term will scale as uJ. In the electromagnetic mode the exhaust velocity may be related to the current through the self-field MPD arc thrust equation.[61]

$$T = \dot{m}u = \mu_o J^2 \left[\ln(r_a/r_c) + 3/4 \right] / 4\pi \qquad (3)$$

Thus for a mass flow independent of current the average exhaust velocity will scale as J^2 implying a J^3 arc voltage dependence is associated with the electromagnetic mode of arcjet operation. Such cubic dependence is indeed exhibited by the region II voltages in Fig. 9. Thus, the transition between region I and region II at approximately 7 kA implies a transition from an electrothermal to an electromagnetic mode of arcjet operation.

The second transition in Fig. 9, from region II to region III at approximately 10 kA, we believe to be associated with insulator ablation. As postulated above, high current arcjet operation is characterized by an arc voltage proportional to the motional emf term of Ohm's law and it seems reasonable to

expect the voltage transition between region II and region III to be due to the onset of phenomena which affect the functional variation of the exhaust velocity with current. Quasi-steady thrusters using ablated electrode material as the propellant are found to ablate mass at a rate proportional to the square of the current.[A-10] For such thrusters the self-field equation (3) implies that exhaust velocities should be independent of arc current, and indeed, velocity measurements in the "starved", highly ablative region III of our Plexiglas characteristic indicate the average exhaust velocity is independent of current.[118] It follows then, that ablation-dominated terminal arc voltages will scale linearly with arc current just as seen in region III of Fig. 9.

For similar levels of incident thermal and/or radiative energy flux, refractory insulating surfaces are less prone to ablate than Plexiglas surfaces. Accordingly boron nitride was substituted for Plexiglas because of its higher thermal diffusivity and ablation temperature. In Fig. 11 the voltage-current characteristic for the same mass injection configuration and mass flow rate as above is now shown with boron nitride as the insulator material instead of Plexiglas. Regions I and II appear much the same as in the Plexiglas case, but no similar transition to region III of ablation-dominated voltage is seen in the boron nitride case. Instead, the high current regime, $J \geq 10$ kA, continues to be characterized by a J^3 voltage dependence in spite of spectral evidence of ionized boron and nitrogen in the discharge plasma. Apparently the refractory nature of the boron nitride insulation reduces the degree of ablation to such an extent that the terminal voltages are no longer ablation dependent.

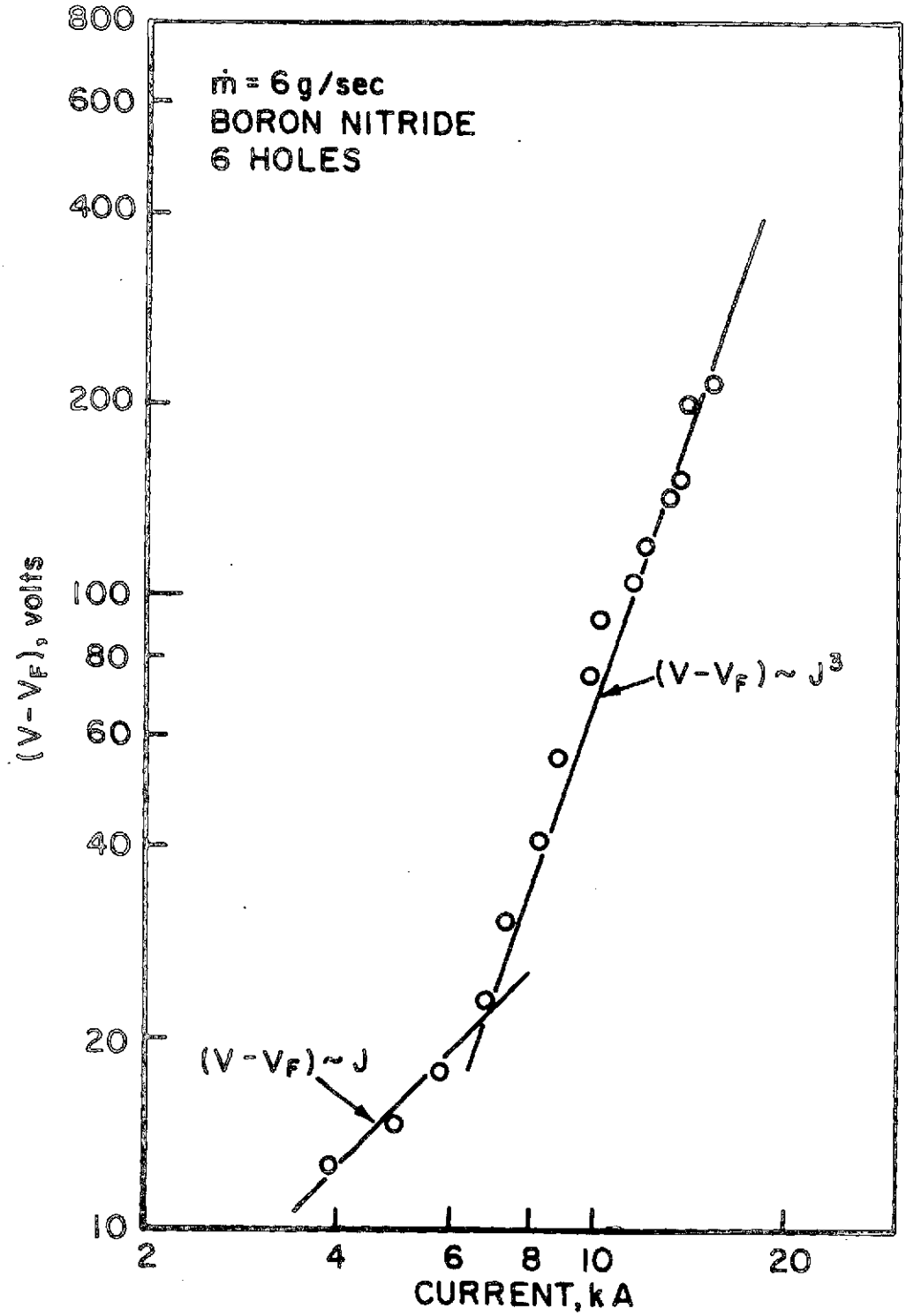

V-J CHARACTERISTIC, SIX-HOLE, BN

FIGURE 11
AP25·4965

It is also found in the boron nitride experiments that the azimuthal jet structure of the discharge seen with Plexiglas is no longer evident. As described below, however, significant effects on the jet velocity remain. That is, the use of boron nitride insulation within the MPD arc chamber reduces the degree of ablation from the previous "significant ablation" level to ablation category (2), "reduced ablation".

Effects of Insulator Ablation on the Exhaust Velocity

Insulator participation in MPD arcjet processes was originally suggested by comparing radial profiles of exhaust velocity with species distributions for an arcjet operating at 15.3 kA with 6 g/sec argon injected through a six-hole Plexiglas end plate.[146] The radial profile of velocity was obtained with a time-of-flight probe at a downstream position near the end of the electromagnetic acceleration region where magnetic field measurements showed that 90% of the total arc current flows upstream of this point. The profile, shown in Fig. 12, consists of a central core region with an average plasma velocity of 21.0 km/sec and two outer wings, each with an average plasma velocity of 8.8 km/sec. Superimposing Bruckner's radial species distribution[139] upon this velocity profile, the ablation products of the Plexiglas insulator (carbon, oxygen, and hydrogen) are found to occupy the central core region while the injected argon propellant occupies the outer wings. It is therefore legitimate to ask whether this velocity profile, particularly the high speed central core, is reflective of a normal $\bar{j} \times \bar{B}$ body force distribution or is a consequence of ablation and the particular insulator material employed within the arc chamber. A related question

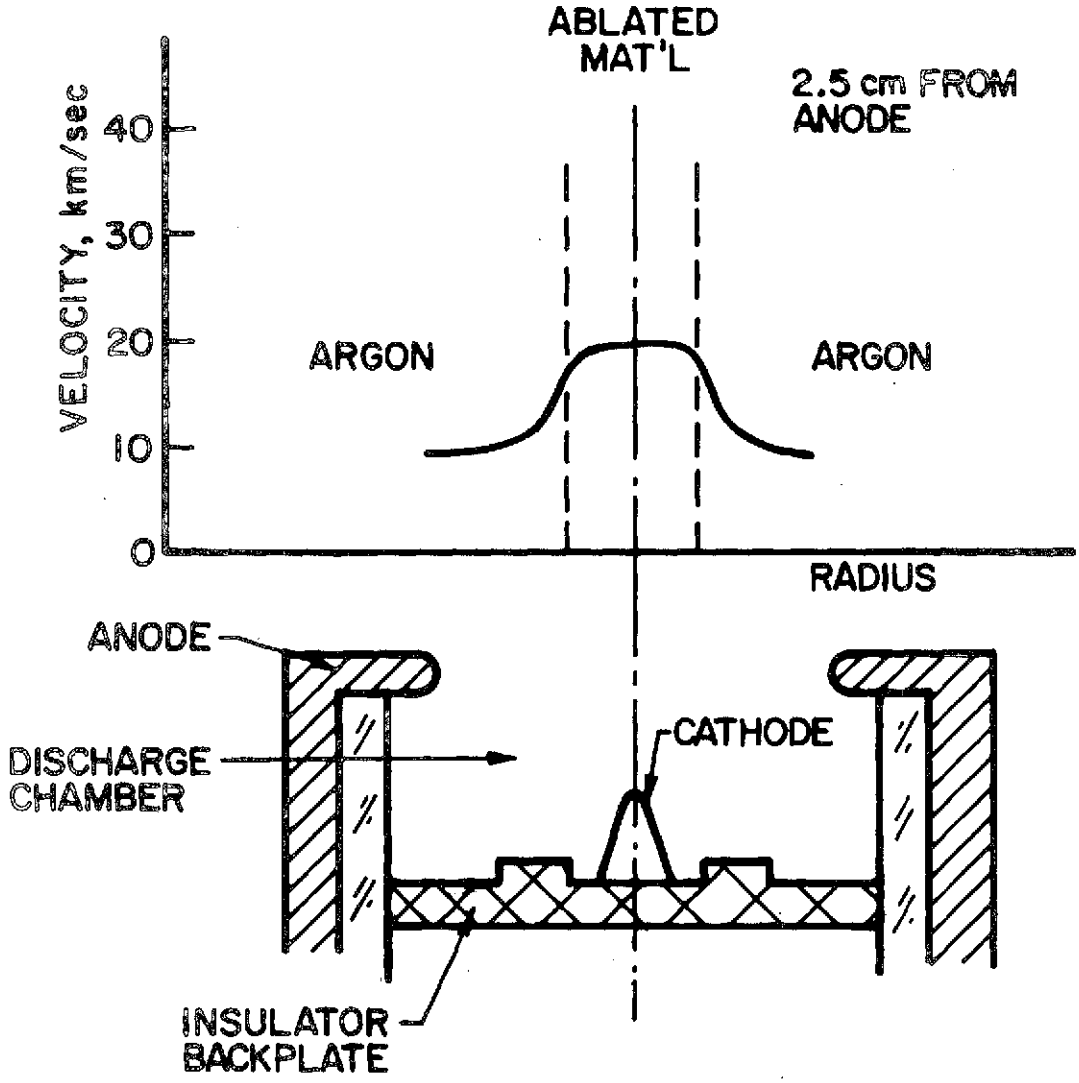

RADIAL DISTRIBUTION OF PLASMA SPECIES AND VELOCITY, $J = 15.3$ kA, $\dot{m} = 6$ g/sec, SIX-HOLE PLEXIGLAS

FIGURE 12
AP25-4966

is whether the specific impulse of 1230 seconds calculated from the measured thrust for this configuration[138] is artificially high compared with what it would be for a pure argon discharge. These questions can be discussed in the context of the Alfvén critical velocity hypothesis.

The Alfvén critical velocity has appeared frequently in the MPD arc literature and is simply defined as the velocity at which an ion's kinetic energy equals its ionization energy.

$$U_c^i = \left(2e\,\phi_i/m_i\right)^{1/2} \qquad (4)$$

The concept as originally suggested by Alfvén in his theory of planetary evolution proposes that an unspecified, highly efficient ionization mechanism is activated when the relative velocity between a neutral gas stream incident upon a magnetized plasma reaches its critical velocity.[A-5,A-11, A-12] In applied field MPD arcs the critical velocity appears as the proportionality constant relating the arc voltage and applied magnetic field.[A-13,147] Exhaust velocities on the order of the critical velocity of the accelerated propellant have been measured in several cases for both applied and self-field arcjets,[A-9,A-14] but the ultimate significance of the critical velocity concept to the MPD arc field has been cause for debate and as of yet no complete theoretical justification of its use exists. Thus, the critical velocity model used in this section is not invoked to explain the physics responsible for the measured velocity profile, but rather is employed in an empirical spirit as an indicator of ablation's influence on the exhaust velocity.

Critical velocity behavior was observed by Malliaris for a variety of noble gas propellants when the self-field MPD arc was operated at conditions such that the parameter $J^2/\dot{m}$

equaled a critical value given in terms of the propellant species and electrode geometry.[A-9] For argon propellant and our electrode geometry, $J^2/\mathring{m} = 39$ kA-sec/g, which is within a few percent of this $(J^2/\mathring{m})_{crit}$ defined by Malliaris. The argon critical velocity defined by equation (4) corresponding to an ionization energy of 15.7 eV and an ion mass of 40 a.m.u. is 8.7 km/sec. The argon ion plasma leaves the electromagnetic acceleration zone with a measured average velocity of 8.8 ± 1.2 km/sec which is within experimental error of the argon critical velocity.

The multispecies nature of the plasma complicates the definition of critical velocity behavior and introduces several ways in which critical velocity phenomena may be manifested. In a kinetic energy model of critical velocity behavior, the kinetic energy per particle of the predominant species continues to be expressed in terms of the critical velocity of that species. Furthermore, the velocity of each remaining ion species is such as to equate its kinetic energy per particle with the kinetic energy per particle of the predominant species. This equipartition of kinetic energy among particles was observed by Malliaris and Libby when an applied field steady-state MPD arc was operated with a bi-species propellant.[A-14] In our particular case, the central "Plexiglas" plasma jet and the outer argon plasma constitute the bi-species nature of the discharge. Because of the continuum nature of the discharge plasma in the near exhaust region, the centerline plasma consisting of the ionized products of Plexiglas ablation (carbon, oxygen and hydrogen-$C_5H_8O_2$) may be treated as a monofluid with an effective ion mass equal to the average weighted atomic mass of the ablation products.

$$m_{plex} = \frac{5m_c + 8m_h + 2m_o}{15} = 6.7 \text{ a.m.u.} \qquad (5)$$

First order estimates of the Plexiglas ablation rate at $J = 15.3$ kA, $\dot{m} = 6$ g/sec amount to less than 15% of the injected argon mass flow rate, thereby establishing argon as the predominant species in the discharge plasma.

According to the above kinetic energy model, the centerline "Plexiglas" plasma velocity should be calculable in terms of an equipartition of kinetic energy per particle.

$$e\phi_a = \tfrac{1}{2} m_a (U_c^a)^2 = \tfrac{1}{2} m_{plex} (u_{plex})^2$$

$$u_{plex} = \left(\frac{m_a}{m_{plex}}\right)^{\frac{1}{2}} U_c^a \qquad (6)$$

Upon substitution of m_a, m_{plex} and the argon critical velocity U_c^a into equation (6), the kinetic energy model predicts a centerline velocity equal to 21.3 km/sec, well within the experimental uncertainty of the measured centerline velocity of 21.0 ± 2.1 km/sec.

As an alternative, one may propose a "velocity model" where the argon and Plexiglas plasmas each leave the electromagnetic acceleration zone with its respective critical velocity. The subtlety of this model arises in assigning a value to the equivalent ionization energy, ϕ_{plex}, in equation (4). In the same spirit as equation (5), ϕ_{plex} is estimated as a weighted average of the ionization potentials of the atomic constituents of Plexiglas

$$\phi_{plex} = \frac{5\phi_c + 8\phi_h + 2\phi_o + \phi_D}{15} = 17.0 \text{ volts} \qquad (7)$$

where the energy of Plexiglas decomposition, $\phi_D = 1470$ kcal/mole, has also been included. Substitution of m_{plex} and ϕ_{plex} into equation (4) predicts a centerline velocity equal to 22.1 km/sec, again within the experimental uncertainty. It should be noted that because of the experimental error involved in measuring

the velocity, one is unable to distinguish between the two models.

In either case it appears that the exhaust velocities exhibit an inverse square root dependence on the mass of the species being accelerated in accordance with the critical velocity hypothesis, and that the high centerline velocity associated with the Plexiglas configuration is a consequence of the low average atomic mass of the centerline plasma and therefore a direct result of insulator ablation. Hence the degree of ablation in region III of the six-hole Plexiglas V-J characteristic is classified as "significant" in that both the arc voltage and exhaust velocity are ablation dominated.

When boron nitride is substituted for the Plexiglas insulation for the same six-hole mass injection geometry, the time-of-flight velocity on the centerline where spectrograms of the discharge indicate ionized boron and nitrogen are confined, is 16.0 $\pm$ 6.0 km/sec. As before, the centerline "boron nitride" plasma may be treated as a monofluid with an effective ion mass of 12.4 a.m.u. and an effective ionization energy of 13.34 volts. Accordingly, the kinetic energy model predicts a centerline "boron nitride" plasma velocity of 15.6 km/sec, while the velocity model yields 14.4 km/sec.

Thus it appears that even though boron nitride insulation reduces the degree of ablation to the extent that the terminal arc voltage is no longer ablation-dominated, the insulator material continues to affect nominal MPD arc operation through its influence on the exhaust velocity for this combination of operating conditions, insulator material and mass injection geometry.

Effects of Mass Injection Geometry on Insulator Ablation

In the previous two sections we described the ablation-dominated nature of the terminal voltage and exhaust velocity when Plexiglas is used as the insulator material. For the given mass injection geometry, substitution of boron nitride for Plexiglas eliminated influence upon the V-J characteristic, but this configuration still displayed an ablation-dominated centerline exhaust velocity. In a further attempt to eliminate the insulator affect upon the exhaust velocity, the manner in which the propellant is injected into the discharge chamber was next explored.

For the six-hole mass injection configuration, visual and spectroscopic data suggest that the insulator ablation is most severe about the base of the centrally located cathode. This is to be expected since the inverse radial dependence of the current density tends to maximize the thermal energy flux from the plasma to the insulating surfaces about the base of the cathode. In addition, the lack of injected argon propellant about the cathode base may create locally "starved" regions which in turn tend to encourage insulator ablation.

Therefore, in an attempt to supply argon propellant to the cathode region and remove solid insulator surfaces from the vicinity of the cathode, a revised boron nitride annular cathode base mass injection configuration was designed and constructed. The annulus channel, one side of which is the rear side of the cathode itself, is angled at 45° to provide a radial component of injected propellant flow, as shown in Fig. 10b.

Figure 13 is the measured V-J characteristic for this boron nitride annular cathode base injection geometry for an argon mass flow rate of 6 g/sec. The revised injection

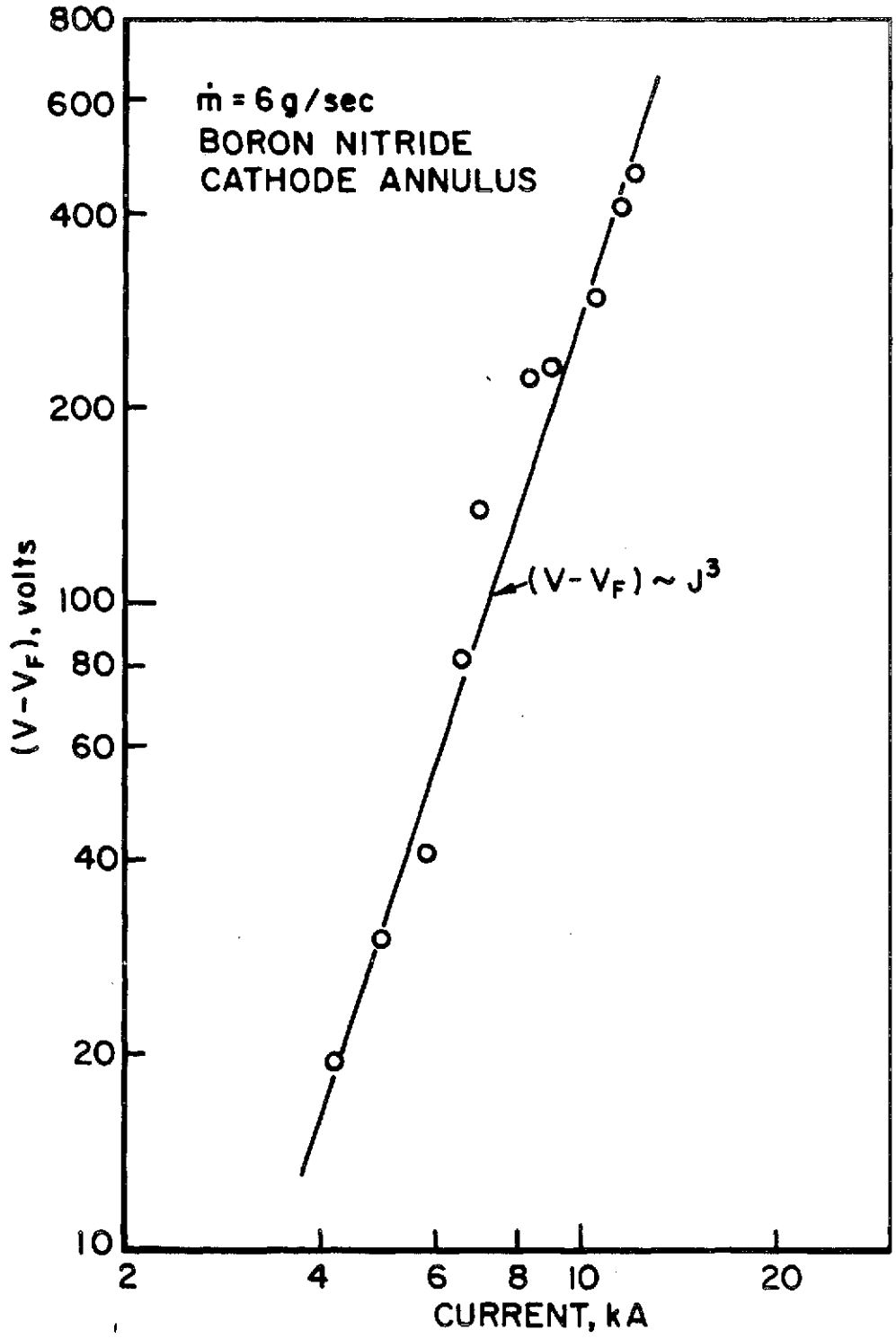

V-J CHARACTERISTIC, CATHODE ANNULUS, BN

FIGURE 13
AP25-4967

geometry still shows no tendency towards transition to ablation-dominated operation in the high current regime. It is also interesting to note that region I of the V-J characteristic has been eliminated and the low current regime now exhibits the cubic dependence of region II. This may suggest that mass injection directly into regions of maximum $\bar{j} \times \bar{B}$ body force helps promote the dominance of the electromagnetic mode of arcjet operation even for relatively low values of total arc current. Even though discharge spectra at J = 15.3 kA, $\dot{m}$ = 6 g/sec continue to indicate the presence of BII, BIII, NII and NIII in the discharge for this new configuration, the centerline exhaust velocity is now measured to be 9.0 km/sec, essentially the critical velocity for argon, suggesting this injection geometry is capable of reducing ablation to a "minimal" level where the exhaust velocity is no longer ablation-dominated.

For comparison, the revised injection geometry was tried using Plexiglas as the insulator material. In this case, while similar improvement in the exhaust velocity was found, the V-J characteristic retained its transition to region III implying that injection geometry changes with Plexiglas can permute the hierarchy of ablation effects rather than induce a change to "minimal" ablation, category (3).

In summary, the combination of an annular cathode base mass injection geometry and a refractory boron nitride insulator result in an arcjet configuration whose voltage characteristic and exhaust velocity are independent of insulator material. However, this has been achieved at the cost of higher terminal voltages as is seen in comparing the absolute magnitudes of the arc voltages for the two different boron nitride injection geometries. For example, at J = 10 kA the six-hole geometry voltage is 95 volts where at the same current

the annular cathode base BN geometry operates at a terminal voltage of 320 volts. Such a dramatic increase in the terminal voltage for a given current implies a significant change in arcjet operation.

Effects of Mass Injection Geometry on Terminal Voltages and Exhaust Velocities

All else remaining the same, MPD arcjet operation at the lowest possible terminal voltage for a given current and mass flow is desirable in terms of the overall efficiency of the device. The empirical experience outlined above suggests that some combination of large and small radius mass injection configurations might provide both lower voltages and arc operation independent of insulator material. To explore this possibility, floating potential surveys were taken for both injection geomtries at $J = 9$ kA, $\dot{m} = 6$ g/sec to identify regions of relative voltage increase.

Potential measurements begin a millimeter from the anode in the anode plane, proceed radially inward to the centerline, and then axially inward to a position a millimeter from the cathode tip. The floating potentials, uncorrected for electron temperature gradients, ion flow, collisional, and magnetic field effects are plotted as a function of radial and axial location along the path described above in Fig. 14. The anode fall potentials, defined as the potential measured at the one millimeter radial position, are equal for both injection configurations. The most pronounced difference between the two profiles is found in the steep radial voltage gradient for the annular cathode base injection geometry case.

This radial voltage gradient suggests that a local starvation of injected propellant exists in the radial conduction regions of the discharge, an effect elsewhere observed to have

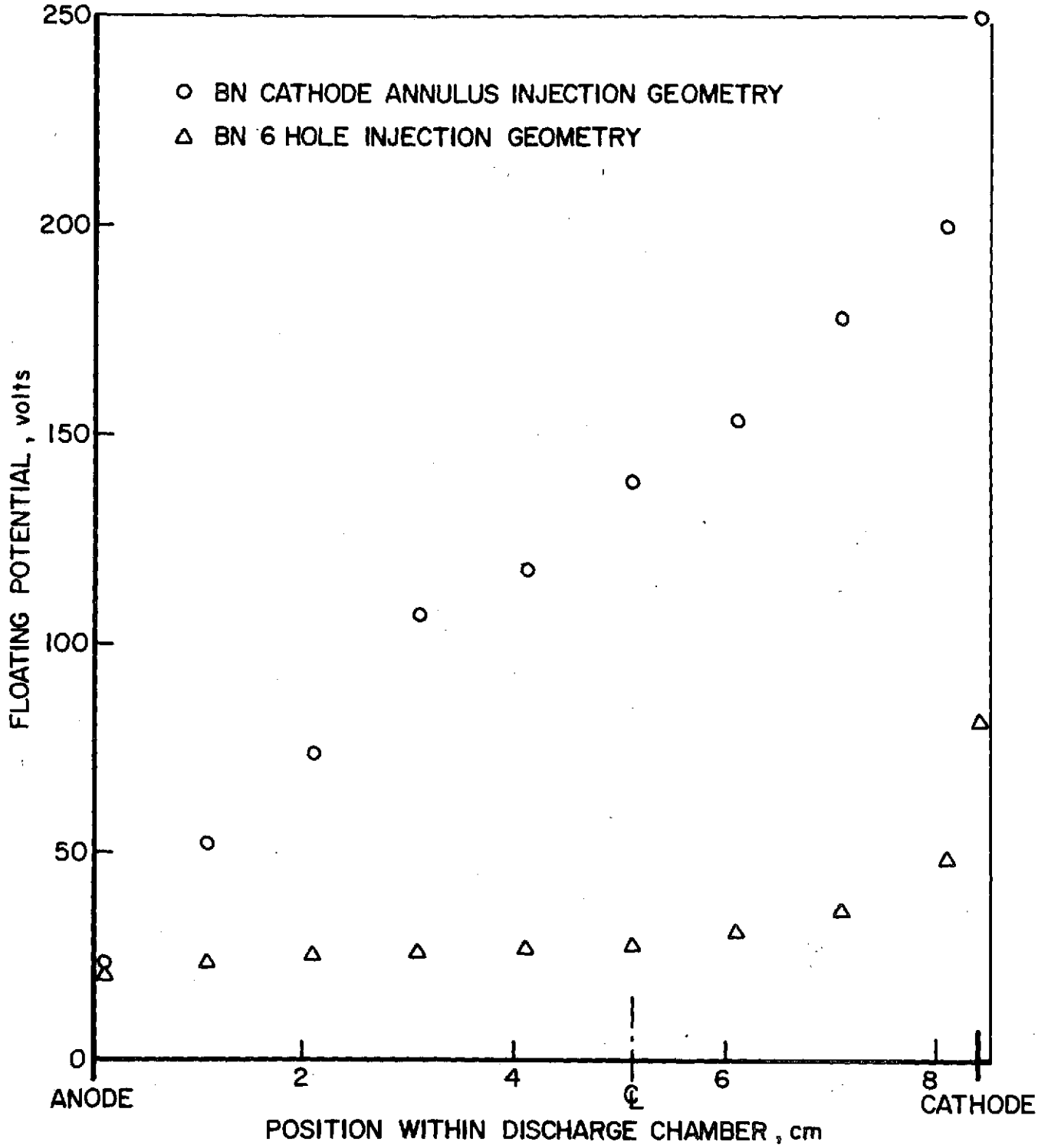

FLOATING POTENTIAL DISTRIBUTIONS
$J = 9.0$ kA , $\dot{m} = 6$ g/sec

FIGURE 14
AP25·4968

a strong influence on the terminal voltage.[132] The cathode base injection configuration apparently tends to concentrate injected mass about the centerline, whereas mass injection at a larger radius (six-hole injection geometry) provides relatively more mass in the radial conduction regions of the discharge.

In order to determine the optimum flow division between the outer radial region and the inner cathode region of the discharge chamber, a new boron nitride mass injection geometry was designed as illustrated in Fig. 10c. Twelve 0.32 cm holes symmetrically distributed about a 3.81 cm radius assure a uniform mass distribution to the radial conduction zone. A 45° cathode base annulus similar to the one used previously allows argon propellant to be delivered about the cathode. A flow divider ring establishes two independent plenums so that the mass flow division between inner annulus and outer holes can be controlled. The percentage flow division is monitored by varying the relative area ratios of the choked orifices feeding the two independent plenums. In such a manner the entire range of flow division between 100% inner flow; 0% outer flow (designated by 100:0) to 0% inner flow; 100% outer flow (0:100) may be spanned.

The V-J characteristics at 6 g/sec as a function of flow division are shown in Fig. 15. It is seen that the functional dependence of arc voltage on arc current is itself dependent on flow division in the low current regime and independent of flow division in the high current regime. Region I continues to scale as voltage proportional to current and region II as the cube of the current. The voltage as a function of percent flow through the inner annulus is presented in Fig. 16 for currents of 5, 10, and 15 kA and a mass flow rate of 6 g/sec. At the lowest current the voltage appears to be insensitive

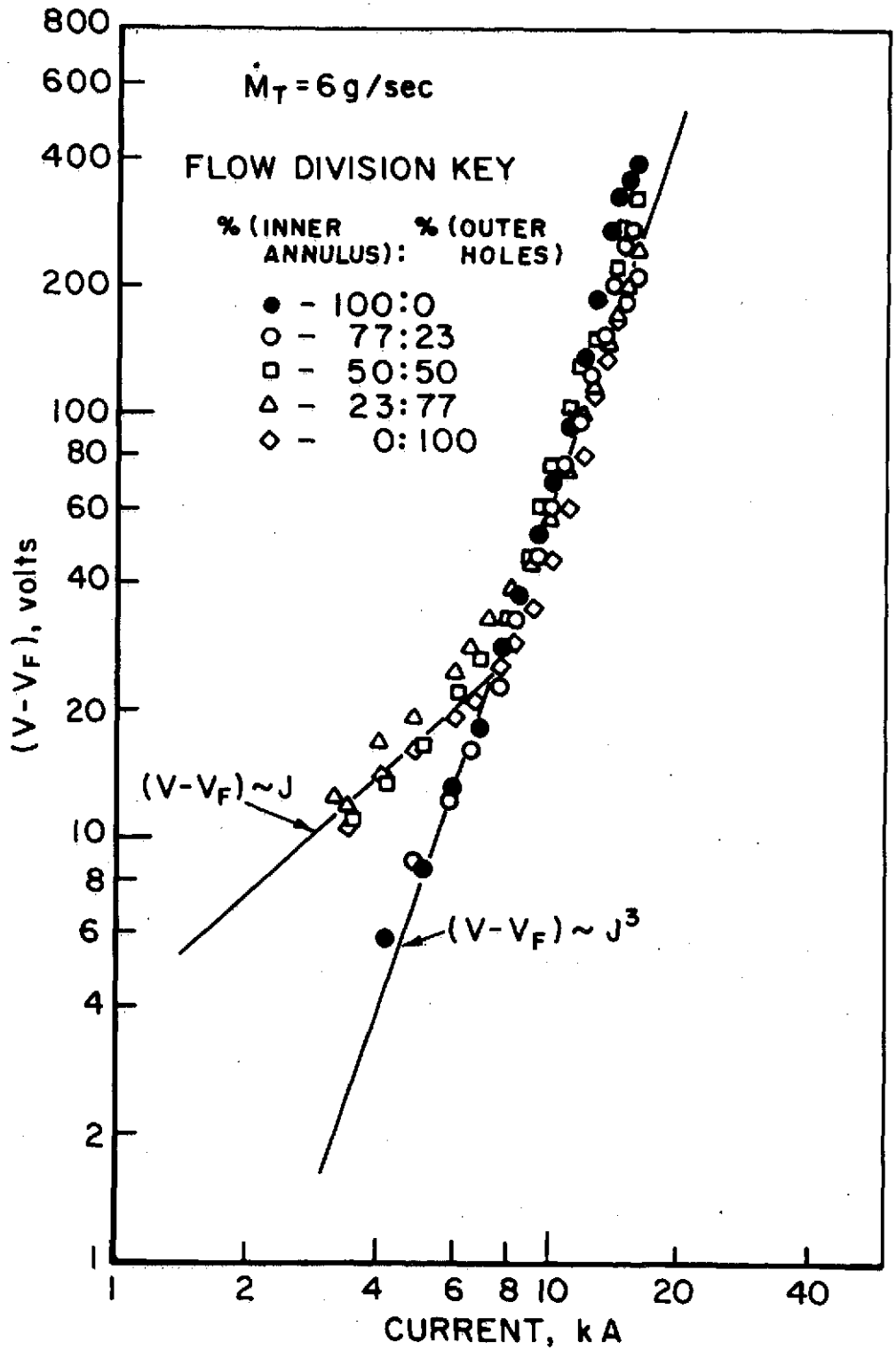

V-J CHARACTERISTICS vs FLOW DIVISION

FIGURE 15
AP25-4969

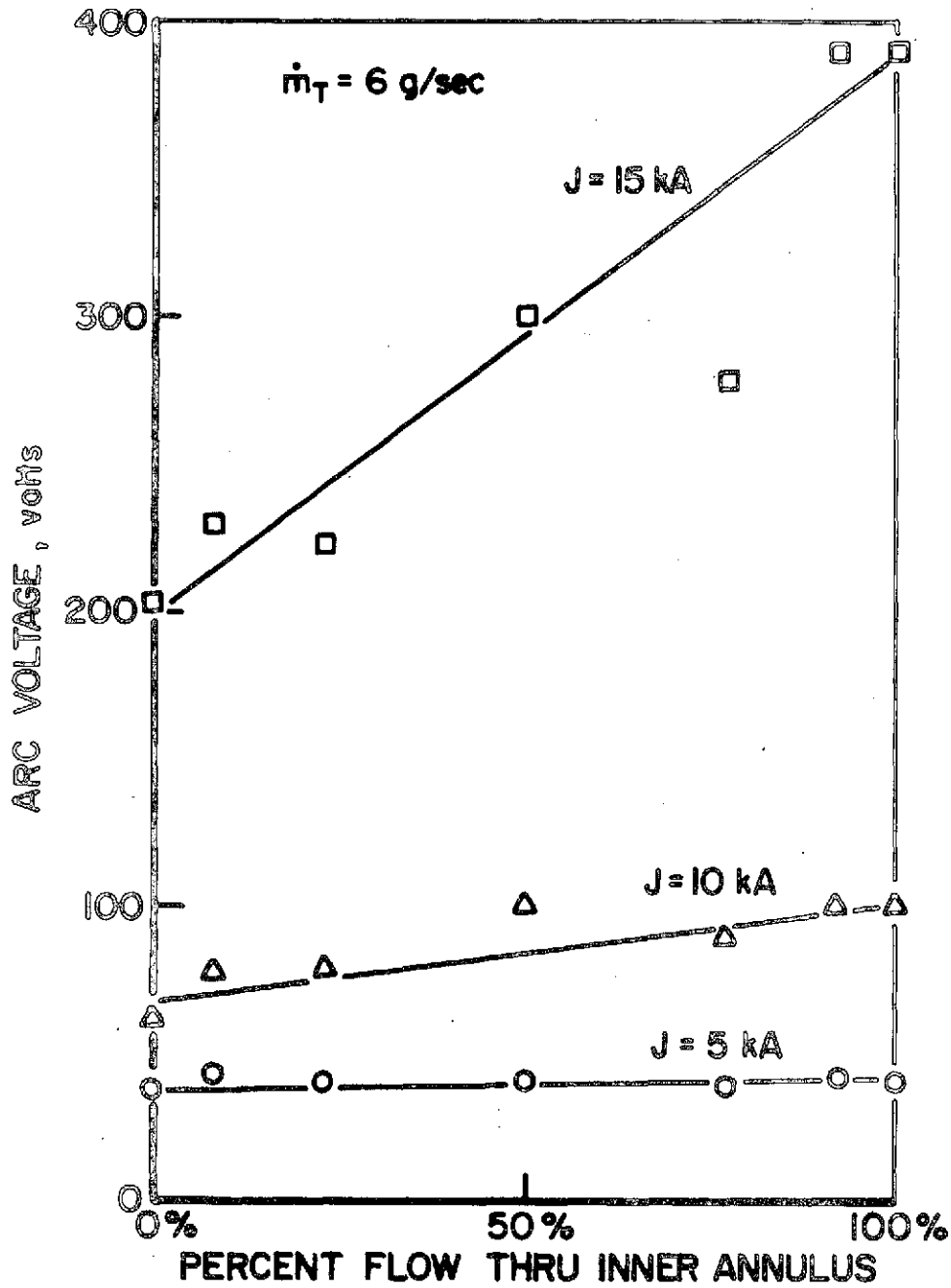

ARC VOLTAGE vs PERCENT FLOW THROUGH INNER ANNULUS

FIGURE 16
AP25-4970

to flow division, whereas at the high currents the voltage monotonically increases with % flow through the inner annulus. Thus, to minimize terminal voltage, the arc should be operated with as little of the flow as possible through the inner annulus, without inducing the ablation-dominated exhaust velocity associated with 0% inner; 100% outer flow division operation. To determine this minimum voltage point of operation it is necessary to obtain the exhaust velocity's dependence on the % flow division. This relationship is presented in Fig. 17 where the velocities are measured on the accelerator centerline 2.5 cm downstream of the anode face. A critical mass flow rate through the inner annulus, $\dot{m}_c$, between 1.4 g/sec and 3.0 g/sec, exists such that for $\dot{m}$ (inner annulus) $> \dot{m}_c$ the exhaust velocity is relatively constant about the argon critical velocity, while for $\dot{m}$ (inner annulus) $< \dot{m}_c$ the exhaust velocity jumps to the neighborhood of the "boron nitride" plasma velocity calculated from the critical velocity models. (Dual critical velocity behavior of a multispecies plasma as a function of species concentration has been reported before by Eninger in a coaxial plasma gun accelerator geometry, although for different levels of current and pressure.[A-15]) Comparison of the voltage and velocity results implies that high current arcjet operation in the electromagnetic mode without insulator ablation effects at a minimum terminal voltage is achieved for this geometry with a 50:50 flow division.

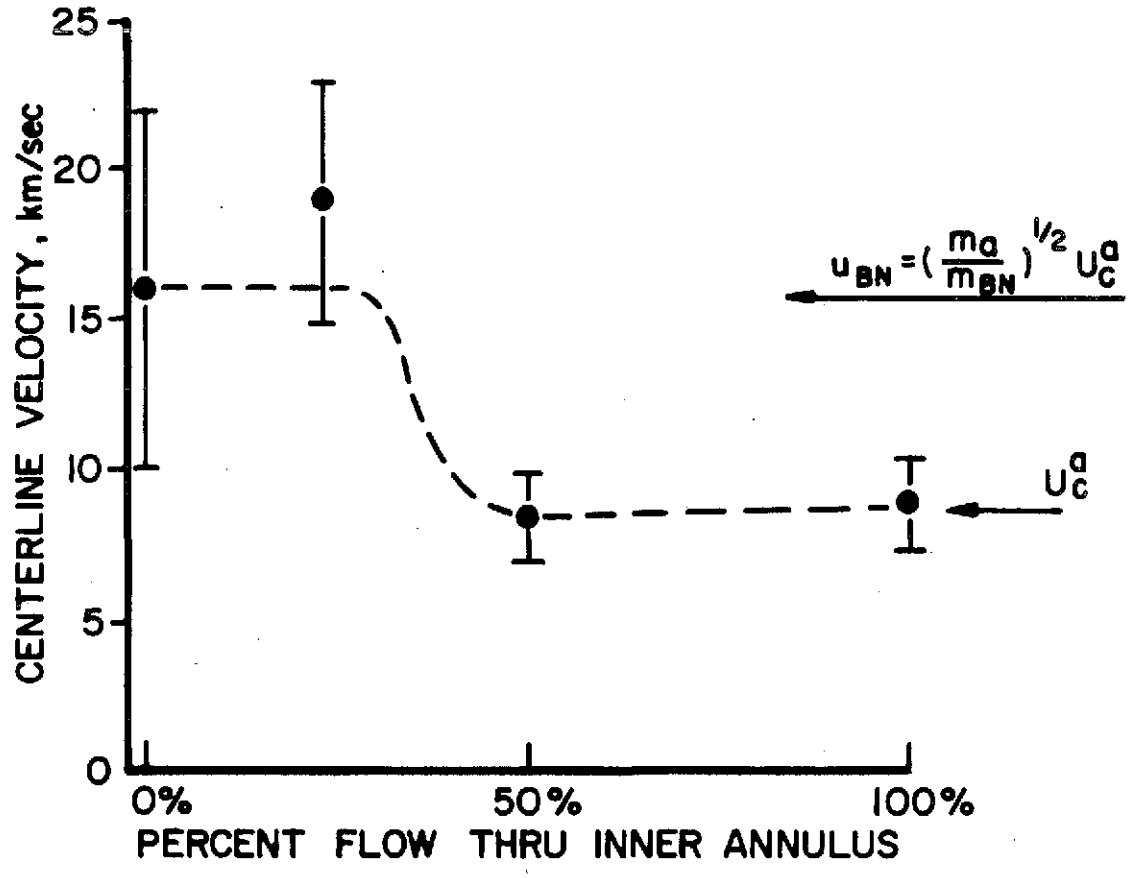

CENTERLINE VELOCITY vs FLOW DIVISION, J = 15.3 kA, $\dot{m}_T$ = 6 g/sec

FIGURE 17
AP25-4971

II-C. Propellant Injection Geometry Effects (Villani)

Sufficient data has been accumulated on the effects of the propellant injection geometry in the MPD discharge to identify certain geometric parameters upon which the arc performance depends sensitively. By varying two such parameters, radial location and injection angle of a single annulus, it has been possible to investigate the effects of propellant starvation on the centerline and at regions of large radius in the discharge chamber, while maintaining constant such macroscopic variables as total mass flow, arc current, and thrust. The effects of propellant starvation are clearly distinguishable through examination of voltage signatures and photographs taken through spectral filters.

Experiments

The experiments were performed in the large Plexiglas vacuum tank by applying a 16.1-kA, 850-μsec-long current pulse to the modular arc head.[143] Argon mass flow was injected by a fast-acting solenoid valve through the rear chamber insulator which served as the propellant distributor.

The various propellant injectors were made of Plexiglas due to its machinability and low cost. Although Plexiglas insulating back plates are known to ablate,[141] this does not interfere with the evaluation of the plates as mass injectors. In fact, the ablating characteristics of Plexiglas have been used to advantage in the photographic portion of this study to identify particular regions of propellant starvation.

Voltage and current as a function of time were monitored on a Tektronix Type 555 dual-beam oscilloscope. Voltage was measured through a Tektronix P6013A 1000 X attenuator attached to the cathode cylinder; current was measured by passive integration of the output of a Rogowski coil wrapped around this same cylinder.

Photographs of certain configurations were taken from the end of the tank on Polaroid type 52 film with a Burlegh Brooks Super Cambo 4 x 5 view camera equipped with a Schneider Tele-Xenar 550 mm telephoto lens. All photographs were taken with a lens setting of f/64, through spectral filters with band-passes centered at 4880 and 5910 Å. The 4880 Å, 10 Å bandwidth filter is transparent to light from singly-ionized argon (AII), and the 5910 Å, 75 Å bandwidth filter transmits light from singly ionized and molecular carbon (CII and C_2). Since the spectral radiant flux in an arc discharge depends both on the number density of a particular species and on the electron temperature, photographic density gradients may be taken as due to either specie density gradients or temperature gradients. A significant difference in luminosity patterns at wavelength bands typical of two different species, however, can be taken with much more confidence to be indicative of a change in relative abundance. Since carbon is a major constituent of the Plexiglas injection stencils used in these experiments, the differences in photographic densities between the argon and carbon photos are used to determine which regions of the discharge are filled with the injected propellant and which are filled with ablation products.

Since the purpose of this injection geometry survey was to specifically seek information on effects which cannot be found in a one-dimensional analysis, two parametric variations were conducted using a single current and mass flow - 16.1 kA and 6 g/sec. Thus, in all cases, the thrust and nominal specific impulse were essentially identical. In the first survey, the shoulder width, which is defined as the radial displacement of the injection annulus from the cathode base, was held constant at 0.31 cm while the propellant injection angle was varied from -16° (flow along the conical cathode surface) to $+90^{\circ}$ (flow outwardly directed along the insulating injector backplate). In

the constant angle survey, data were taken with shoulder widths of 2.46, 1.27, 0.47, 0.24 and 0.0 cm, at an injection angle of $+45^{\circ}$. Voltage-time signatures were recorded for all configurations, and spectral photographs were taken of selected cases.

Voltage Behavior

Typical voltage-time signatures for the constant-shoulder-width survey are shown in Fig. 18. The current is shown on the upper trace of each oscillogram while the voltage, measured with respect to the anode ground, is shown in the lower trace. The traces show that as the injection angle, θ_i, decreases, the voltage becomes larger and considerably more unsteady. This dependence of peak voltage on injection angle is shown in Fig. 19a. A schematic sketch of the arc head defining the parameters "shoulder width" and "injection angle" is also shown in this figure. The graph shows that as the injection angle is decreased below approximately $+20^{\circ}$, i.e. as the inlet flow is directed more downstream and away from the anode, the voltage increases by up to 60% over its minimum value. Since the current is fixed and thus the thrust is approximately constant, this increased voltage directly translates into a similar increase in the power loss mechanisms within the discharge.

Oscillograms and a graph of the voltages for the constant-injection-angle survey are shown in Figs. 20 and 19b. As in the constant-shoulder-width survey, the maximum voltages are plotted. Except for the $w_s = 0.0$ cm data, the voltage shows a monotonic increase as the injection annulus is moved farther from the cathode. The results at $w_s = 0.0$ cm are considered somewhat questionable because the surface of the cathode was employed as the inner wall of the channel in this injection stencil (see Fig. 21). Two data points were obtained, one with this surface uninsulated, Fig. 21b, and one with a thin coat (less than 0.05 cm) of insulation on it, Fig. 21c. The uninsulated cathode voltage was very high, approximately 220 volts,

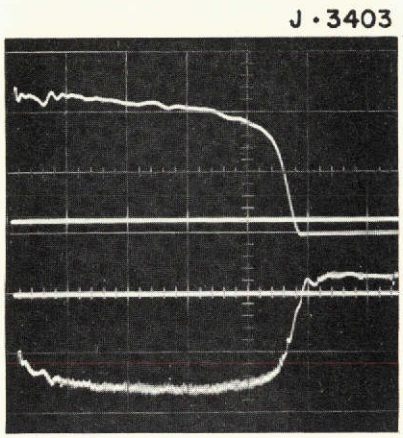

a) $\theta_i = 67.5°$

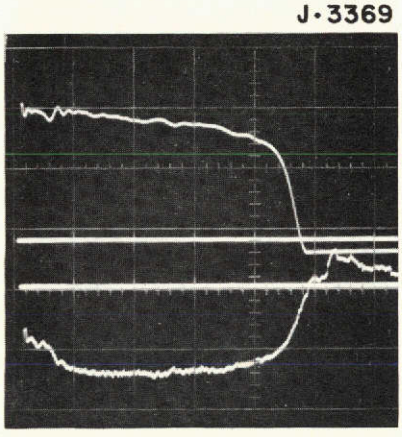

b) $\theta_i = 22.5°$

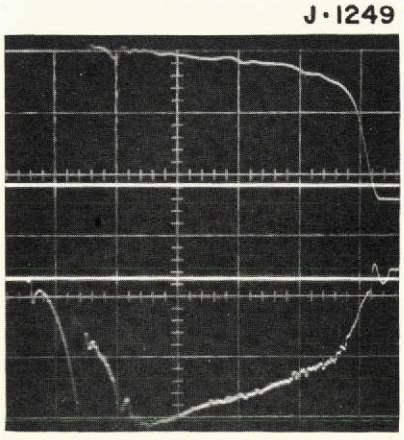

c) $\theta_i = -16°$

VOLTAGE AND CURRENT SIGNATURES
$w_s = 0.31$ cm

FIGURE 18
AP25·P· 430

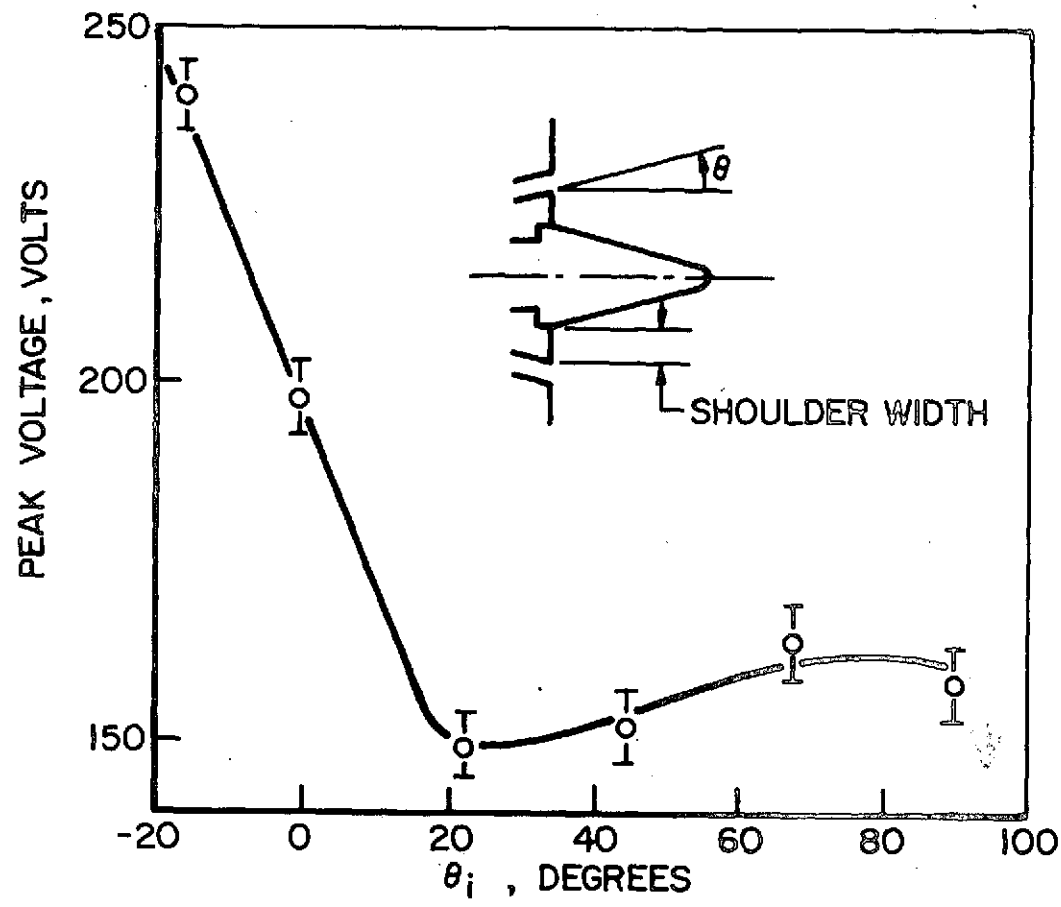

a) w_s = 0.31 cm

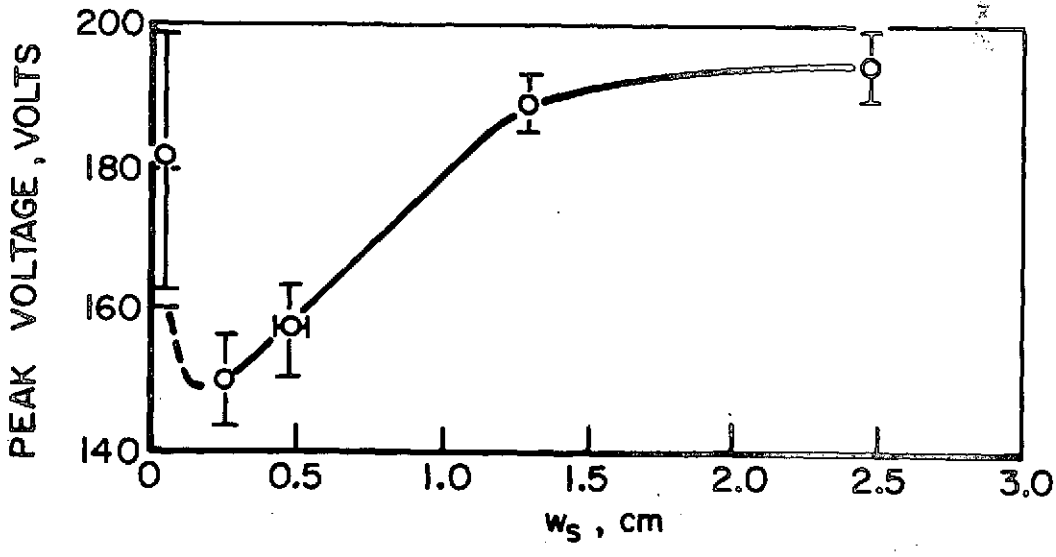

b) θ_i = 45°

VOLTAGE DEPENDENCE ON INJECTION ANGLE θ_i AND SHOULDER WIDTH w_s

FIGURE 19
AP 25 · 4972

J·3451

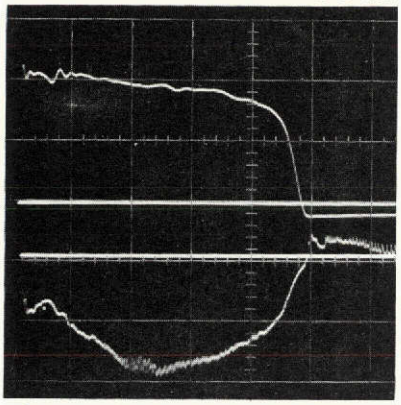

J, 7.7 kA/DIV

V, 100 V/DIV

a) INSULATED, $w_s \approx 0$

J·2886

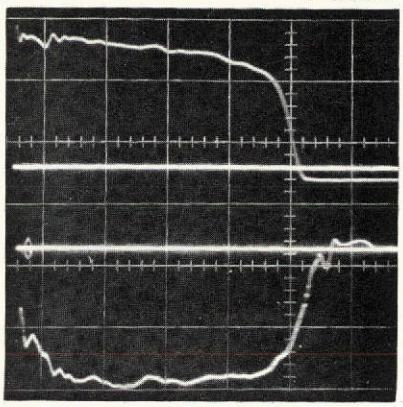

b) UNINSULATED, $w_s = 0$

J·3646

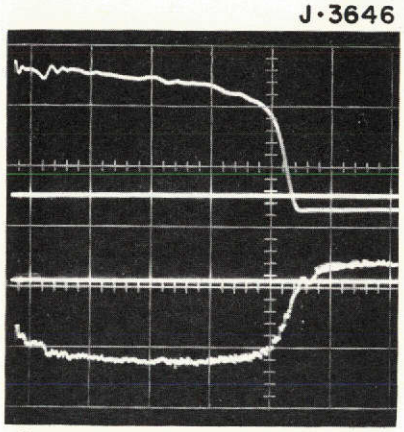

J, 7.7 kA/DIV

V, 100 V/DIV

c) $w_s = 0.24$ cm

J·3294

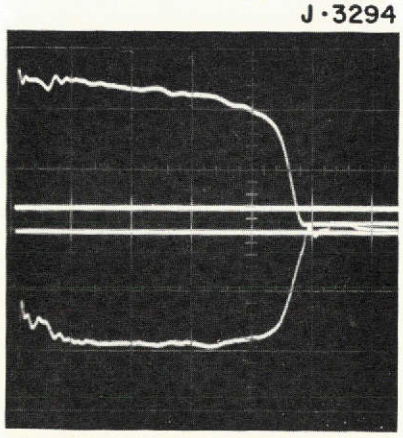

J, 7.7 kA/DIV

V, 100 V/DIV

d) $w_s = 1.27$ cm

VOLTAGE AND CURRENT SIGNATURES
$\theta_i = 45°$

FIGURE 20
AP25·P·429

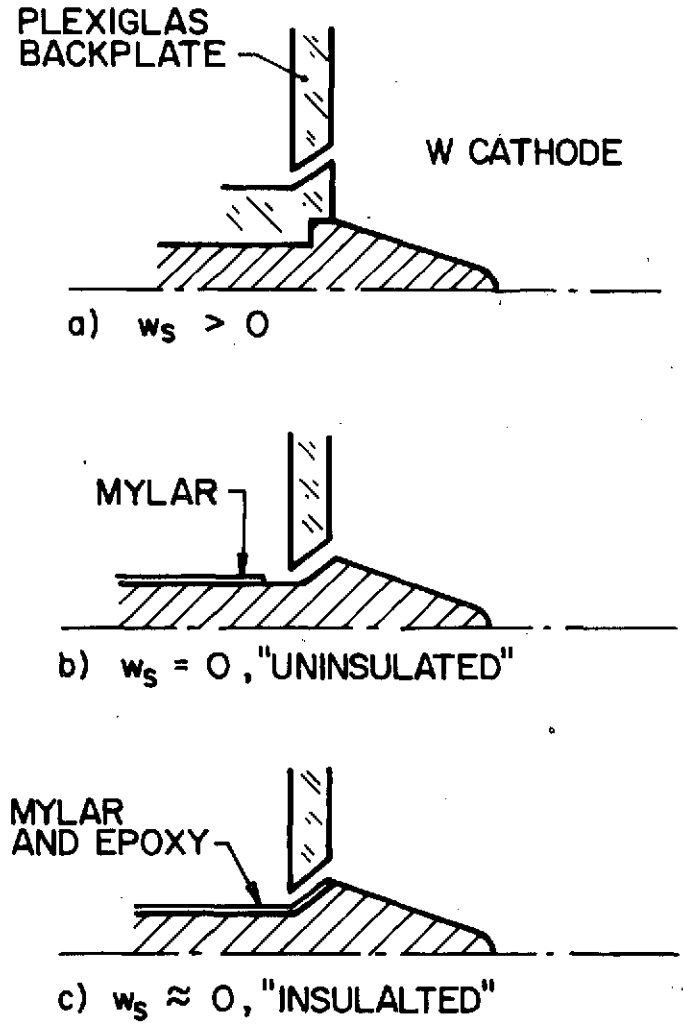

INJECTION ANNULUS CONFIGURATIONS

FIGURE 21
AP25-4973

and there was evidence from the condition of the cathode surface that some arc current was attaching to the cathode surface back inside the channel. Since this current would produce a $\bar{j} \times \bar{B}$ force directed towards the centerline, it was considered likely that in this case the effective turning angle of the injection stencil/cathode combination was much less than 45°. The insulated cathode produced a much lower voltage as expected, although there was a systematic tendency for the later shots to exhibit higher voltages than the earlier shots due to ablation of the thin insulating layer. It is likely that the shots most characteristic of nominal behavior of this configuration are the first few shots taken, which exhibit voltages in the vicinity of 145 volts. The dotted lines in Fig. 19 indicate the uncertainty in the voltage dependence between w_s = 0.0 and 0.24 cm.

Spectral Photographs

End-on spectral photographs of the discharge have been obtained for the constant injection angle ($\theta_i = +45^{\circ}$), varying shoulder width survey. These are shown in Figs. 22a (4880 Å AII filter) and 22b (5910 Å CII and C_2 filter). It can be seen that as the injection annulus is moved to larger radii the argon luminosity becomes more faint and the bright luminous area in the carbon photos increases in size continuously. This trend toward an apparent increase in number density of ablated species in the discharge corresponds to an increase in the terminal voltage, as indicated in Fig. 19b.

The photographs for the insulated and uninsulated no-shoulder injectors (top of Figs. 22a and b) support the discussion of these configurations in the terminal voltage section. The relative densities of the argon photos are such that the "uninsulated" photo is more dense than the "insulated" photo at small radius, even slightly beyond the cathode radius, and

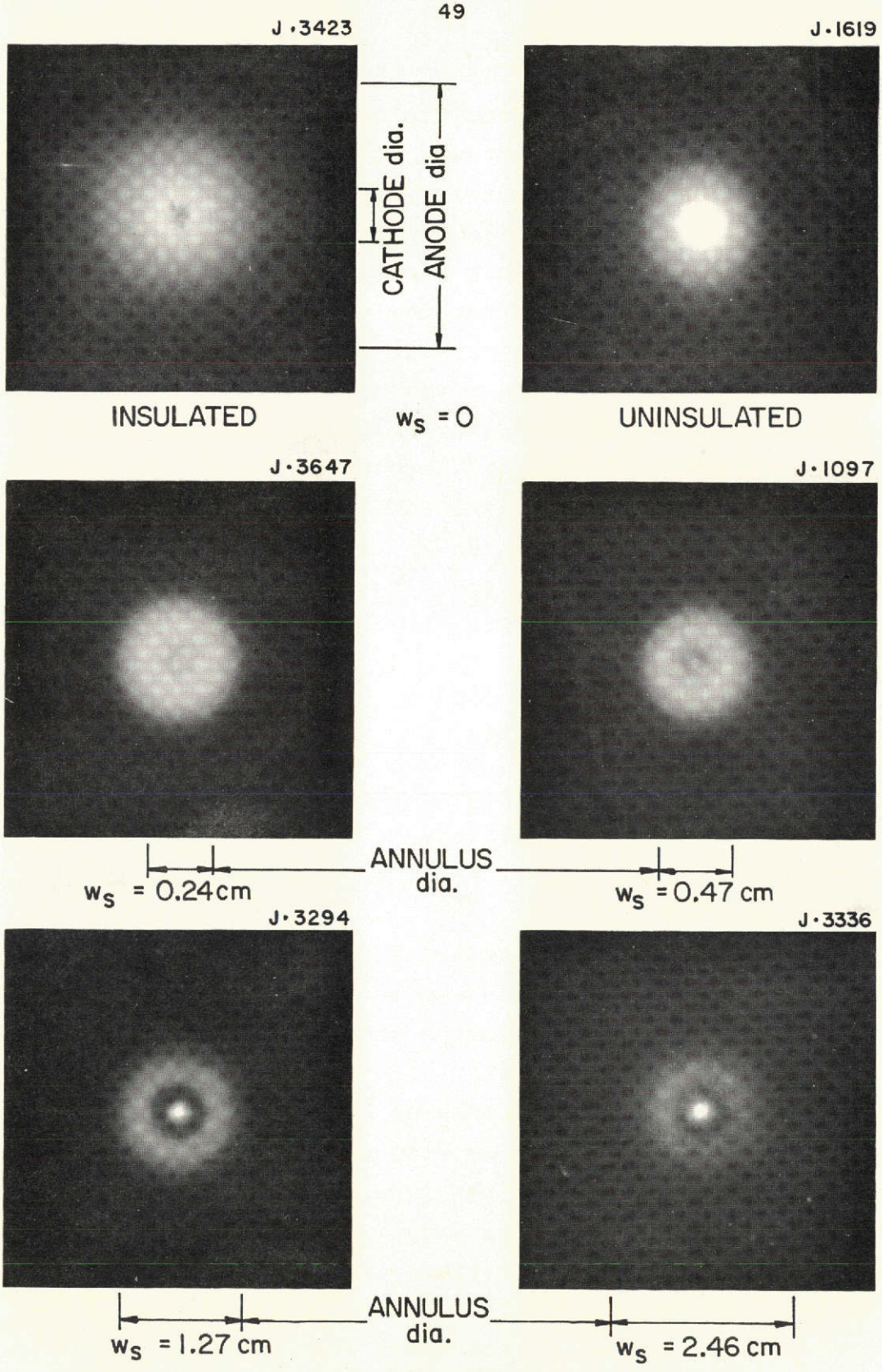

SPECTRAL FILTER PHOTOGRAPHS WITH $\theta_i = 45°$

$\lambda = 4880$ Å - AII

FIGURE 22 a

AP25·P·428

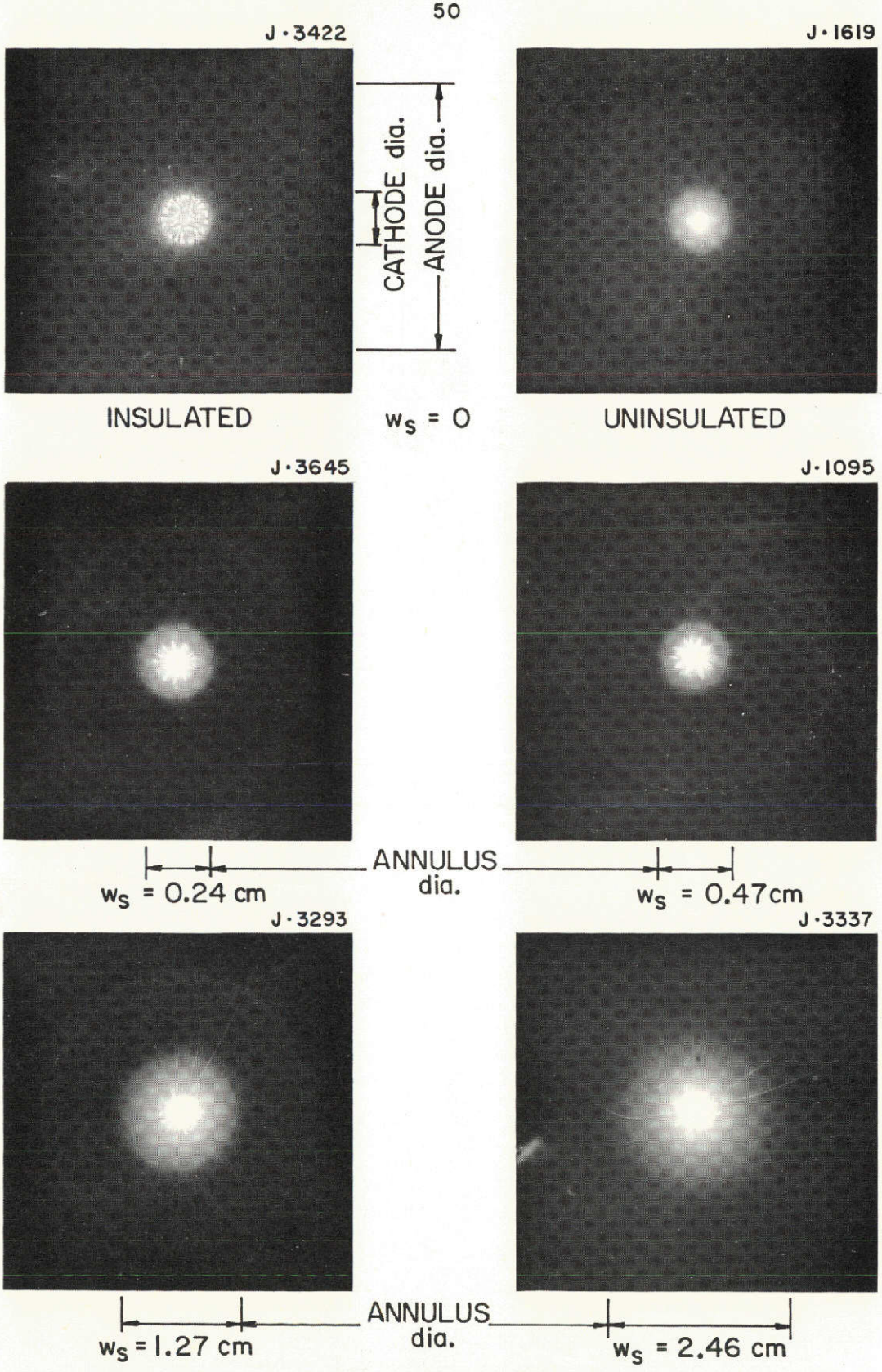

SPECTRAL FILTER PHOTOGRAPHS WITH $\theta_i = 45°$
λ = 5910 Å CII AND C_2

FIGURE 22 b
AP25·P·427

less dense than the insulated photo at large radius. The relative density levels can be explained by a luminosity distribution which is more peaked in the center for the uninsulated configuration. Examination of the corresponding carbon photos (top of Fig. 22b) shows some carbon luminosity in the uninsulated case at large radius, where the argon photo is relatively dark. This luminosity suggests that the temperature is sufficiently high to excite the species present. Thus, the comparison of the photographs suggests a peaking of argon concentration about the centerline supporting the hypothesis that the extension of current back into the channel of the injection annulus affects the distribution of propellant.

Internal Diagnostics

The arc voltage is ultimately the result of the E-field produced in the arc in response to an interrelated pattern of local current density, plasma state, transport properties and the interaction between flow velocity and magnetic field. Knowledge of the potential and current distributions in the arc can provide answers to questions such as: Does the increased voltage for some injectors appear as additional "electrode falls" or does it arise in the body of the plasma? Do the additional potential drops appear in the same region as propellant mass starvation, with the latter indicated by the spectral photos, or are the loss mechanisms nonlocal in nature? Is the current pattern, and thus the force field perturbed significantly by the changes in the propellant distribution?

To answer these questions, a survey has been made of the patterns of enclosed current and floating potential in the discharge for two $\theta_i = 45^o$ configurations: the $w_s = 0.47$ cm case V = 160 volts) and the $w_s = 0.0$ cm, uninsulated case (V = 220 volts). Enclosed current contours are obtained by taking

advantage of the simple axisymmetric geometry in that Maxwell's equation $\nabla \times \bar{B} = \mu_o \bar{j}$ integrates to

$$|B| = \frac{\mu_o J_{enclosed}}{2\pi r}. \qquad (8)$$

B is measured by inserting a 0.5-cm-diameter, 8-turn coil at the desired point in the chamber, whose output voltage is proportional to $\frac{dB}{dt}$. This is passively integrated, and the output of the integrator, which is proportional to B, is displayed on an oscilloscope.

Floating potential is measured by exposing the tip of a small length of insulated wire to the plasma at the desired position. The wire is then connected to ground through a high impedance, usually a Tektronix P6013A attenuator, and its potential displayed on an oscilloscope.

Initial results of the current and potential surveys are shown in Fig. 23. Although the data reduction will be extended to extract local values of current density, j, local body forces $\bar{j} \times \bar{B}$, local total power input $\bar{E} \cdot \bar{j}$, and local ohmic heating j^2/σ, some initial conclusions can be drawn from the data in its relatively unprocessed form.

Since the cross sections in Fig. 23 represent axisymmetric distributions, each region defined by the space between two adjacent equipotential lines and two adjacent enclosed current contours actually corresponds to a quasi-toroidal volume of space. For equal areas on the figure, the associated volume is proportional to the distance from the centerline. Furthermore, since the interval between all adjacent equipotentials is a constant 2 V and the interval between adjacent current streamlines is a constant 2 kA, the same amount of power, 40 kW, is being deposited in each volume so defined. It follows that for a constant radial position, the power deposition per unit volume is simply inversely proportional to the area of the "power quadrilateral" at that point.

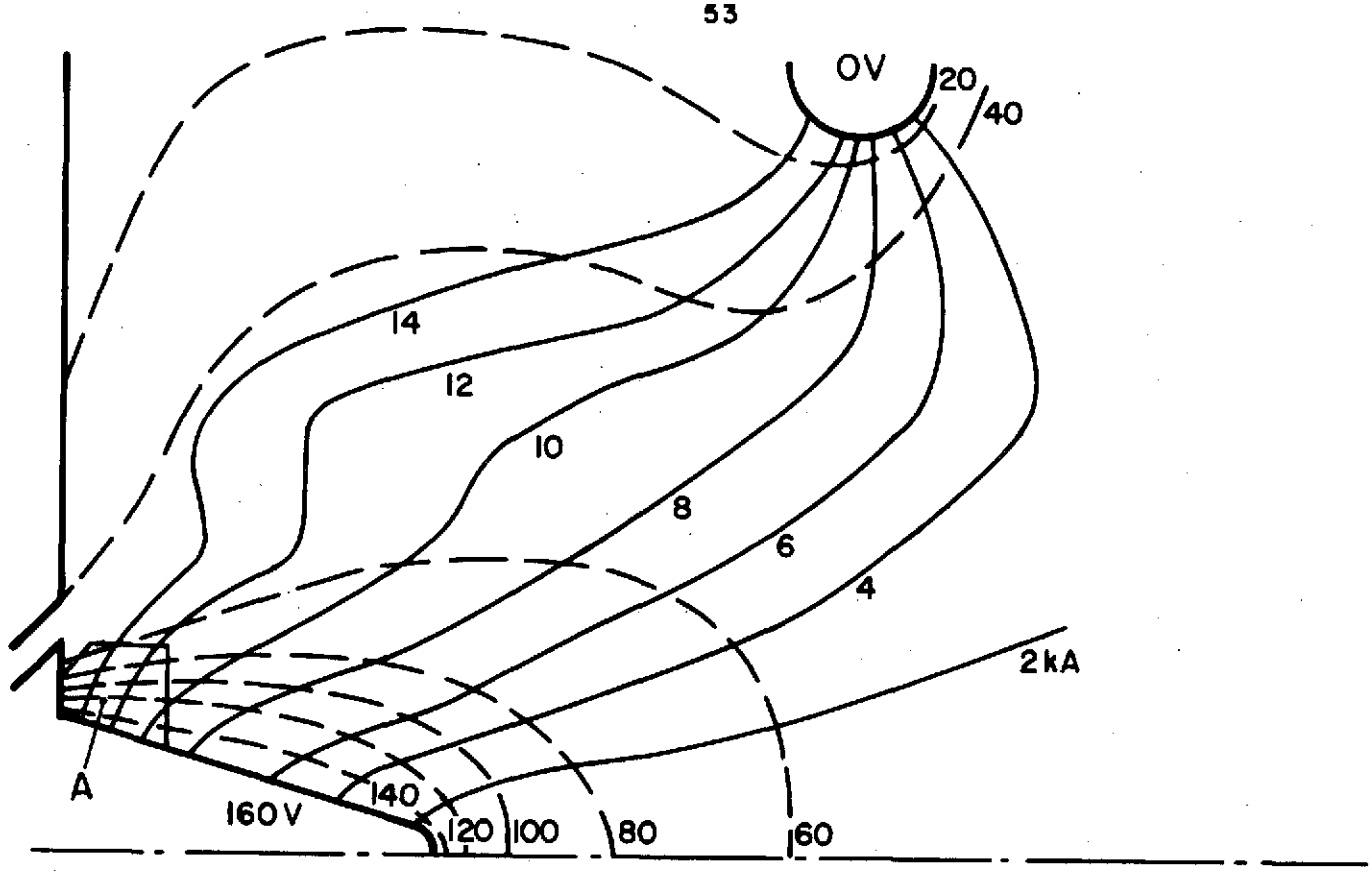

a) $\theta_i = 45°$, $w_s = 0.47$ cm

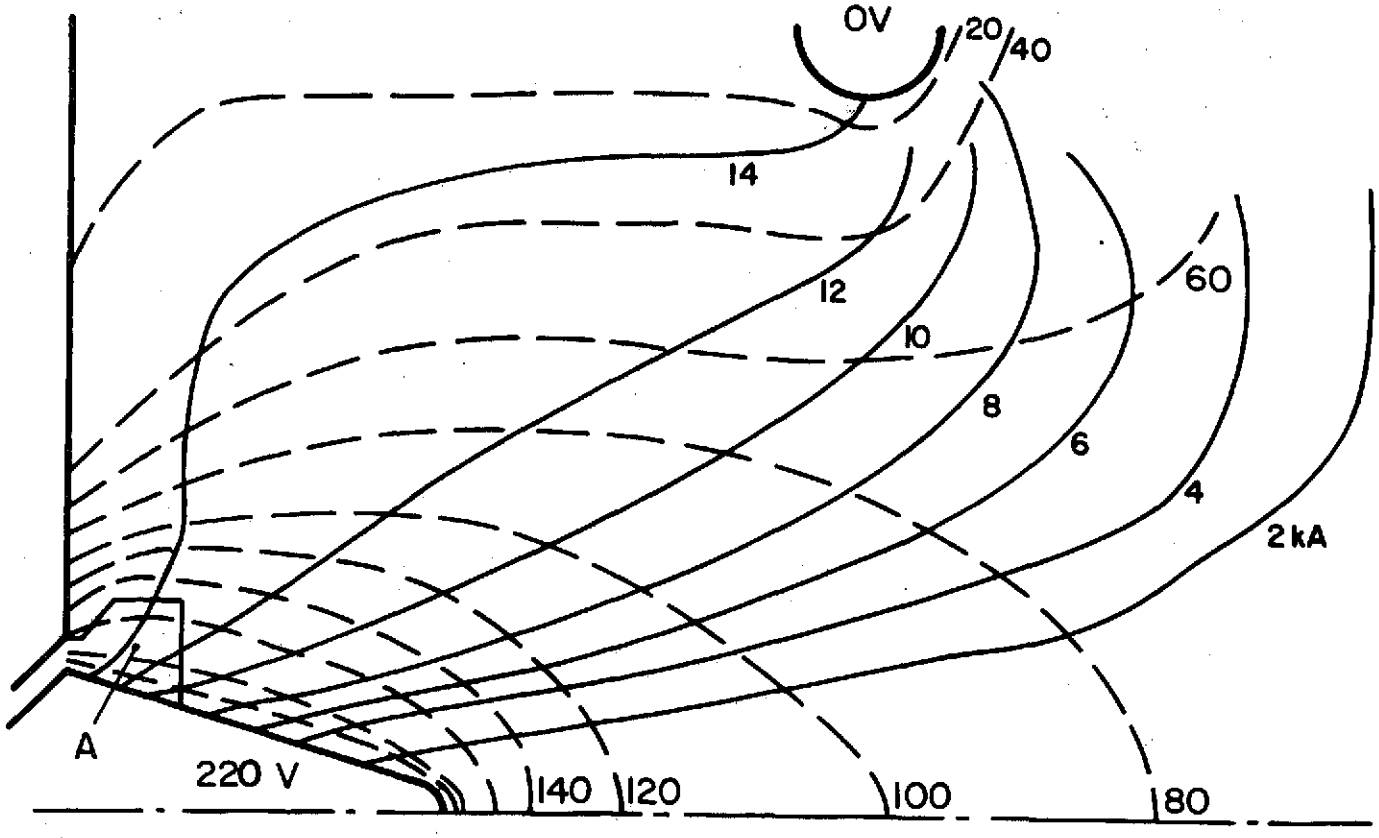

b) $\theta_i = 45°$, $w_s = 0$, UNINSULATED

CURRENT AND POTENTIAL CONTOURS
16.1 kA x 6 g/sec

FIGURE 23
AP25-4974

Examination of the contours shows that the power density in the region marked (A) of the $w_s = 0.47$ cm configuration, Fig. 23a, is approximately twice that of the same region in the $w_s = 0$ configuration, Fig. 23b. This is the region which, according to the spectral photographs shown in Fig. 22, is most highly starved for this configuration. However, since the total power is much greater for the $w_s = 0$ configuration (3.6 MW for $w_s = 0$ vs 2.5 MW for $w_s = 0.47$ cm), the power density at other locations in the chamber must be much higher for the $w_s = 0$ case to make up the difference. Examination confirms this: the power density at both large and small radii in the downstream half of the arc chamber is approximately 50% to 100% higher for the $w_s = 0$ configuration than for the $w_s = 0.47$ cm case.

This in itself gives us some insight into the physical processes involved in the energy losses. The Maecker expression for thrust, Eq. (3), has been shown to have a high degree of validity in the operating regime of this device. The thrust equation involves only total current and electrode geometry; it does not involve total mass flow, much less injected mass distribution. Thus, for fixed injected mass flow, electrode geometry, and total current, an arc running at higher power must be considered to be running at lower efficiency, indicating the activation of some loss mechanism. The fact that the excess power between the two cases shown here appears in a region far from any electrodes (i.e. downstream half of chamber, intermediate and small radii) shows that the loss mechanisms are due to phenomena occurring in the body of the plasma rather than to phenomena associated with the plasma-electrode interface. Furthermore, exhaust plume measurements on a similar device have shown profile and divergence losses to be each approximately 20% of the total directed kinetic energy (0.16 MW and 0.17 MW respectively);[138] it is therefore highly unlikely that increases

in these components of the power balance can account for the 1 MW difference between the two configurations shown here. The conclusion is that the excess losses of the $w_s = 0$ configuration must appear as either multiple ionization, thermal energy, or radiation.

Physical Processes

The ultimate goal of this research is an understanding of the physical mechanisms responsible for impeding the current flow in the arcjet and causing high voltages, with the subsequent aim of reducing them to a minimum. Aside from electrode phenomena, which are the subject of other research programs in this laboratory, the likely candidate phenomena are increased plasma resistivity, Hall parameter effects, or $\bar{v} \times \bar{B}$ back EMF. Since the latter two are non-dissipative, they must induce additional phenomena if they are to cause an increase in arc power without a corresponding increase in thrust.

An example of this can be found in the current-potential contours shown in Fig. 23. It can be shown that the power density in a conducting fluid, $\bar{j} \cdot \bar{E}$, can be broken up into two terms:

$$\bar{j} \cdot \bar{E} \equiv \bar{v} \cdot \bar{j} \times \bar{B} + \eta j^2 \qquad (9)$$

where η is the scalar resistivity of the plasma.

The term $\bar{v} \cdot \bar{j} \times \bar{B}$ is simply the power being deposited in directed kinetic energy of the local plasma by the local $\bar{j} \times \bar{B}$ force. The term ηj^2 is the local ohmic heating. While it is true that a given element of plasma traversing the entire arc chamber may have some of its directed kinetic energy thermalized due to passage through high-Mach-number shocks, and some of its thermal energy converted into directed kinetic energy by expansion due to a magnetic nozzle effect, it seems reasonable to expect that an arc in which the integral of ηj^2 throughout

the chamber volume is large compared with the integral of the $\bar{v} \cdot \bar{j} \times \bar{B}$ term will have greater losses than one in which the relative values of these integrals are reversed. Without invoking any major changes in σ, it is possible to examine the differences between the two configurations shown in terms of the quantity $\int_{\mathcal{V}} j^2 d\mathcal{V}$, where $\mathcal{V}$ is the chamber volume.

The current streamlines for the $w_s = 0$ configuration, Fig. 23b, are distended downstream considerably more than those for $w_s = 0.47$ cm in Fig. 23a, even near the cathode where the arc with $w_s = 0$ could be expected to operate in a medium with sufficient charge carriers. This is an example of the possible non-local effects of a local mass starvation; the current streamlines are forced to spread out axially to traverse the "starved" jacket region, and the current in the core region is then forced to flow further downstream in order to secure current-continuity between the two regions. At first it may appear that the $w_s = 0$ current pattern is more diffuse than the $w_s = 0.47$ cm pattern due to its greater axial extent. However, the quantity j^2 is equal to $(\nabla J_{enclosed})^2/(2\pi r)^2$ and because of the $1/r^2$ dependence, the region within one cathode radius of the centerline is found to comprise most of the integral. In this region, it is obvious from the closely spaced current streamlines that j^2 is considerably higher in the $w_s = 0$ configuration.

Preliminary calculations of the integral in the two cases shown indicate that the ratio of the quantity $\int_{\mathcal{V}} j^2 d\mathcal{V}$ between the $w_s = 0$ and $w_s = 0.47$ configurations is approximately 1.6. By comparison the ratio of total power between the two configurations is approximately 1.4. The ratio of directed kinetic energy between the two is not yet known.

Although neither the experimental program nor the data analysis is yet complete, it can be seen from the above that a model is emerging which can account for some variations in "ohmic" losses for different injection configurations despite the fact

that the plasma resistivity itself depends only logarithmically on density. In the case of "jacket" starvation, it appears likely that some effect in the jacket impedes the current flow at large radius, forcing the pattern to distend downstream and causing an increase in axial current density and ηj^2 at small radius.

III. HOLLOW CATHODE DISCHARGES (Krishnan)

During the past several years, hollow cathodes have replaced more conventional electron emitters in advanced ion engine thrusters due to their demonstrated lower specific heating power, decreased erosion, and improved discharge stability.[A-16] Despite these advantages, hollow cathode deterioration after several thousand hours of operation is one of the principal causes of reduced ion thruster system lifetime and reliability.[A-17] A diagnostic study of the interior plasma, which is clearly necessary in order to understand hollow cathode operation and ultimately to reduce its long term wear characteristics to a tolerable level, has been precluded up to now by the small dimensions of these cathodes. As a consequence, only a few detailed analyses of the physical processes inside the cathode cavity have been attempted and even empirical scaling laws and scaling parameters for these cathodes have not yet been well established.[A-18]

In the present program at this laboratory, a much larger hollow cathode has been incorporated in a high current, quasi-steady MPD discharge. Once characteristic hollow cathode operation is established in this configuration, the larger cavity in the quasi-steady discharge will allow detailed study of the interior emission and ionization processes. In this way it should be possible to determine 1.) whether the same advantages found in ion engine hollow cathodes prevail at these higher currents and 2.) the nature and extent of scaling laws for characteristic hollow cathode operation.

The previous semi-annual report described in detail the quasi-steady hollow cathode apparatus, its calibration, and the results of early experiments in which the terminal properties and discharge luminosity were recorded over a wide range of currents, mass flows, and flow division between cathode and

chamber injectors.[146] The most interesting results were obtained at high current (29 kA) and low mass flow (0.3 g/sec) through the cathode only. In this case, bright argon radiance was observed emanating from within the hollow cathode suggesting that a significant fraction of the input current is attaching inside the cavity.

In order to determine the fraction of the total current emitted from the cathode interior, the magnetic field distribution in and around the cathode was measured using a 0.1-cm-diameter magnetic field coil in a thin glass tube to insulate it from the plasma. Figure 24 is a sketch of the enclosed current contours within and near the hollow cathode for this 29 kA, 0.3 g/sec operating condition. Almost all of the input current attaches either on the face or on the external surface of the tungsten cathode, with at most 800 amperes inside the cavity. Raising the mass flow to 6 g/sec or decreasing it to 0.04 g/sec at the same current had a marginal effect on this distribution, the maximum of 1.3 kA inside current observed at the lowest mass flow.

To force more of the current inside the cavity, the outer cylindrical cathode surface, which carries approximately one-half of the total current, was insulated with a nylon tube. This cathode configuration is shown in Fig. 25b compared to the uninsulated version in Fig. 25a. Magnetic probe measurements, however, showed that the same small fraction of the total current attached in the cavity as with the uninsulated cathode, while the cathode face now carried the balance of the current.

The insulation of the outer electrode surface was therefore extended to include the cathode face and the downstream section of the cavity surface. This configuration, shown schematically in Fig. 25c, forces the current to attach inside the 20-mm-long cavity, still permitting diagnostic access through the 9.4-mm-diameter by 19-mm-long insulated channel.

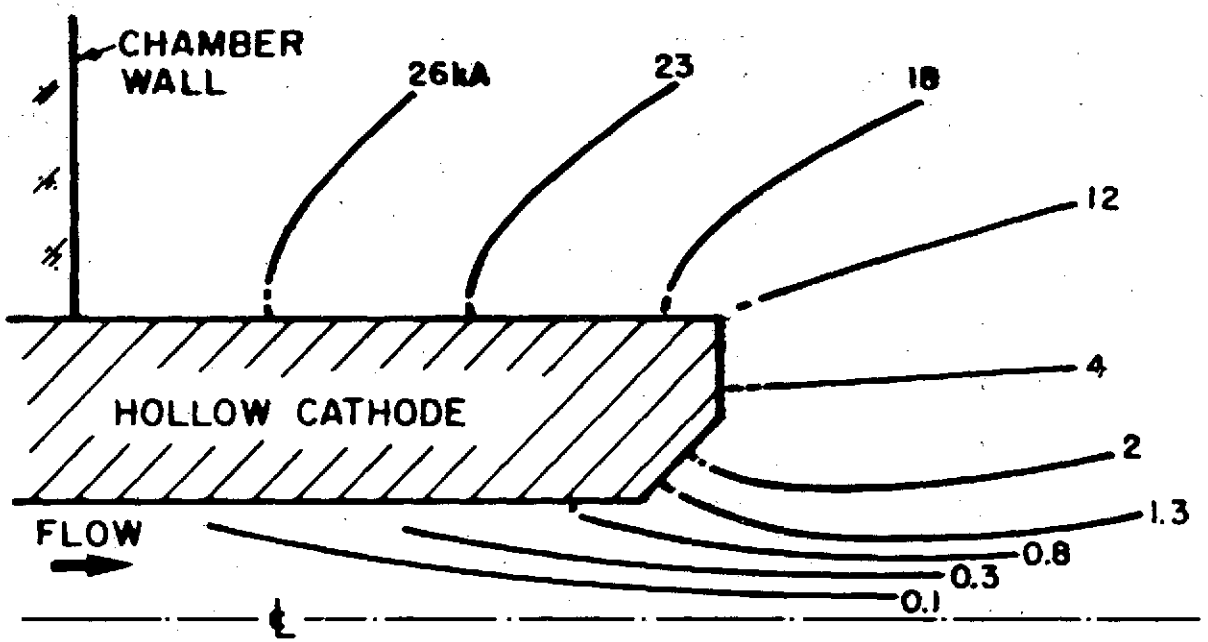

ENCLOSED CURRENT CONTOURS; $\dot{m} = 0.3$ g/sec

FIGURE 24
AP25-4939

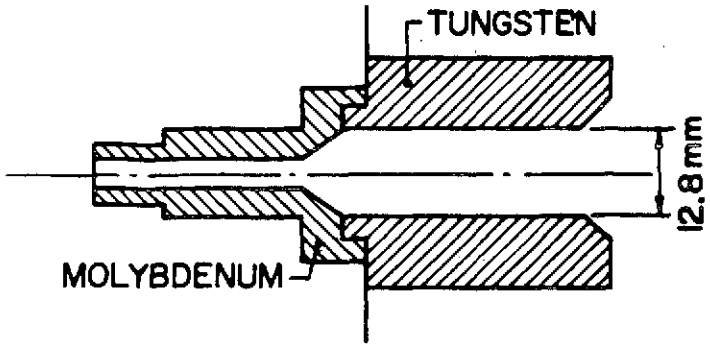

a) UNINSULATED CATHODE

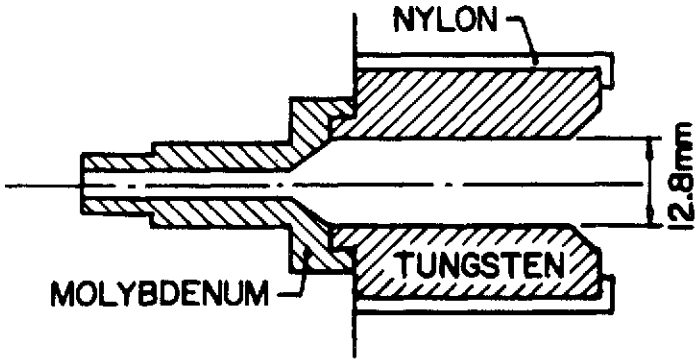

b) PARTIALLY INSULATED CATHODE

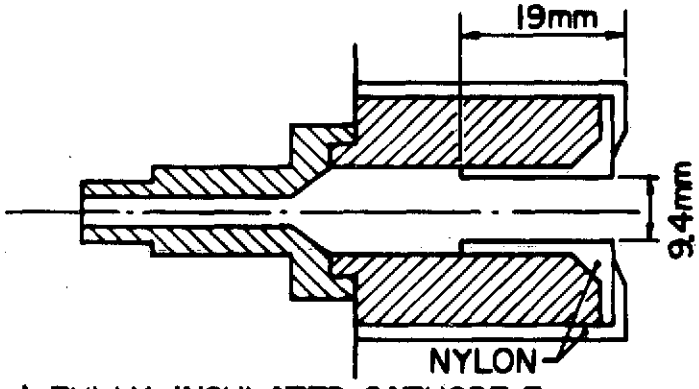

c) FULLY INSULATED CATHODE I

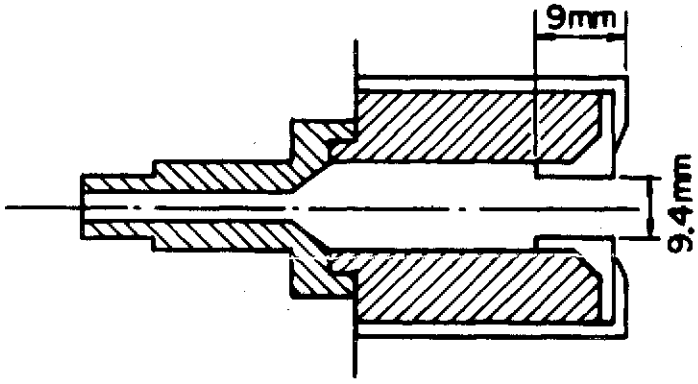

d) FULLY INSULATED CATHODE II

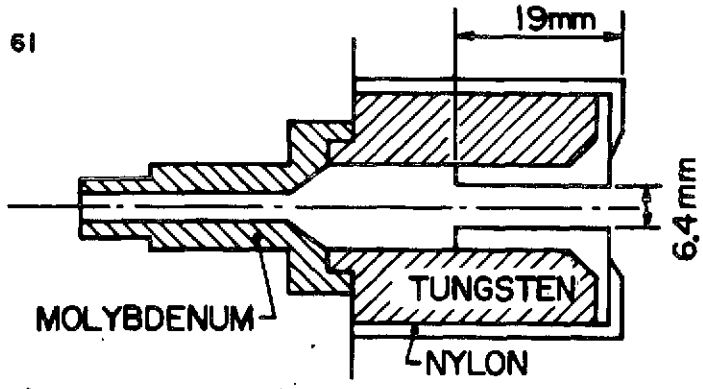

e) FULLY INSULATED CATHODE III

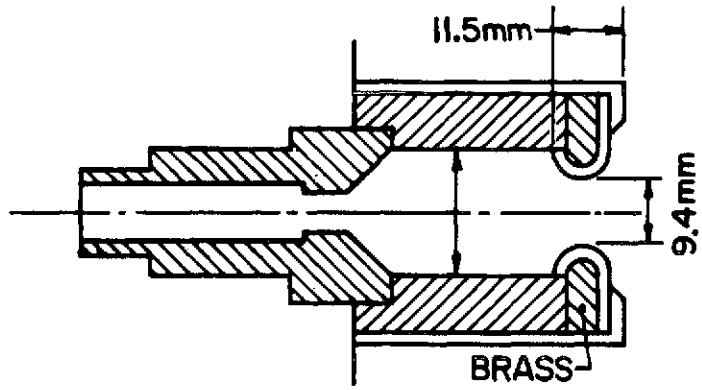

f) FULLY INNSULATED CATHODE IV

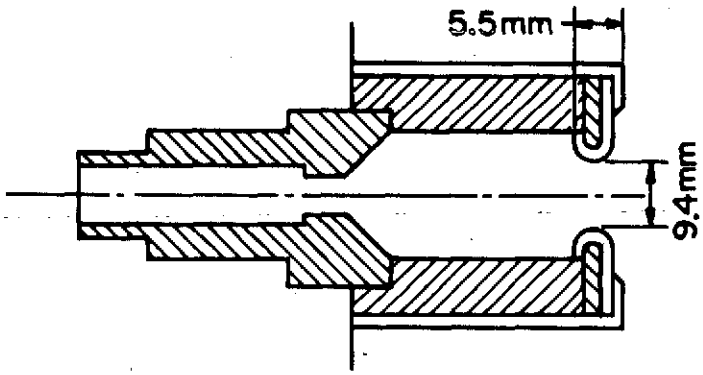

g) FULLY INSULATED CATHODE V

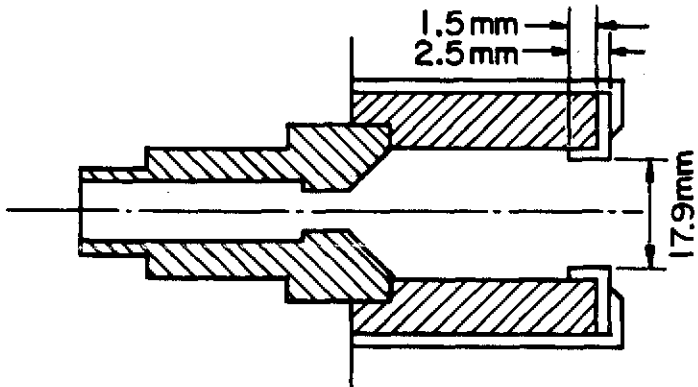

h) FULLY INSULATED CATHODE VI

HOLLOW CATHODE CONFIGURATIONS

FIGURE 25

AP25-4975

For this insulated cathode, the current distribution was determined by translating the magnetic probe axially from the insulated channel upstream to the end of the cavity at a fixed radius of 2.4 mm. The measured enclosed currents, shown normalized with respect to the value at the upstream end of the channel insulator, are plotted in Fig. 26 for a current of 7 kA and mass flows of 0.4 and 4.0 g/sec. The cathode and its insulator are shown for comparison on this and later figures. For the $\dot{m}$ = 4.0 g/sec condition, the steep gradient of enclosed current over the first 11 mm of the cavity indicates that 90% of the current attaches over this length. This in turn implies a current density at the wall of 1300 A/cm^2, which is considerably higher than the current density for hollow cathodes in ion engines. For $\dot{m}$ = 0.4 g/sec the current distribution is seen to extend somewhat further upstream. Thus, for this range of mass flows, most of the current attaches over a relatively short region at the front of the cavity.

In order to explore the profiles of the potential over the same regions for which the enclosed currents were measured, a single floating-potential Langmuir probe was used. It consists of an insulated 0.25-mm-diameter tungsten wire, of which only the front 3 mm is exposed, and which is connected to an oscilloscope through a Tektronix P-6013A voltage probe. The floating potentials, which in all cases were steady and reproducible, were measured relative to the anode ground so that voltages relative to the cathode had to be reduced from the separately measured terminal voltage.

In a potential survey it is the plasma potential which is of principal interest rather than the floating potential. However, the correction term to be applied, usually of the order of a few volts, includes the electron temperature which

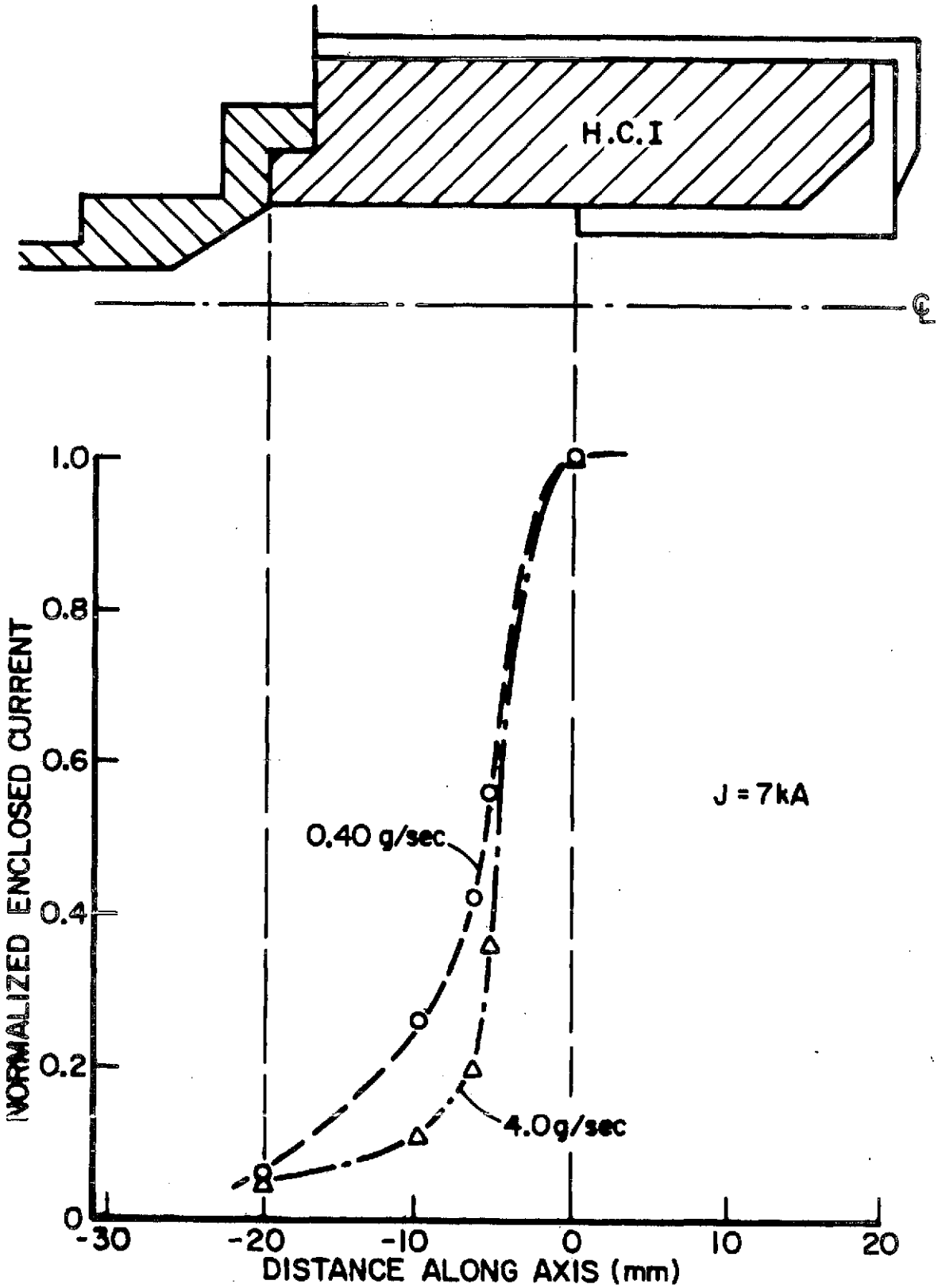

ENCLOSED CURRENT IN HOLLOW CATHODE I

FIGURE 26
AP25·4976

has not yet been measured for these operating conditions. Consequently, the values displayed in the following figures are floating potentials relative to the cathode and thus represent the minimum voltage difference between cathode and probe location. In Fig. 27 the relative floating potentials along the cathode axis are presented for the $J = 7$ kA, $\dot{m} = 4.0$ and 0.4 g/sec operating conditions. For the $\dot{m} = 0.4$ g/sec condition, there exists a plateau in the potential over the front 11 mm of the cavity, exactly where most of the current attaches (Fig. 26). Similarly, for $\dot{m} = 4.0$ g/sec, a plateau is detected over the first 6 mm of the cavity, again the region of primary current attachment. These relatively field-free potential plateaus (less than 8 V/cm) may indicate the presence of an electron trapping mechanism, which has been proposed for lower current hollow cathode operation.

A second interesting feature of the potential profiles is the very steep gradient connecting the interior cavity plasma with the outer discharge. The large electric field associated with this gradient (approximately 100 V/cm) may reflect a low conductivity in the outer plasma between cathode and anode, where there is no injected argon, or it may in fact be the field necessary to conduct the 7 kA current through the long, small-diameter insulating channel. In either case the field is undesirable because it causes a large power deposition in this region.

The first hypothesis was negated by measuring the centerline potential profile for a case where the flow was split into a 4 g/sec inside flow and a 4 g/sec outside chamber flow. For this running condition, the terminal voltage is virtually unchanged and the potential profile through the insulator channel, as shown by the solid square data points in Fig. 27, closely follows that for the case of 4.0 g/sec mass flow injected solely through the cathode. However, it should be noted

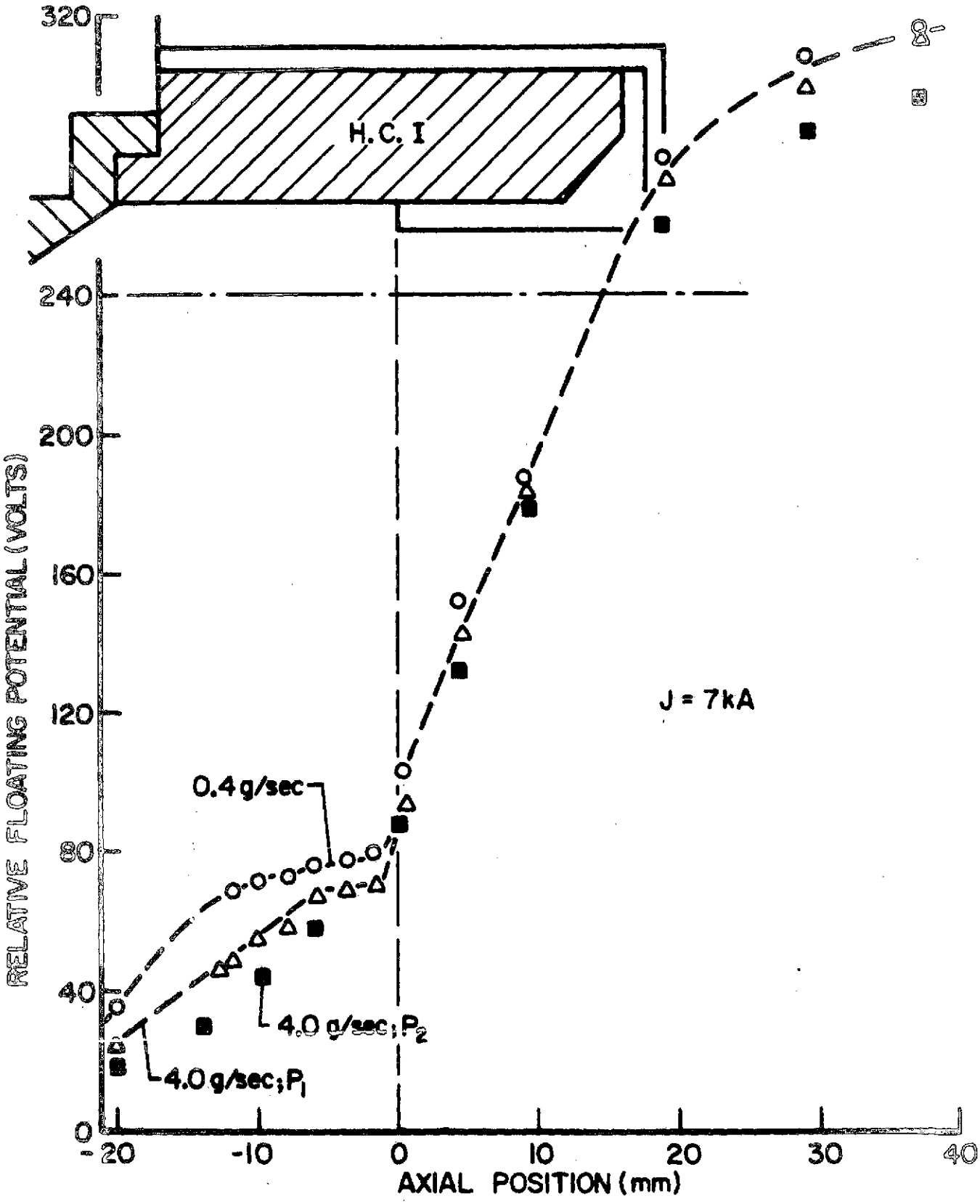

FLOATING POTENTIAL IN CATHODE I

FIGURE 27
AP25-4977

that the potential plateau inside the cavity has disappeared. It may be speculated that the loss of the plateau is related to a decreased excitation or ionization mean free path within the cavity caused in turn by the higher pressure, p_2, and different orifice sizes necessary to split the flow.

Since the large field is apparently caused by the restrictive insulating channel, two alternative insulators were installed to determine whether the length or diameter is responsible. One of these configurations consisted of a shorter insulator of the same inner diameter as the original (cathode II, Fig. 25d), while the second was of the same length but smaller diameter (cathode III, Fig. 25e).

The profiles of floating potential and enclosed current for the short insulator configuration at a current of 7 kA and mass flows of 4.0 and 0.4 g/sec are shown in Figs. 28 and 29. In Fig. 28, the potential profiles are compared with the corresponding profiles for the long channel hollow cathode configuration. The voltage gradient in the short insulated channel is approximately 100 volts/cm as in the longer channel, but it prevails now over only one-half of the previous channel length and thus accounts for a smaller potential drop of only 100 volts. This change is reflected in the terminal voltage which decreases from 375 V to 250 V for $\dot{m}$ = 4.0 g/sec and from 395 V to 290 V for $\dot{m}$ = 0.4 g/sec.

A further interesting difference in the profiles is that the lower portion of the steep gradient now extends approximately 0.5 cm into the cavity where it joins a potential plateau at 30 volts which extends from 0.6 cm to 1.7 cm further upstream. It should be noted that the latter is approximately 50 volts below the potential of the plateaus in the long channel configuration, and that it begins and extends considerably further upstream. This may be due to the divergence of the equipotentials around the chamfer on the face of the tungsten electrode.

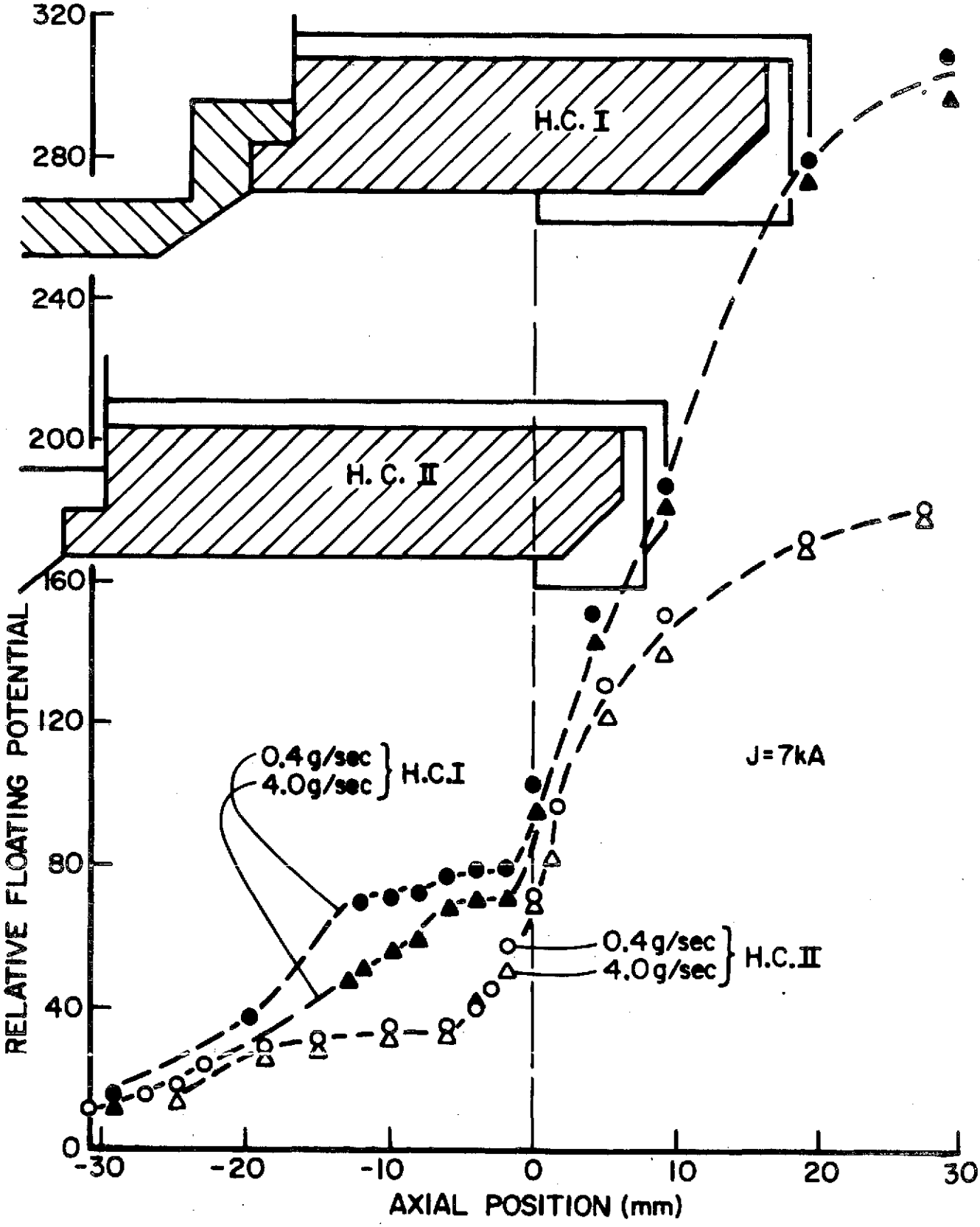

FLOATING POTENTIAL IN CATHODE I AND II

FIGURE 28
AP25-4978

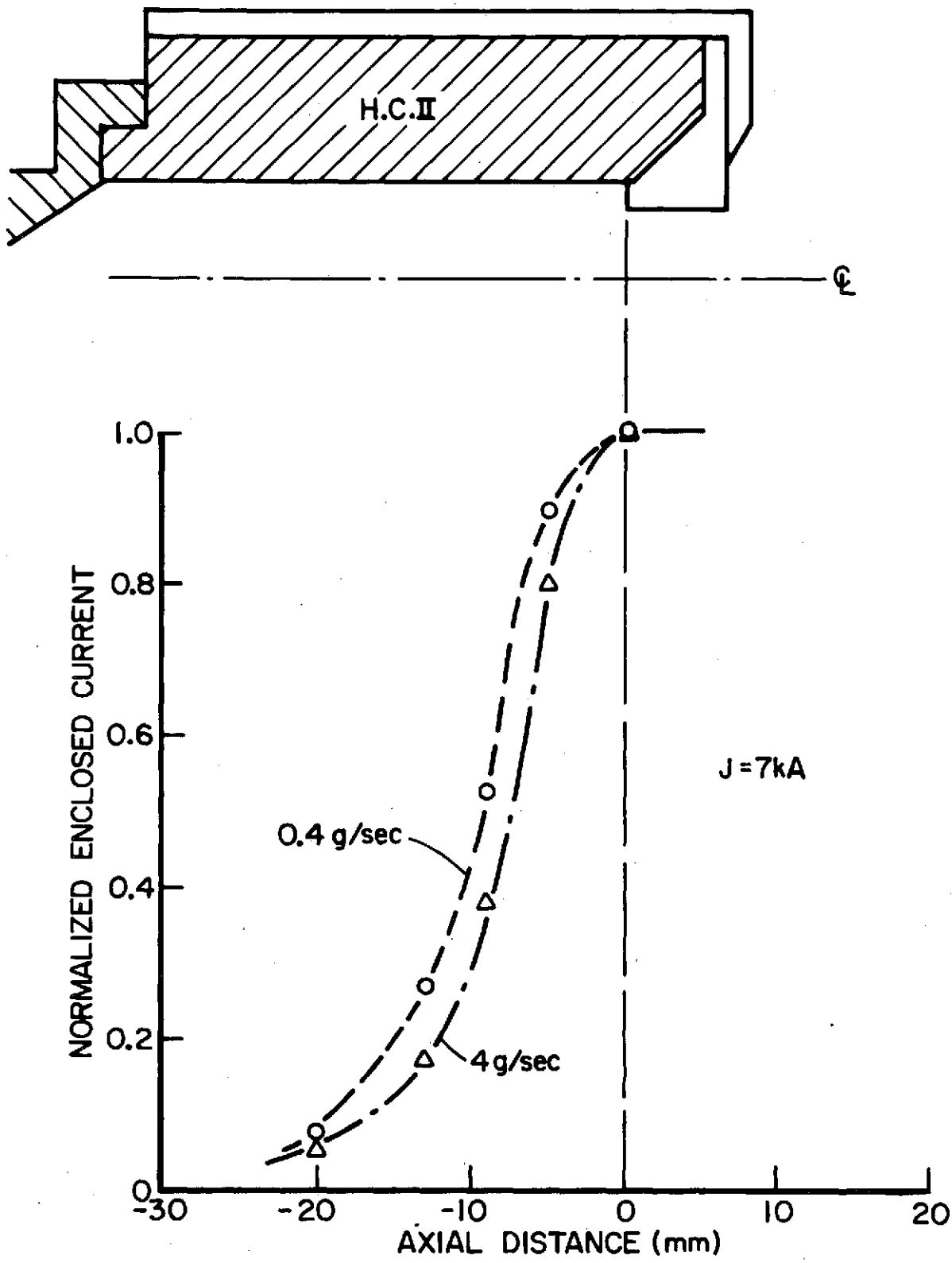

ENCLOSED CURRENT IN CATHODE II

FIGURE 29
AP25-4979

An inspection of the current distribution for the same mass flows in the short channel configuration, Fig. 29, shows that about 70% of the current at 4.0 g/sec and 80% of the current at 0.4 g/sec still attaches in that portion of the cavity where the potential plateau is observed. Thus, it can be stated that over a limited range of conditions, both cathode configurations exhibit current densities on the cavity wall of approximately 1500 A/cm^2 coexistent with axial potential plateaus of less than 10 V/cm.

The potential profile for the long channel with the smallest diameter hole (cathode III, Fig. 25e) is considerably steeper in the insulator region (150 V/cm as compared to 100 V/cm previously), resulting in a terminal voltage of 510 V for the 7 kA, 4.0 g/sec condition. Thus, comparing the voltage gradients of cathodes I, II and III, it appears that the electric field along the insulator channel is determined primarily by the channel diameter. It follows that the total voltage drop through the channel is then established by the channel length.

To obtain further information on the physical processes in the hollow cathode a few near infrared spectrograms of the discharge were recorded. This spectral region contains a number of strong neutral argon lines which are more readily identifiable than those in the visible portion of the spectrum, since the latter tend to be dominated by ionized argon and impurity lines. Figure 30 compares the spectral interval from 6500 Å to 8600 Å for the uninsulated hollow cathode in the 29 kA, 0.3 g/sec argon discharge with that for the fully insulated hollow cathode I at $J = 7$ kA and $\dot{m} = 0.4$ g/sec. Both spectrograms were recorded looking upstream, directly into the cavity along the axis. However, in the case of the uninsulated cathode at the 29 kA, 0.3 g/sec condition (Fig. 30a), there existed a radiant region immediately downstream of the cathode orifice

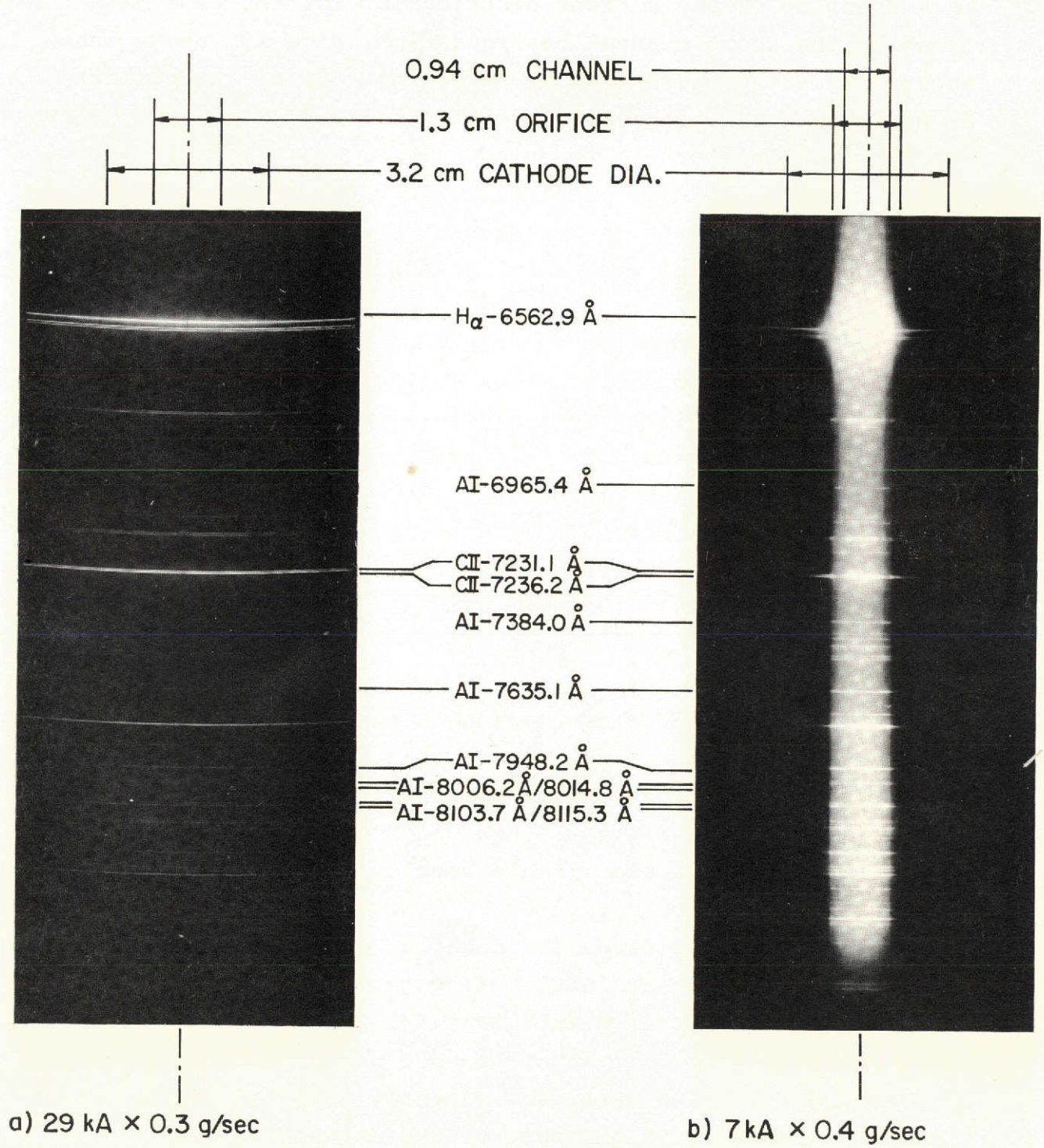

SPECTRA OF HOLLOW CATHODE DISCHARGE

FIGURE 30
AP25·P·426

through which the line of sight also passed. No such detached radiant region was observed for the insulated cathode at the 7 kA, 0.4 g/sec condition (Fig. 30b).

Figure 30a shows that the distribution of radiance of the spectral lines does not reflect any of the cathode features despite the measured 0.8 kA attaching inside the cavity for this 29 kA, 0.3 g/sec condition. The AI lines are barely discernible and there is no continuum radiation. (In contrast the AII lines between 4300 Å and 6000 Å are clearly observable, but not shown here.) An estimate of the electron density from the broadened H_β line (not shown) indicates several times 10^{15} electrons/cm^3 somewhere along the line-of-sight, most likely inside the cavity.

The spectrum of the discharge in the fully insulated cathode shows, in dramatic contrast, a sharply defined continuum in the cavity with AI and AII lines brightly superimposed on it. (Fig. 30b). There is little radiation recorded beyond the cavity diameter at this exposure, indicating the high level of radiant flux emerging from the cavity. The large widths of the broadened H_α and H_β lines in this spectrum indicate an electron density of several times $10^{17}/cm^3$ in the cavity, two orders of magnitude larger than in the uninsulated cathode, despite a total arc current only one quarter as large. The distinctly bounded bright "brems" continuum radiation dominates even in the low sensitivity region of the film, confirming a high level of electron density. The AI lines appear brightest at the edge of the cavity while AII radiance is most pronounced along the axis. Spectrograms recorded at higher mass flows and the same current of 7 kA show a correspondingly higher radiance of AI and AII spread over a larger radial extent, but the continuum appears distinctly bounded by the cavity, as in Fig. 30b, and at approximately the same visual density on the film.

In summary, first evidence has been obtained that a hollow cathode can be successfully operated in a high power quasi-steady MPD discharge without the assistance of auxiliary heating, low work function inserts, or external keeper electrodes. The relatively large dimensions of the hollow cathode have permitted detailed probing of the potential profiles and enclosed current distributions inside and outside of the cathode cavity. These measurements yield current densities in the cavity of approximately 1500 A/cm^2 in a region of axial potential gradient of less than 10 V/cm. Electron number density in the cavity exceeds $10^{17}/cm^3$, which is at least one order of magnitude higher than previously observed in solid cathode MPD discharges of twice the arc current level.

IV. PLASMADYNAMIC LASER STUDIES

The preceding semi-annual report discussed two initial steps taken in the program to determine the extent to which an MPD discharge can be used as a laser source. In the first of these, photoelectrically measured radiance profiles were used to determine the optical depth of selected transitions within the MPD discharge. These measurements, which can be related to the gain or absorption of the particular transition, have been extended recently using calibrated optical components and the improved injection configuration discussed in section II-B. Early results are reported in the first of the two succeeding sections.

In the second of the previously reported experiments, the distribution of neutral argon in the discharge chamber and exhaust flow was obtained using a spectroscopic-photographic technique. When combined with other records of singly ionized argon distribution, these data indicate a substantial recombination in the exhaust flow within 36 cm of the discharge chamber, thus implying that population inversions could be produced in that region. To determine whether this complete recombination process proceeds collisionally or radiatively, the ultraviolet radiation characteristics of the discharge have been recorded. The technique and the first results obtained with it are described in the second section.

IV-A Optical Depth Measurements (Campbell, von Jaskowsky)

In earlier work with the parallel plate discharge apparatus the gain coefficient over a 15-cm path, ℓ, transverse to both the discharge current and flow direction, $\alpha = (1/\ell)\ \ln\ (L/L_o)$, was measured for the 4880 Å line using an argon ion laser of radiance L_o.[92] For the 120 kA x 20 μsec pulse in 50 mTorr of ambient argon, the gain coefficient was found to be negative during most of the discharge except for a small positive excursion of less than 0.005 for approximately 10 μsec. Although reproducible, this positive value could not be firmly established due to the 1.5% experimental error bar.

These earlier experiments clearly show the need for optical measurements with accuracies better than 1%. The first step in achieving this goal is the calibration of the reflectivities and transmissivities of the various elements in the optical train. The arrangement shown in Fig. 31a was used to calibrate the components required for the measurement of the optical depth as shown in Fig. 31b. In the calibration, a 15 cm integrating sphere in Fig. 31a, was used with an IP28 photomultiplier (PM-1) because the latter alone did not yield the needed accuracy due to the differences in sensitivity over the multiplier cathode. A second photomultiplier (PM-2) was used in a "null"-bridge method to balance out any fluctuations of the Sylvania C-10 concentrated-arc light source. In this arrangement, the PM-1 and PM-2 detectors were connected in opposition across two 50,000 Ω, 10-turn potentiometers. The sliding contacts were then adjusted for zero potential difference between them by monitoring a differential input oscilloscope. The high sensitivity of the oscilloscope and the fine scale of the potentiometers produced a detector accuracy of 0.3%. For the calibration, 10 readings with and without

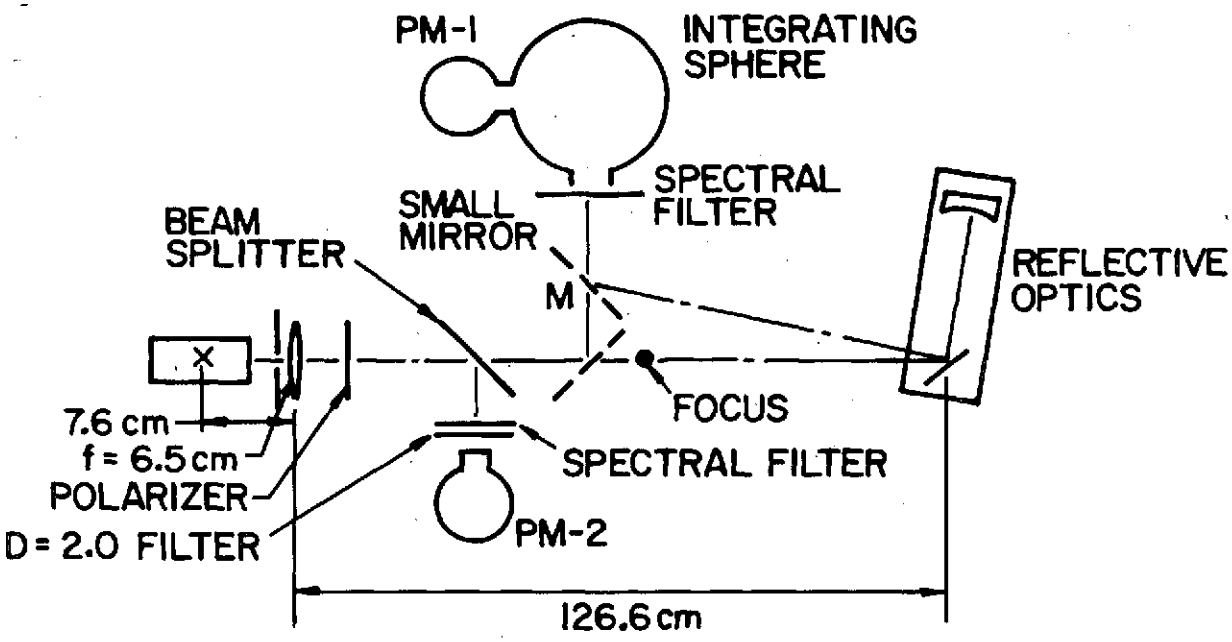

a) CALIBRATION

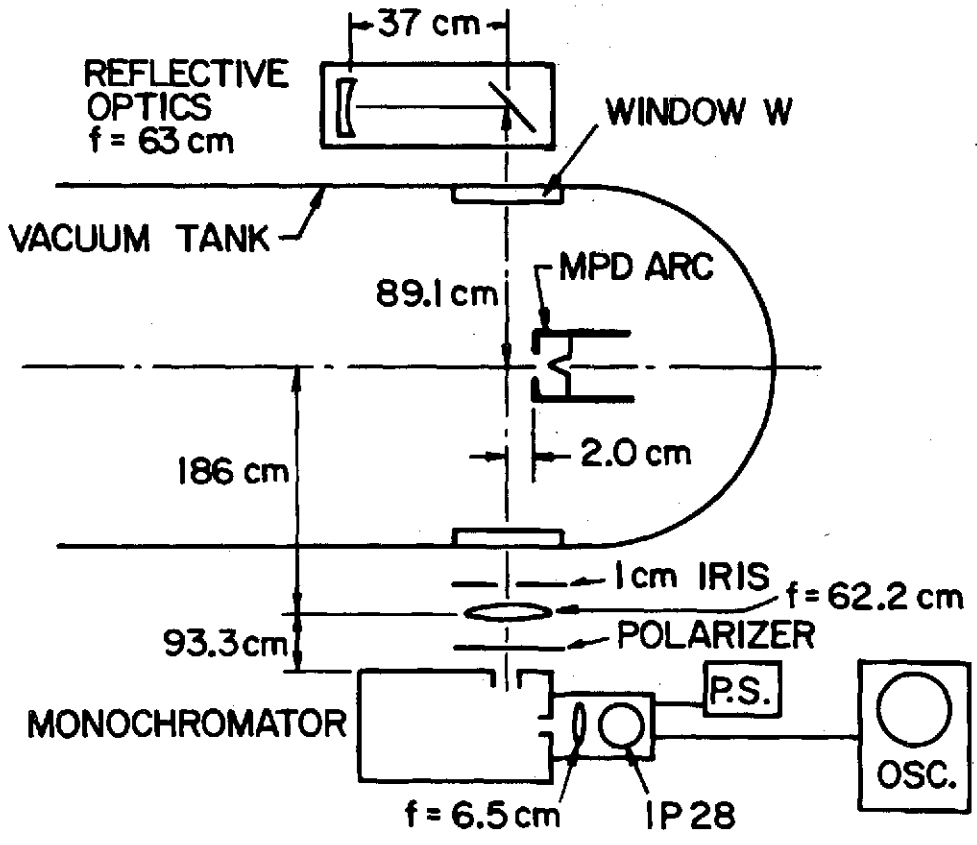

b) OPTICAL DEPTH STUDIES

EXPERIMENTAL ARRANGEMENTS

FIGURE 31
AP25-4980

the reflective optics in the optical train were recorded by simple repositioning of the small mirror M in Fig. 31a.

The reflectivity of the reflective optics was determined at three spectral locations, ≈ 4530 Å (Wratten #47B), ≈ 4910 Å (Wratten #75) and ≈ 5510 Å (80 Å wide interference filter). The measured values are shown plotted against wavelength λ in Fig. 32a. The standard deviation for these data was 0.38%. In a similar way, the transmission of the tank window W in Fig. 31b was determined at 16 positions on the window by simply inserting it into the optical train. The measured transmissivity, again plotted versus wavelength, is shown in Fig. 32b. The transmissivity is seen to depend on the beam diameter due to scattering which can be shown to scale with the radiance in the beam and therefore will scale inversely with the beam cross section. The overall standard deviation in any of the transmission measurements was 0.2%, somewhat better than the reflectivity measurements in which the small mirror M had to be moved.

The window and the reflective optics were installed as shown in Fig. 31b for measuring the optical depth of ionized argon lines at the 15.3 kA x 6 g/sec operating condition. It should be noted that an iris of 1 cm opening restricted the nominal focal ratio 1/F to approximately 1/200 providing considerable depth of focus and good resolution.

A typical oscillogram of the radiance signals with and without reflective optics at an axial station 2 cm downstream of the anode is shown in Fig. 33, together with the terminal voltage in the upper trace for reference. Assuming the plasma radiates equal spectral fluxes in both directions along the optical path, the radiance signals S and S_R on the oscillogram are reduced using the following expression for the radiance with reflective optics of reflectivity R and window

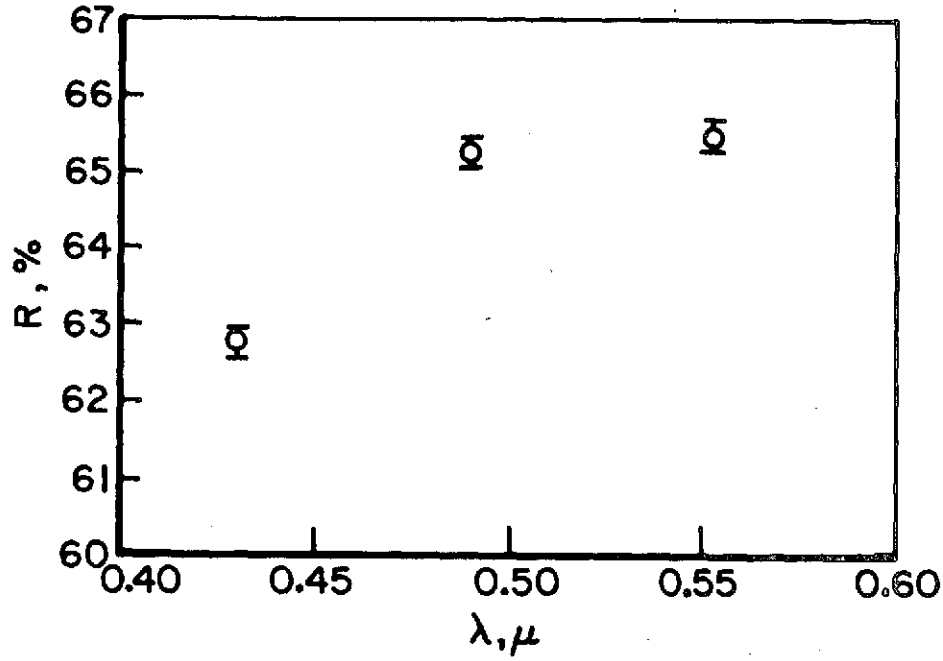

a) REFLECTIVITY, R

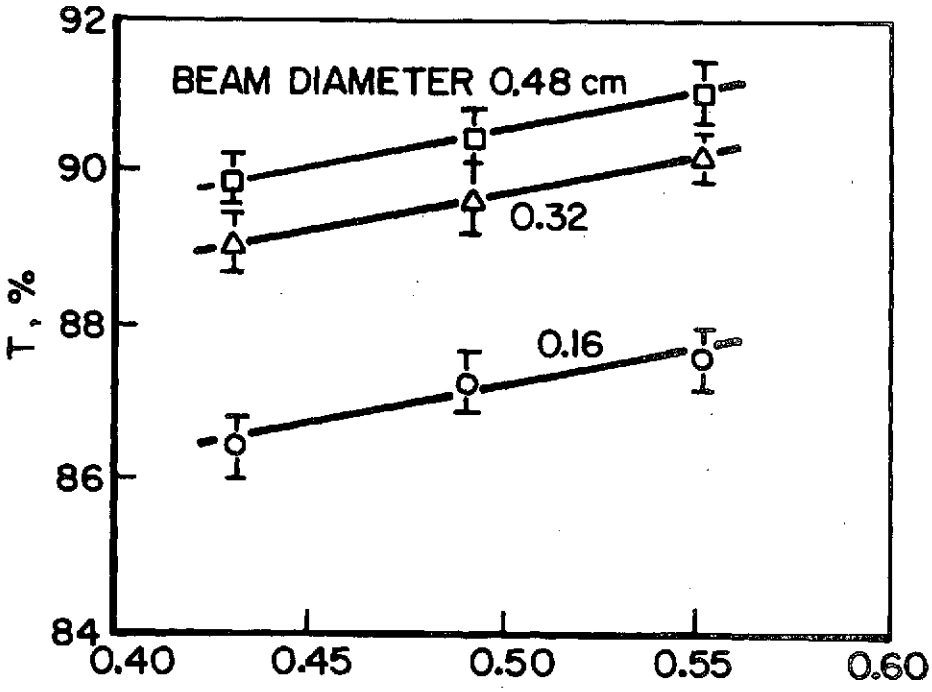

b) TRANSMISSION

REFLECTIVITY AND TRANSMISSIVITY

FIGURE 32
AP25-4981

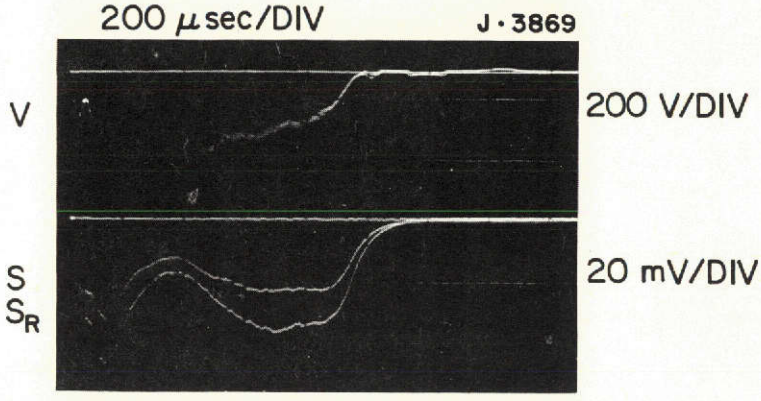

4764.9 Å RADIANCE

FIGURE 33
AP25·P·425

transmissivity T:

$$S_R = L \cdot T^2 \, e^{-\tau} + L \tag{10}$$

where L is the radiance from the plasma and τ its optical depth. The relative difference in the radiances with and without reflective optics is then:

$$(S_R - S)/S = RT^2 e^{-\tau}$$

and the radiation enhancement (for $\tau < 0$)

$$e^{-\tau} = \frac{1}{RT^2} \, \frac{S_R - S}{S} \tag{11}$$

In the sample trace at t $\approx$ 0.8 msec, $e^{-\tau} = 1.06$ and therefore $\tau = -0.06$.

It should be noted that this sample of the 4764.8 Å AII line is a preliminary measurement in the ongoing investigation rather than an exhibition of a particular optical depth. Such measurements for several lines over a range of operating conditions are in progress now with the improved injection geometry (see Sections IIB and IIC) and the refractory discharge chamber insulator. Clearly this technique must also demonstrate a high degree of reproducibility in a number of successive discharges. One simple discharge with, and a succeeding one without reflective optics as in the example of Fig. 33 is insufficient. Attractive alternate methods to be explored further employ either a light chopper in the reflected optical path or the simultaneous measurement of both incident and reflected components with two photodetectors.

IV-B. Vacuum Ultraviolet Radiation Studies (von Jaskowsky)

The study of the relative magnitudes of AI and AII radiance has shown recombination to be effective in the flow from the MPD discharge.[146] The spectroscopic presence of AI, however, does not in itself establish whether the recombination process is entirely radiative or dominated by 3-body collisions. It is this latter collisional recombination process which is of particular significance for the establishment of a population inversion by fast cascading from the upper levels of the recombined ion or atom. Such an inversion may be expected to involve energy levels above the lower lying resonance levels from which the radiative transitions are faster than the collisional de-excitation process. A study of the presence of resonance radiation should therefore indicate whether collisional de-excitation involves only the upper levels of the ion or atom or whether it extends all the way to the resonance and metastable levels. Since these levels lie some 13 and 16 eV above the ground level of the ion and some 11 and 14 eV above the ground level of the atom, a vacuum ultraviolet technique must be used.

In the present investigation a 6199 photomultiplier tube was used in tandem with a glass substrate coated with a 1.8 mg/cm^2 (or 1.3 mg/cm^2) layer of sodium salicylate. This material fluoresces with an absolute and constant quantum efficiency of 0.65 under incident radiation from approximately 300 Å to 3500 Å wavelength.[A-19] The radiance emitted from the fluorescent coating peaks at approximately 4200 Å, which is close to the peak sensitivity of the multiplier tube.

In order to distinguish spectral regions of the radiance emitted by the relaxing MPD plasma flow, interchangeable filters of calcium fluoride, quartz, and glass, as well as two aperture stops were positioned in front of the fluorescent

screen as shown schematically in Fig. 34a. The photomultiplier responds to a) the fluorescence of the sodium salicylate screen and b) the radiation transmitted through the filters and the fluorescent screen without fluorescent response. Table 1 shows the wavelength regions of these two components of radiant flux.

Table 1

	a) Fluorescence due to	b) Transmission
No filter	300 - 3500 Å	3500 - 7000 Å
CaF_2 (0.2 cm)	1220 - 3500 Å	3500 - 7000 Å
Quartz (0.31 cm)	1700 - 3500 Å	3500 - 7000 Å
Glass (0.3 cm)	3100 - 3500 Å	3500 - 7000 Å

The 7000 Å limit is set by the sensitivity cut-off of the photomultiplier. Figure 34b shows the multiplier in the gate valve mounting installed at the location of the second window, $z = 0.39$ m, covering a field of view of 0.34 m of the flow on the axis of the vacuum tank.

A typical set of side-on photomultiplier records (1.3 g/cm^2 of sodium salcylate) with and without filters is shown in Fig. 35 for the 16 kA, 16 g/sec operating condition. The terminal voltage of the MPD discharge is shown for comparison in the upper half of Fig. 35a.

It is instructive to divide the oscillograms into three temporal regions: the initial transient peak, the quasi-steady portion, and the afterglow or radiance emitted after cessation of the current pulse. It should be noted that these three regions do not show the same spectral characteristics. For example, when the spectral detection region is extended from that transmitted by glass to wavelengths below 1220 Å, the initial peak at $t_2 = 0.145$ msec increases by 80% and the afterglow at $t_4 = 1.2$ msec by 340%, while the quasi-steady portion increases by only 20%.

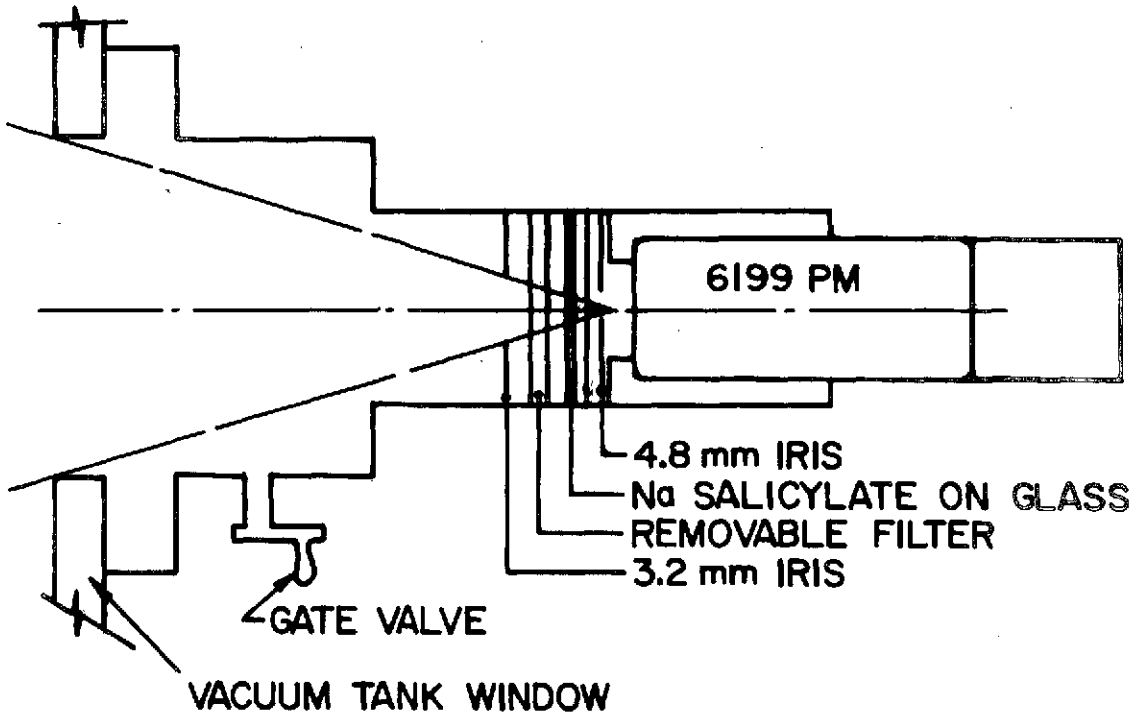

a) PHOTOMULTIPLIER ARRANGEMENT

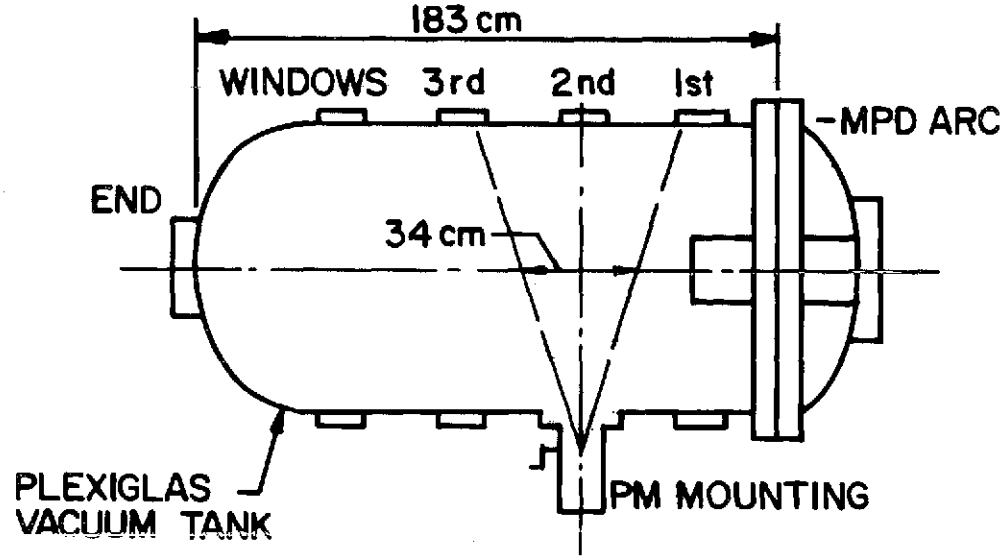

b) DISCHARGE APPARATUS

VUV - EXPERIMENT

FIGURE 34
AP25·4982

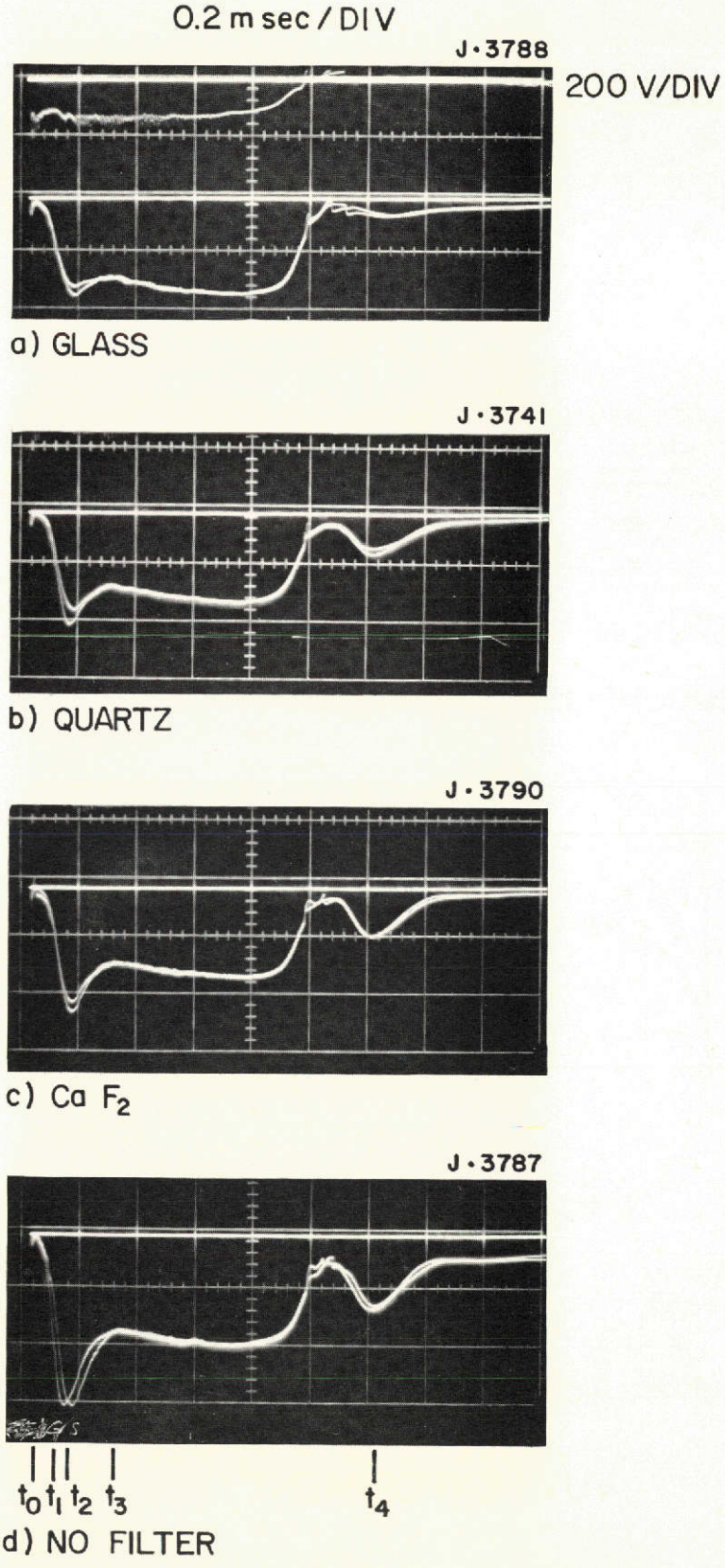

RADIANCE OF 16 kA × 16 g/sec DISCHARGE

FIGURE 35
AP25·P·524

The first peak may be indicative of the passage of a strongly radiating front[92] through the field of view of the photomultiplier. The leading edge of this front arrives in the center of the field of view at $t_1 = 0.08$ msec, fully occupies it at $t_2 = 0.14$ msec and leaves it at $t_3 = 0.29$ msec as indicated in Fig. 35d. The half-width of approximately one-tenth millisecond indicates the residence time of the front in the field of view. These times and the known dimensions of the field of view yield a width of approximately 0.26 m for the front travelling at 2 km/sec which is considerably slower than the flow velocity in the quasi-steady part of the pulse.[88,97]

For a more complete radiation profile at the same 16 kA x 16 g/sec operating condition, the radiance was also recorded with the same filters at the 1st and 3rd vacuum tank windows. The oscillograms, shown in Fig. 36, were obtained with a 1.8 mg/cm^2 coating of sodium salicylate, which was found to have a lower fluorescent efficiency than the previous coating of 1.3 mg/cm^2. Figures 36a,c and e show the detector signals with the glass filter, while no filter was used for the recordings in Figs. 36b,d and f. The radiance oscillograms at the 2nd window, Figs. 36c and d show the delay in the arrival of the radiating front relative to Figs. 36a and b recorded at the 1st window. The absence of the ultraviolet peak at the 1st window location is to be noted as well as an approximately 20 fold decrease in recording sensitivity for the high radiance level. At this upstream location the signal increases by some 40% in the quasi-steady portion due to ultraviolet radiation, while there is no afterglow peak such as observed further downstream at the second window location, Fig. 36d.

Further downstream at the 3rd window location, the beginning of the radiation pulse is further delayed relative to the second window and does not rise to a prominent peak. At

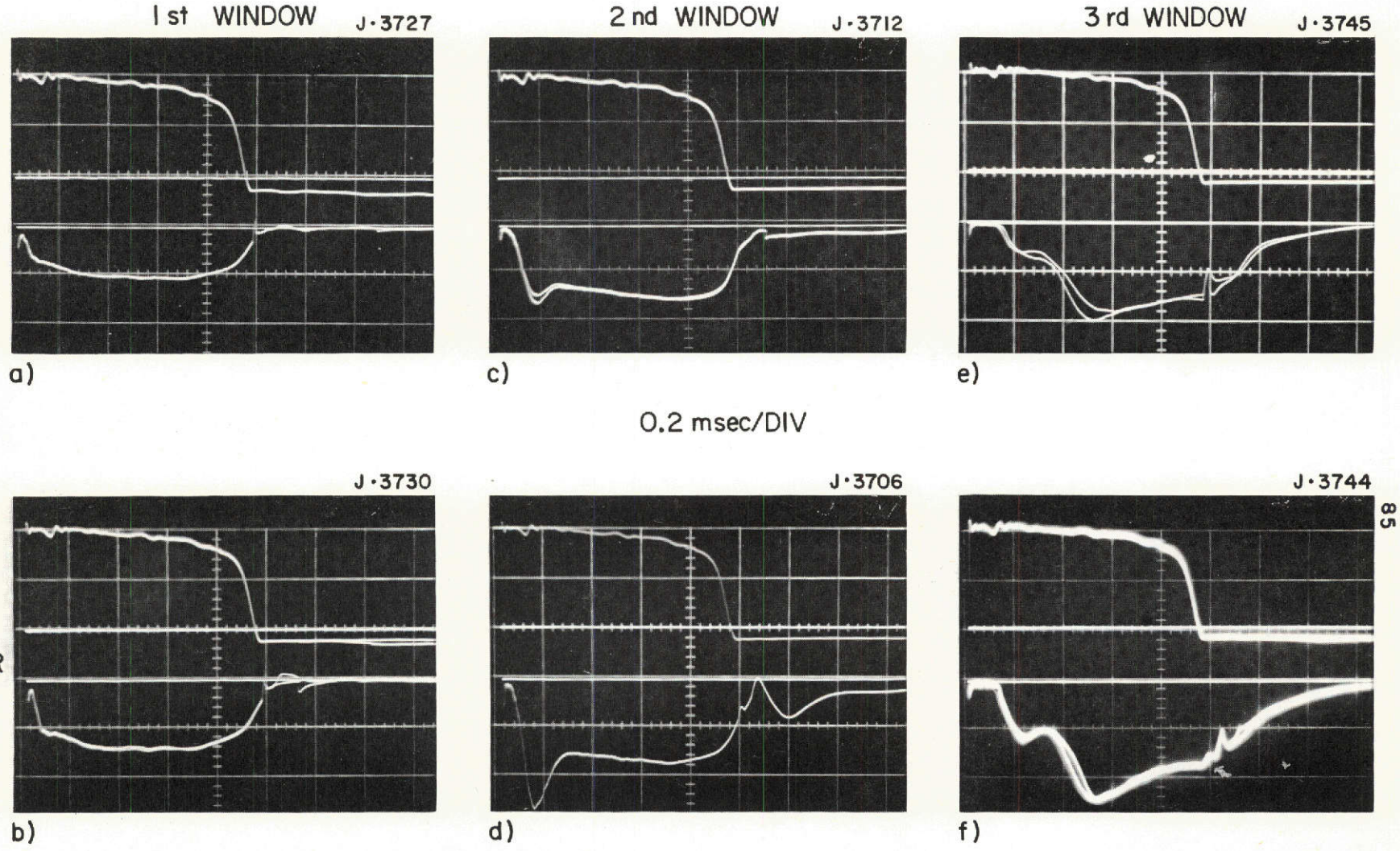

FIGURE 36
AP25·P·523

RADIANCE OF 16 kA × 16 g/sec DISCHARGE

the pulse front a considerably level of ultraviolet is radiated, as well as at the end of the pulse where it slowly decays without the typical afterglow peak. It should also be noted that the "quasi-steady" region observed at the first and second windows has been significantly shortened, occurring only over the last quarter of the current pulse which is shown in the upper part of the oscillogram.

The radiance records with the glass filter and with no filter for two other mass flows at the same 16 kA current are shown in Fig. 37. For a mass flow of 6 g/sec, Figs. 37a and b, the radiance level is rather comparable to that at the 16 kA x 16 g/sec operating condition, but now a second pronounced peak of radiance appears at 0.31 msec whose origin is not understood at this time. The radiance at the 16 kA x 32 g/sec condition, shown in Figs. 37c and d is quite similar to that at 16 kA x 16 g/sec, Figs. 36c and d, but at a level reduced by approximately 25%.

The large proportion of vacuum ultraviolet radiation throughout the discharge pulse is attributed to energetic argon resonance radiation. However, it is not possible to assign this radiation to either AII or AI since the resonance transitions for both ionized and neutral argon occur at wavelengths below 1200 Å, which is the cut-off of the CaF filter. The vacuum ultraviolet radiation indicates that the resonance levels have not been depleted by collisional de-excitation, thus indicating the possible existence of inversions in the levels above the resonance levels due to rapid cascading in the recombination process.

The large population of the resonance levels provokes the intriguing thought of stimulated emission in the vacuum ultraviolet from these levels. In the atom these transitions must be expected to be rapidly self-terminating; in the ion the possibility exists of extending the point of self termination by rapid recombination. However, this same collisional process may also deplete the resonance level and destroy the inversion.

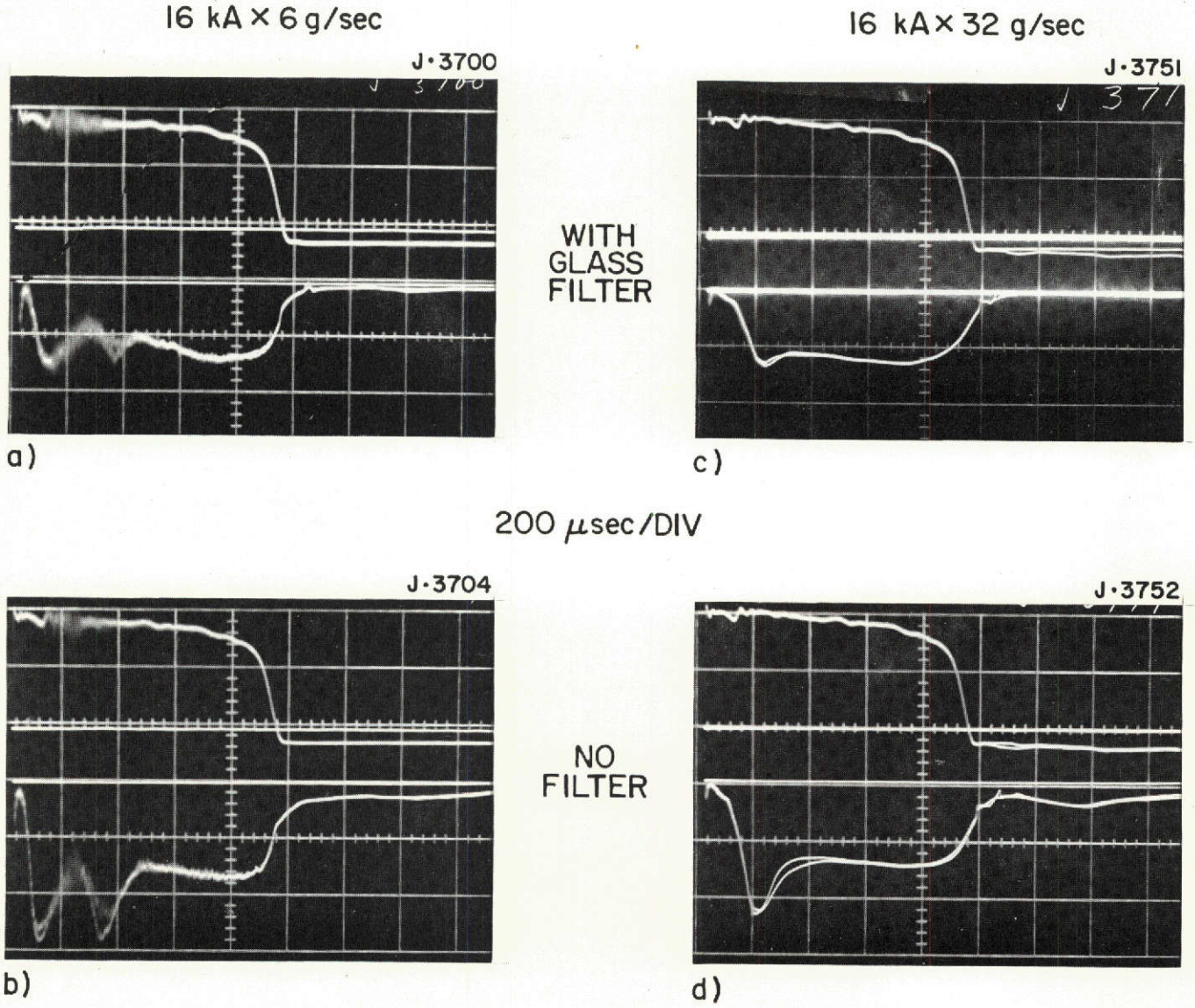

FIGURE 37
AP25·P·522

RADIANCE AT 2nd WINDOW LOCATION

PROJECT REFERENCES

[1]Jahn, R. G., Bernstein, I. B. and Kunen, A. E., "Proposed Studies of the Formation and Stability of an Electromagnetic Boundary in a Pinch," Proposal for NASA Research Grant NsG-306-63, Mar. 5, 1962, Princeton Univ., Princeton, N. J.

[2]Jahn, R. G. and von Jaskowsky, W. F., "Pulsed Electromagnetic Gas Acceleration," NASA NsG-306-63 progress report for the period 1 July 1962 to 31 December 1962, Aeron. Eng. Rept. No. 634, Jan. 1963, Princeton Univ., Princeton, N. J.

[3]Jahn, R. G. and von Jaskowsky, W. F., "The Plasma Pinch as a Gas Accelerator," A.I.A.A. Preprint 63013, A.I.A.A. Electric Propulsion Conference, Colorado Springs, Colo., 11-13 Mar. 1963.

[4]Jahn, R. G. and von Jaskowsky, W. F., "Pulsed Electromagnetic Gas Acceleration," NASA NsG-306-63 progress report for the period 1 January 1963 to 30 June 1963, Aeron. Eng. Report No. 634a, June 1963, Princeton Univ., Princeton, N. J.

[5]Jahn, R. G. and von Jaskowsky, W. F., "Structure of a Large-radius Pinch Discharge," A.I.A.A. Journal, Vol. 1, No. 8, Aug. 1963, pp. 1809-1814.

[6]Jahn, R. G., von Jaskowsky, W. F. and Casini, A. L., "A Gas-triggered Inverse Pinch Switch," NASA NsG-306-63, Aeron. Eng. Tech. Note No. 660, Aug. 1963, Princeton Univ., Princeton, N. J.

[7]Jahn, R. G., von Jaskowsky, W. F. and Casini, A. L., "Gas triggered Inverse Pinch Switch," The Review of Scientific Instruments, Vol. 34, No. 12, Dec. 1963, pp. 1439-1440.

[8]Jahn, R. G. and von Jaskowsky, W. F., "Pulsed Electromagnetic Gas Acceleration," (Paper delivered at the 4th NASA Intercenter Conference on Plasma Physics, Washington, D. C., 2-4 Dec. 1963), p. 8.

[9]Jahn, R. G. and von Jaskowsky, W. F., "Pulsed Electromagnetic Gas Acceleration," NASA NsG-306-63 progress report for period 1 July 1963 to 31 December 1963, Aeron. Eng. Rept. No. 634b, Dec. 1963, Princeton Univ., Princeton, N. J.

PROJECT REFERENCES

[10]Jahn, R. G. and von Jaskowsky, W. F., "Current Distributions in Large-radius Pinch Discharges," A.I.A.A. Preprint 64-25, A.I.A.A. Aerospace Sciences Meeting, New York, N. Y., 20-22 Jan. 1964.

[11]Jahn, R. G. and von Jaskowsky, W. F., "Current Distributions in Large-radius Pinch Discharges," A.I.A.A. Bulletin, Vol. 1, No. 1, Jan. 1964, p. 12.

[12]Jahn, R. G. and von Jaskowsky, W. F., "Pulsed Electromagnetic Gas Acceleration," NASA NsG-306-63 renewal proposal for 15-months extension, Jan. 15, 1964, Princeton Univ., Princeton, N. J.

[13]Jahn, R. G. and von Jaskowsky, W. F., "Pulsed Electromagnetic Gas Acceleration," NASA NsG-306-63 progress report for the period 1 January 1964 to 30 June 1964, Aeron. Eng. Rept. No. 634c, July 1964, Princeton Univ., Princeton, N. J.

[14]Jahn, R. G., von Jaskowsky, W. F. and Casini, A. L., "Gas-triggered Pinch Discharge Switch," NASA NsG-306-63, Aerospace and Mechanical Sciences Tech. Note No. 101, July 1964, Princeton Univ., Princeton, N. J.

[15]Corr, J. M., "Double Probe Studies in an 8" Pinch Discharge," M.S.E. thesis, Sept. 1964, Princeton Univ., Princeton, N. J.

[16]Jahn, R. G. and von Jaskowsky, W. F., "Exhaust of a Pinched Plasma From an Axial Orifice," A.I.A.A. Bulletin, Vol. 1, No. 10, Oct. 1964, p. 570.

[17]Jahn, R. G. and von Jaskowsky, W. F., "Current Distributions in Large-radius Pinch Discharges," A.I.A.A. Journal, Vol. 2, No. 10, Oct. 1964, pp. 1749-1753.

[18]Jahn, R. G., von Jaskowsky, W. F. and Casini, A. L., "Gas-triggered Pinch Discharge Switch", The Review of Scientific Instruments, Vol. 36, No. 1, Jan. 1964, pp. 101-102.

[19]Jahn, R. G. and von Jaskowsky, W. F., "Exhaust of a Pinched Plasma from an Axial Orifice," A.I.A.A. Paper 65-92, A.I.A.A. 2nd Aerospace Sciences Meeting, New York, N. Y., 25-27 Jan. 1964.

PROJECT REFERENCES

[20]Jahn, R. G. and von Jaskowsky, W. F., "Pulsed Electromagnetic Gas Acceleration," NASA NsG-306-63 progress report for the period 1 July 1964 to 31 December 1964, Aerospace and Mechanical Sciences Rept. No. 634d, Jan. 1965, Princeton Univ., Princeton, N. J.

[21]Wright, E. S., "The Design and Development of Rogowski Coil Probes for Measurement of Current Density Distribution in a Plasma Pinch," M.S.E. thesis, May 1965, Princeton Univ., Princeton, N. J.

[22]Jahn, R. G. and von Jaskowsky, W. F., "Pulsed Electromagnetic Gas Acceleration," NASA NsG-306-63 renewal proposal for 12-months extension, June 7, 1964, Princeton Univ., Princeton, N. J.

[23]Jahn, R. G. and Black, N. A., "On the Dynamic Efficiency of Pulsed Plasma Accelerators," A.I.A.A. Journal, Vol. 3, No. 6, June 1965, pp. 1209-1210.

[24]Black, N. A., "Linear Pinch Driven by a High-current Pulse-forming Network," A.I.A.A. Bulletin, Vol. 2, No. 6, June 1965, p. 309.

[25]Wright, E. S. and Jahn, R. G., "The Design and Development of Rogowski Coil Probes for Measurement of Current Density Distribution in a Plasma Pinch," NASA NsG-306-63, Aerospace and Mechanical Sciences Rept. No. 740, June 1965, Princeton Univ., Princeton, N. J.

[26]Rowell, G. A., "Cylindrical Shock Model of the Plasma Pinch," M.S.E. thesis, July 1965, Princeton Univ., Princeton, N. J.

[27]Black, N. A., "Linear Pinch Driven by a High-current Pulse-forming Network," A.I.A.A. Paper 65-336, A.I.A.A. 2nd Annual Meeting, San Francisco, Calif., 26-29 July 1965.

[28]Jahn, R. G. and von Jaskowsky, W. F., "Pulsed Electromagnetic Gas Acceleration," NASA NsG-306-63 progress report for the period 1 January 1965 to 30 June 1965, Aerospace and Mechanical Sciences Rept. No. 634e, July, 1965, Princeton Univ., Princeton, N. J.

[29]Jahn, R. G. and Ducati, A. C., "Design and Development of a Thermo-Ionic Electric Thrustor," 5QS 085-968 Interim Report, NASA Contract NASw-968, Aug. 1965, Giannini Scientific Corp., Santa Ana, Calif.

PROJECT REFERENCES

[30]Jahn, R. G., von Jaskowsky, W. F. and Burton, R. L., "Ejection of a Pinched Plasma From an Axial Orifice," A.I.A.A. Journal, Vol. 3, No. 10, Oct. 1965, pp. 1862-1866.

[31]Jahn, R. G. and Wright, E. S., "Miniature Rogowski Coil Probes for Direct Measurement of Current Density Distribution in Transient Plasmas," The Review of Scientific Instruments, Vol. 36, No. 12, Dec. 1965, pp. 1891-1892.

[32]Jahn, R. G. and von Jaskowsky, W. F., "Pulsed Electromagnetic Gas Acceleration," NASA NsG-306-63 progress report for the period 1 July 1965 to 31 December 1965, Aerospace and Mechanical Sciences Rept. No. 634f, Jan. 1966, Princeton Univ., Princeton, N. J.

[33]Burton, R. L. and Jahn, R. G., "Electric and Magnetic Field Distributions in a Propagating Current Sheet," A.I.A.A. Bulletin, Vol. 3, No. 1, Jan. 1966, p. 35.

[34]Rowell, G. A., Jahn, R. G. and von Jaskowsky, W. F., "Cylindrical Shock Model of the Plasma Pinch," NASA NsG-306-63, Aerospace and Mechanical Sciences Rept. No. 742, Feb. 1966, Princeton Univ., Princeton, N. J.

[35]Burton, R. L. and Jahn, R. G., "Electric and Magnetic Field Distributions in a Propagating Current Sheet," A.I.A.A. Paper 66-200, A.I.A.A. 5th Electric Propulsion Conference, San Diego, Calif., 7-9 Mar. 1966.

[36]Black, N. A., "Pulse-forming Networks for Propulsion Research," Proceedings of the 7th Symposium on Engineering Aspects of Magnetohydrodynamics, Princeton Univ., Princeton, N. J., Mar. 30-April 1, 1966, pp. 10-11.

[37]Jahn, R. G., "Electromagnetic Propulsion," Astronautics and Aeronautics, Vol. 4, No. 2, February, 1966, pp. 73-75.

[38]Black, N. A., "Dynamics of a Pinch Discharge Driven by a High-current Pulse-forming Network," Ph.D. thesis, May 1966, Princeton Univ., Princeton, N. J.

[39]Black, N. A. and Jahn, R. G., "Dynamics of a Pinch Discharge Driven by a High-current Pulse-forming Network," NASA NsG-306-63, Aerospace and Mechanical Sciences Rept. No. 778, May 1966, Princeton Univ., Princeton, N. J.

PROJECT REFERENCES

[40]Jahn, R. G., "Pulsed Plasma Propulsion," Proceedings of the 5th NASA Intercenter and Contractors Conference on Plasma Physics, Washington, D. C., 24-26 May 1966, pt. V, pp. 75-81.

[41]Jahn, R. G. and von Jaskowsky, W. F., "Pulsed Electromagnetic Gas Acceleration," NASA NsG-306-63 renewal proposal for 24-months extension, May 25, 1966, Princeton Univ., Princeton, N. J.

[42]Ducati, A. C., Jahn, R. G., Muehlberger, E. and Treat, R. P., "Design and Development of a Thermo-Ionic Electric Thrustor," FR-056-968 Final Report, NASA CR-54703, May 1966, Giannini Scientific Corp., Santa Ana, Calif.

[43]Jahn, R. G. and Clark, K. E., "A Large Dielectric Vacuum Facility," A.I.A.A. Journal, Vol. 4, No. 6, June 1966, p. 1135.

[44]John, R. R., Bennett, S. and Jahn, R. G., "Current Status of a Plasma Propulsion," A.I.A.A. Bulletin, Vol. 3, No. 5, May 1966, p. 264.

[45]John, R. R., Bennett, S. and Jahn, R. G., "Current Status of a Plasma Propulsion," A.I.A.A. Paper 66-565, A.I.A.A. 2nd Propulsion Joint Specialist Conference, Colorado Springs, Colo., 13-17 June 1966.

[46]Jahn, R. G. and von Jaskowsky, W. F., "Pulsed Electromagnetic Gas Acceleration," NASA NsG-306-63 progress report for the period 1 January 1966 to 30 June 1966, Aerospace and Mechanical Sciences Rept. No. 634g, July 1966, Princeton Univ., Princeton, N. J.

[47]Burton, R. L., "Structure of the Current Sheet in a Pinch Discharge," Ph.D. thesis, Sept. 1966, Princeton Univ., Princeton, N. J.

[48]Burton, R. L. and Jahn, R. G., "Structure of the Current Sheet in a Pinch Discharge," NASA NsG-306-63, Aerospace and Mechanical Sciences Rept. No. 783, Sept. 1966, Princeton Univ., Princeton, N. J.

[49]Jahn, R. G. and von Jaskowsky, W. F., "Pulsed Electromagnetic Gas Acceleration," NASA NsG-306-63 progress report for the period 1 July 1966 to 31 December 1966, Aerospace and Mechanical Sciences Rept. No. 634h, Jan. 1967, Princeton Univ., Princeton, N. J.

PROJECT REFERENCES

[50]Burton, R. L. and Jahn, R. G., "Structure of the Current Sheet in a Pinch Discharge," Bulletin of the American Physical Society, Vol. 12, Ser. II, Paper L1, May 1967, p. 848.

[51]Jahn, R. G., "Plasma Propulsion for Deep Space Flight," Bulletin of the American Physical Society, Vol. 12, Ser. II, Paper BC-1, May 1967, p. 646.

[52]Ellis, W. R., Jr., "An Investigation of Current Sheet Structure in a Cylindrical Z-Pinch," Ph.D. thesis, July 1967, Princeton Univ., Princeton, N. J.

[53]Ellis, W. R., Jr. and Jahn, R. G., "An Investigation of Current Sheet Structure in a Cylindrical Z-Pinch," NASA NsG-306-63, Aerospace and Mechanical Sciences Rept. No. 805, July 1967, Princeton Univ., Princeton, N. J.

[54]Jahn, R. G. and von Jaskowsky, W. F., "Pulsed Electromagnetic Gas Acceleration," NASA NsG-306-63 progress report for the period 1 January 1967 to 30 June 1967, Aerospace and Mechanical Sciences Rept. No. 634i, July 1967, Princeton Univ., Princeton, N. J.

[55]Clark, K. E. and Jahn, R. G., "The Magnetoplasmadynamic Arc," Astronautica Acta, Vol. 13, No. 4, 1967, pp. 315-325.

[56]Jahn, R. G., "The MPD Arc," NASA Contract NASw-1513, Aug. 1967, Giannini Scientific Corp., Santa Ana, Calif.

[57]Eckbreth, A. C., Clark, K. E. and Jahn, R. G., "Current Pattern Stabilization in Pulsed Plasma Accelerators," A.I.A.A. Bulletin, Vol. 4, No. 9, Sept. 1967, p. 433.

[58]Clark, K. E., Eckbreth, A. C. and Jahn, R. G., "Current Pattern Stabilization in Pulsed Plasma Accelerators," A.I.A.A. Paper 67-656, A.I.A.A. Electric Propulsion and Plasmadynamics Conference, Colorado Springs, Colo., 11-13 Sept. 1967.

[59]Jahn, R. G. and von Jaskowsky, W. F., "Pulsed Electromagnetic Gas Acceleration," NASA NsG-306-63 progress report for the period 1 July 1967 to 31 December 1967, Aerospace and Mechanical Sciences Rept. No. 634j, Jan. 1968, Princeton Univ., Princeton, N. J.

PROJECT REFERENCES

[60]Ducati, A. C., Jahn, R. G., Muehlberger, E. and Treat, R. P., "Exploratory Electromagnetic Thruster Research," TR 117-1513 Annual Report, NASA CR 62047, Feb. 1968, Giannini Scientific Corp., Santa Ana, Calif.

[61]Jahn, R. G., PHYSICS OF ELECTRIC PROPULSION, McGraw-Hill Book Company, New York, 1968.

[62]Burton, R. L. and Jahn, R. G., "Acceleration of Plasma by a Propagating Current Sheet," The Physics of Fluids, Vol. 11, No. 6, June 1968, pp. 1231-1237.

[63]Jahn, R. G. and von Jaskowsky, W. F., "Pulsed Electromagnetic Gas Acceleration," NASA NGR 31-001-005 step-funding renewal proposal for the period 1 October 1968 to 30 September 1971, June 1, 1968, Princeton Univ., Princeton, N. J.

[64]Jahn, R. G. and von Jaskowsky, W. F., "Pulsed Electromagnetic Gas Acceleration," NASA NsG-306/31-001-005 progress report for the period 1 January 1968 to 30 June 1968, Aerospace and Mechanical Sciences Rept. No. 634k, July 1968, Princeton Univ., Princeton, N. J.

[65]Wilbur, P. J., "Energy Transfer from a Pulse Network to a Propagating Current Sheet," Ph.D. thesis, Sept. 1968, Princeton Univ., Princeton, N. J.

[66]Wilbur, P. J. and Jahn, R. G., "Energy Transfer from a Pulse Network to a Propagating Current Sheet," NASA NGR 31-001-005, Aerospace and Mechanical Sciences Rept. No. 846, Sept. 1968, Princeton Univ., Princeton, N. J.

[67]Ducati, A. C., Jahn, R. G., Muehlberger, E. and Treat, R. P., "Exploratory Electromagnetic Thruster Research, Phase II," 2SS108-1513 Interim Report, NASA Contract NASw-1513, Oct. 1968, Giannini Scientific Corp., Santa Ana, Calif.

[68]Eckbreth, A. C., Clark, K. E. and Jahn, R. G., "Current Pattern Stabilization in Pulsed Plasma Accelerators," A.I.A.A. Journal, Vol. 6, No. 11, Nov. 1968, pp. 2125-2132.

PROJECT REFERENCES

[69]Eckbreth, A. C., "Current Pattern and Gas Flow Stabilization in Pulsed Plasma Accelerators," Ph.D. thesis, Dec. 1968, Princeton Univ., Princeton, N. J.

[70]Eckbreth, A. C. and Jahn, R. G., "Current Pattern and Gas Flow Stabilization in Pulsed Plasma Accelerators," NASA NGL 31-001-005, Aerospace and Mechanical Sciences Rept. No. 857, Dec. 1968, Princeton Univ., Princeton, N. J.

[71]York, T. M., "Pressure Distribution in the Structure of a Propagating Current Sheet," Ph.D. thesis, Dec. 1968, Princeton Univ., Princeton, N. J.

[72]York, T. M. and Jahn, R. G., "Pressure Distribution in the Structure of a Propagating Current Sheet," NASA NGL 31-001-005, Aerospace and Mechanical Sciences Rept. No. 853, Dec. 1968, Princeton Univ., Princeton, N. J.

[73]Eckbreth, A. C. and Jahn, R. G., "Current Pattern and Gas Flow Stabilization in Pulsed Plasma Accelerators," A.I.A.A. Bulletin, Vol. 5, No. 12, Dec. 1968, p. 730.

[74]Wilbur, P. J. and Jahn, R. G., "Energy Transfer From a Pulse Network to a Propagating Current Sheet," A.I.A.A. Bulletin, Vol. 5, No. 12, Dec. 1968, p. 730.

[75]Ellis, W. R. and Jahn, R. G., "Ion Density and Current Distributions in a Propagating Current Sheet, Determined by Microwave Reflection Technique," Rept. No. CLM-P-187, Dec. 1968, Culham Laboratory, Abingdon, Berkshire, Great Britain.

[76]Jahn, R. G. and von Jaskowsky, W. F., "Pulsed Electromagnetic Gas Acceleration," NASA NGL 31-001-005 progress report for the period 1 July 1968 to 31 December 1968, Aerospace and Mechanical Sciences Rept. No. 634, Jan. 1969, Princeton Univ., Princeton, N. J.

[77]Eckbreth, A. C. and Jahn, R. G., "Current Pattern and Gas Flow Stabilization in Pulsed Plasma Accelerators," A.I.A.A. Paper 69-112, A.I.A.A. 7th Aerospace Sciences Meeting, New York, N. Y., 20-22 Jan. 1969.

PROJECT REFERENCES

[78]Wilbur, P. J. and Jahn, R. G., "Energy Transfer From a Pulse Network to a Propagating Current Sheet," A.I.A.A. Paper 69-113, A.I.A.A. 7th Aerospace Sciences Meeting, New York, N. Y., 20-22 Jan. 1969.

[79]Ellis, W. R. and Jahn, R. G., "Ion Density and Current Distributions in a Propagating Current Sheet, Determined by Microwave Reflection Technique," Journal of Plasma Physics, Vol. 3, Pt. 2, 1969, pp. 189-213.

[80]York, T. M. and Jahn, R. G., "Pressure Distribution in the Structure of a Propagating Current Sheet," A.I.A.A. Bulletin, Vol. 6, No. 2, Feb. 1969, p. 75.

[81]Clark, K. E. and Jahn, R. G., "Quasi-steady Plasma Acceleration," A.I.A.A. Bulletin, Vol. 6, No. 2, Feb. 1969, p. 75.

[82]York, T. M. and Jahn, R. G., "Pressure Distribution in the Structure of a Propagating Current Sheet," A.I.A.A. Paper 69-264, A.I.A.A. 7th Electric Propulsion Conference, Williamsburg, Va., 3-5 Mar. 1969.

[83]Clark, K. E. and Jahn, R. G., "Quasi-steady Plasma Acceleration," A.I.A.A. Paper 69-267, A.I.A.A. 7th Electric Propulsion Conference, Williamsburg, Va., 3-5 Mar. 1969.

[84]Jahn, R. G. and Mickelsen, W. R., "Electric Propulsion Notebook," A.I.A.A. Professional Study Series, Williamsburg, Va., 1-2 Mar. 1969.

[85]Boyle, M. J., "Plasma Velocity Measurements with Electric Probes," B.S.E. thesis, April 1969, Princeton Univ., Princeton, N. J.

[86]Clark, K. E., "Quasi-steady Plasma Acceleration," Ph.D. thesis, May 1969, Princeton Univ., Princeton, N. J.

[87]Clark, K. E. and Jahn, R. G., "Quasi-steady Plasma Acceleration," NASA NGL 31-001-005, Aerospace and Mechanical Sciences Rept. No. 859, May 1969, Princeton Univ., Princeton, N. J.

PROJECT REFERENCES

[88]Boyle, M. J., "Plasma Velocity Measurements with Electric Probes," Paper No. 4 (Paper presented at the Northeastern Regional Student Conference, Princeton Univ., Princeton, N. J., 9-10 May 1969).

[89]Mickelsen, W. R. and Jahn, R. G., "Status of Electric Propulsion," A.I.A.A. Bulletin, Vol. 6, No. 6, June 1969, p. 257.

[90]Mickelsen, W. R. and Jahn, R. G., "Status of Electric Propulsion," A.I.A.A. Paper 69-497, A.I.A.A. 5th Propulsion Joint Specialist Conference, U. S. Air Force Academy, Colo., 9-13 June 1969.

[91]Ducati, A. C. and Jahn, R. G., "Electron Beam from a Magnetoplasmadynamic Arc," The Physics of Fluids, Vol. 12, No. 6, June 1969, pp. 1177-1181.

[92]Jahn, R. G. and von Jaskowsky, W. F., "Pulsed Electromagnetic Gas Acceleration," NASA NGL 31-001-005 progress report for the period 1 January 1969 to 30 June 1969, Aerospace and Mechanical Sciences Rept. No. 634m, July 1969, Princeton Univ., Princeton, N. J.

[93]Jahn, R. G. and von Jaskowsky, W. F., "Pulsed Electromagnetic Gas Acceleration," NASA NGR 31-001-005 step-funding renewal proposal for the period 1 October 1969 to 30 September 1970, July 1, 1969, Princeton Univ., Princeton, N. J.

[94]Jahn, R. G., Clark, K. E., Oberth, R. C. and Turchi, P. J., "Acceleration Patterns in Quasi-steady MPD Arcs," A.I.A.A. Bulletin, Vol. 6, No. 12, Dec. 1969, p. 701.

[95]Ducati, A. C. and Jahn, R. G., "Repetitively Pulsed, Quasi-steady Vacuum MPD Arc," A.I.A.A. Bulletin, Vol. 6, No. 12, Dec. 1969, p. 701.

[96]Jahn, R. G., von Jaskowsky, W. F. and Clark, K. E., "Pulsed Electromagnetic Gas Acceleration: Acceleration Processes in Quasi-steady Arcs," (Paper delivered at the 6th NASA Intercenter and Contractors Conference on Plasma Physics, NASA Langley Research Center, Hampton, Va., 8-10 Dec. 1969), pp. 8-15.

PROJECT REFERENCES

[97]Jahn, R. G., von Jaskowsky, W. F. and Clark, K. E., "Pulsed Electromagnetic Gas Acceleration," NASA NGL 31-001-005 progress report for the period 1 July 1969 to 31 December 1969, Aerospace and Mechanical Sciences Rept. No. 634n, Jan. 1970, Princeton Univ., Princeton, N. J.

[98]Eckbreth, A. C. and Jahn, R. G., "Current Pattern and Gas Flow Stabilization in Pulsed Plasma Accelerators," A.I.A.A. Journal, Vol. 8, No. 1, Jan. 1970, pp. 138-143.

[99]Jahn, R. G., Clark, K. E., Oberth, R. C. and Turchi, P. J., "Acceleration Patterns in Quasi-steady MPD Arcs," A.I.A.A. Paper 70-165, A.I.A.A. 8th Aerospace Sciences Meeting, New York, N. Y., 19-21 Jan. 1970.

[100]Ducati, A. C. and Jahn, R. G., "Repetitively Pulsed, Quasi-steady Vacuum MPD Arc," A.I.A.A. Paper 70-167, A.I.A.A. 8th Aerospace Sciences Meeting, New York, N. Y., 19-21 Jan. 1970.

[101]Wilbur, P. J. and Jahn, R. G., "Energy Transfer from a Pulse Network to a Propagating Current Sheet," A.I.A.A. Journal, Vol. 8, No. 1, Jan. 1970, pp. 144-149.

[102]Clark, K. E. and Jahn, R. G., "Quasi-steady Plasma Acceleration," A.I.A.A. Journal, Vol. 8, No. 2, Feb. 1970, pp. 216-220.

[103]York, T. M. and Jahn, R. G., "Pressure Distribution in the Structure of a Propagating Current Sheet," The Physics of Fluids, Vol. 13, No. 5, May 1970, pp. 1303-1309.

[104]Jahn, R. G., "Pulsed Electromagnetic Gas Acceleration," NASA NGL 31-001-005 step-funding renewal proposal for period 1 October 1970 to 30 September 1971, June 11, 1970, Princeton Univ., Princeton, N. J.

[105]Jahn, R. G., von Jaskowsky and Clark, K. E., "Pulsed Electromagnetic Gas Acceleration," NASA NGL 31-001-005, progress report for the period 1 January 1970 to 30 June 1970, Aerospace and Mechanical Sciences Rept. No. 634o, July 1970, Princeton Univ., Princeton, N. J.

PROJECT REFERENCES

[106]Turchi, P. J. and Jahn, R. G., "The Cathode Region of a Quasi-steady MPD Arcjet," A.I.A.A. Bulletin, Vol. 7, No. 9, Sept. 1970, p. 449.

[107]Clark, K. E., DiCapua, M. S., Jahn, R. G. and von Jaskowsky, W. F., "Quasi-steady Magnetoplasmadynamic Arc Characteristics," A.I.A.A. Bulletin, Vol. 7, No. 9, Sept. 1970, p. 449.

[108]Turchi, P. J. and Jahn, R. G., "The Cathode Region of a Quasi-steady MPD Arcjet," A.I.A.A. Paper 70-1094, A.I.A.A. 8th Electric Propulsion Conference, Stanford, Calif., 31 Aug.-2 Sept. 1970.

[109]Clark, K. E., DiCapua, M. S., Jahn, R. G. and von Jaskowsky, W. F., "Quasi-steady Magnetoplasmadynamic Arc Characteristics," A.I.A.A Paper 70-1095, A.I.A.A. 8th Electric Propulsion Conference, Stanford, Calif., 31 Aug.-2 Sept. 1970.

[110]Turchi, P. J., "The Cathode Region of a Quasi-steady Magnetoplasmadynamic Arcjet," Ph.D. thesis, Sept. 1970, Princeton Univ., Princeton, N. J.

[111]Turchi, P. J. and Jahn, R. G., "The Cathode Region of a Quasi-steady Magnetoplasmadynamic Arcjet," NASA NGL 31-001-005, Aerospace and Mechanical Sciences Rept. No. 940, Oct. 1970, Princeton Univ., Princeton, N. J.

[112]Oberth, R. C., "Anode Phenomena in High-Current Discharges," Ph.D. thesis, Dec. 1970, Princeton Univ., Princeton, N. J.

[113]Oberth, R. C. and Jahn, R. G., "Anode Phenomena in High-Current Discharges," NASA NGL 31-001-005, Aerospace and Mechanical Sciences Rept. No. 961, Dec. 1970, Princeton Univ., Princeton, N. J.

[114]Di Capua, M. S. and Jahn, R. G., "Voltage-Current Characteristics of Parallel-Plate Plasma Accelerators," A.I.A.A. Bulletin, Vol. 8, No. 1, Jan. 1971, p. 40.

[115]Oberth, R. C. and Jahn, R. G., "Anode Phenomena in High-Current Accelerators," A.I.A.A. Bulletin, Vol. 8, No. 1, Jan. 1971, p. 40.

[116]Di Capua, M. S. and Jahn, R. G., "Energy Deposition in Parallel-Plate Plasma Accelerators," A.I.A.A. Paper 71-197, A.I.A.A. 9th Aerospace Sciences Meeting, New York, N. Y., 25-27 Jan. 1971.

PROJECT REFERENCES

[117] Oberth, R. C. and Jahn, R. G., "Anode Phenomena in High-Current Accelerators," A.I.A.A. Paper 71-198, A.I.A.A. 9th Aerospace Sciences Meeting, New York, N. Y., 25-27 Jan. 1971.

[118] Jahn, R. G., Clark, K. E., Oberth, R. C. and Turchi, P. J., "Acceleration Patterns in Quasi-steady MPD Arcs," A.I.A.A. Journal, Vol. 9, No. 1, Jan. 1971, pp. 167-172.

[119] Jahn, R. G., von Jaskowsky, W. F. and Clark, K. E., "Pulsed Electromagnetic Gas Acceleration," NASA NGL 31-001-005, semi-annual report for period 1 July 1970 to 31 December 1970, Aerospace and Mechanical Sciences Rept. No. 634p, January 1971, Princeton University, Princeton, N. J.

[120] Jahn, R. G., von Jaskowsky, W. F. and Clark, K. E., "Pulsed Electromagnetic Gas Acceleration," NASA NGL 31-001-005 step-funding renewal proposal for the period 1 October 1971 to 30 September 1972, June 16, 1971, Princeton Univ., Princeton, N. J.

[121] Clark, K. E., Jahn, R. G. and von Jaskowsky, W. F., "Exhaust Characteristics of a Quasi-steady MPD Accelerator," DGLR Symposium on Electric Space Thruster System, Braunschweig, Germany, June 22-23, 1971, DLR Mitt. 71-21, Teil 1, pp. 81-100.

[122] Turchi, P. J. and Jahn, R. G., "Cathode Region of a Quasi-steady MPD Arcjet," A.I.A.A. Journal, Vol. 9, No. 7, July 1971, pp. 1372-1379.

[123] Jahn, R. G., von Jaskowsky, W. F. and Clark, K. E., "Pulsed Electromagnetic Gas Acceleration," NASA NGL 31-001-005, semi-annual report for period 1 January 1971 to 30 June 1971, Aerospace and Mechanical Sciences Dept. No. 634q, July 1971, Princeton University, Princeton, N. J.

[124] Cory, John S., "Mass,Momentum and Energy Flow from an MPD Accelerator," Ph.D. thesis, August 1971, Princeton University, Princeton, N. J.

PROJECT REFERENCES

[125] Cory, J. S. and Jahn, R. G., "Mass, Momentum and Energy Flow from an MPD Accelerator," NASA NGL 31-001-005, Aerospace and Mechanical Sciences Rept. No. 999, September 1971, Princeton University, Princeton, N. J.

[126] Jahn, R. G., von Jaskowsky, W. F. and Clark, K. E., "Quasi-steady Plasma Acceleration," International Symposium on Dynamics of Ionized Gases, University of Tokyo, September 1971.

[127] Di Capua, M. S., "Energy Deposition in the Parallel-Plate Plasma Accelerator," Ph.D. thesis, November 1971, Princeton University, Princeton, N. J.

[128] Di Capua, M. S. and Jahn, R. G., "Energy Deposition in Parallel-Plate Plasma Accelerators," NASA 31-001-005, Aerospace and Mechanical Sciences Rept. No. 1015, December 1971, Princeton University, Princeton, N. J.

[129] Parmentier, N., "Hollow Cathode, Quasi-steady MPD Arc," M.S.E. thesis, December 1971, Princeton University, Princeton, N. J.

[130] Parmentier, N. and Jahn, R. G., "Hollow Cathode, Quasi-steady MPD Arc," NASA NGL 31-001-005, Aerospace and Mechanical Sciences Rept. No. 1023, December 1971, Princeton University, Princeton, N. J.

[131] Jahn, R. G., von Jaskowsky, W. F. and Clark, K. E., "Pulsed Electromagnetic Gas Acceleration," NASA NGL 31-001-005, semi-annual report for period 1 July 1971 to 31 December 1971, Aerospace and Mechanical Sciences Report No. 634r, January 1972, Princeton University, Princeton, N. J.

[132] Oberth, R. C. and Jahn, R. G., "Anode Phenomena in High-Current Accelerators," A.I.A.A. Journal, Vol. 10, No. 1, January 1972, pp. 86-91.

[133] Clark, K. E., "Electric Propulsion," Astronautics and Aeronautics, Vol. 10, No. 2, February 1972, pp. 22-23.

[134] Hixon, T. L., "Near-Ultraviolet Spectroscopic Studies of a Quasi-Steady Magnetoplasmadynamic Arc," B.A. thesis, April 1972, Princeton University, Princeton, N. J.

[135] Hixon, T. L., "Near-Ultraviolet Spectrographic Studies of AIII in an MPD Arc Discharge," Paper presented at the Northeastern Regional Student Conference, Rutgers University, New Brunswick, N. J., April 29, 1972.

PROJECT REFERENCES

[136]Clark, K. E., Jahn, R. G. and von Jaskowsky, W. F., "Distribution of Momentum and Propellant in a Quasi-Steady MPD Discharge," A.I.A.A. Bulletin, Vol. 9, No. 4, April 1972, p. 165.

[137]Bruckner, A. P. and Jahn, R. G., "Exhaust Plume Structure in a Quasi-steady MPD Arc," A.I.A.A. Bulletin, Vol. 9, No. 4, April 1972, p. 166.

[138]Clark, K. E., Jahn, R. G. and von Jaskowsky, W. F., "Measurements of Mass, Momentum and Energy Distributions in a Quasi-Steady MPD Discharge," A.I.A.A. Paper 72-497, A.I.A.A. 9th Electric Propulsion Conference, Bethesda, Md., 17-19 April 1972.

[139]Bruckner, A. P. and Jahn, R. G., "Exhaust Plume Structure in a Quasi-Steady MPD Arc," A.I.A.A. Paper 72-499, A.I.A.A. 9th Electric Propulsion Conference, Bethesda, Md., 17-19 April, 1972.

[140]Bruckner, A. P., "Spectroscopic Studies of the Exhaust Plume of a Quasi-steady MPD Accelerator," Ph.D. thesis, May 1972, Princeton University, Princeton, N. J.

[141]Bruckner, A. P. and Jahn, R. G., "Spectroscopic Studies of the Exhaust Plume of a Quasi-steady MPD Accelerator,"NASA NGL 31-001-005, Aerospace and Mechanical Sciences Rept. No. 1041, May, 1972, Princeton University, Princeton, N. J.

[142]Jahn, R. G., von Jaskowsky, W. F. and Clark, K. E., "Pulsed Electromagnetic Gas Acceleration," NASA NGL 31-001-005 step-funding renewal proposal for the period 1 October 1972 to 30 September 1973, June 1972, Princeton University, Princeton, N. J.

[143]Jahn, R. G., von Jaskowsky, W. F. and Clark, K. E., "Pulsed Electromagnetic Gas Acceleration," NASA NGL 31-001-005, semi-annual report for period 1 January 1972 to 30 June 1972, Aerospace and Mechanical Sciences Report No. 634s, July 1972, Princeton University, Princeton, N. J.

[144]Kelly, A. J. and Clark, K. E., "Plasma Propulsion Systems," Aerospace and Mechanical Sciences Rept. No. 1074, September 1973, Princeton University, Princeton, N. J.

[145]Greco, R. V., Bliss, J. R., Murch, C. K., Clark, K. E., and Kelly, A. J., "Resistojet and Plasma Propulsion System Technology," AIAA Paper 72-1124 (1972).

PROJECT REFERENCES

[146] Jahn, R. G., von Jaskowsky, W F. and Clark, K. E., "Pulsed Electromagnetic Gas Acceleration," NASA NGL 31-001-005, semi-annual report for period 1 July 1972 to 31 December 1972, Aerospace and Mechanical Sciences Report No. 634t, January 1973, Princeton University, Princeton, N. J.

[147] Fradkin, D. B., "Analysis of Acceleration Mechanisms and Performance of an Applied Field MPD Arcjet," Ph.D. thesis, March 1973, Princeton University, Princeton, N. J.

[148] Jahn, R. G., von Jaskowsky, W F. and Clark, K. E., "Quasi-Steady Plasma Acceleration," in Dynamics of Ionized Gases, Proceedings of the International Symposium on Dynamics of Ionized Gases sponsored by the International Union of Theoretical and Applied Mechanics, Tokyo, Japan, September 13-17, 1971, University of Tokyo Press, 1973, Edited by M. J. Lighthill, I. Imai and H. Sato.

[149] Jahn, R. G., von Jaskowsky, W. F. and Clark, K. E., "Pulsed Electromagnetic Gas Acceleration," renewal proposal for the period 1 October 1973 to 30 September 1974, June 1973, Princeton University, Princeton, N. J.

GENERAL REFERENCES

A-1 Shih, K. T. et al., "Experimental Anode Heat-Transfer Studies in a Coaxial Arc Configuration," AIAA J., Vol. 6, No. 8, August 1968, pp. 1482-1487.

A-2 Ducati, A. C. et al., "Recent Progress in High Specific Impulse Thermo-Ionic Acceleration," AIAA Paper 65-96, January 1965.

A-3 Schott, L., "Electrical Probes," Chap. 11 in "Plasma Diagnostics," W. Lochte-Holdgreven, Ed., North Holland, 1968.

A-4 Kanal, M., "Theory of Current Collection of Moving Cylindrical Probes," J. Applied Physics, Vol. 35, No. 6, June 1964, pp. 1697-1703.

A-5 Alfvén, H., "Collision Between a Nonionized Gas and a Magnetized Plasma," Rev. Modern Physics, Vol. 32, 1960, pp. 710-713.

A-6 Swift, J. D. and M. J. R. Schwar, "Electrical Probes for Plasma Diagnostics," Iliffe, London, 1968.

A-7 Chen, F. F., "Electric Probes," in "Plasma Diagnostic Techniques," Huddlestone, R. H. and Leonard, S. L., Eds., Academic Press, New York, 1965, pp. 113-200.

A-8 Malliaris, A. C., John, R. R., Garrison, R. L. and Libby, D. R., "Performance of Quasi-steady MPD Thrusters at High-Powers," AIAA Journal, Vol. 10, No. 2, February 1972, pp. 121-122.

A-9 Malliaris, A. C., John, R. R., Garrison, R. L. and Libby, D. R., "Quasi-steady MPD Propulsion at High-Power," Final Tech. Rept. AVSD-0146-71-44, NASA CR 111872, February 1971.

A-10 Ducati, A. C. and Jahn, R. G., "Investigation of Pulsed Quasi-steady MPD Arcjets," Report FR-061-10140, Plasmadyne, Santa Ana, California, June 1971.

A-11 Alfvén, H., On the Origin of the Solar System, Oxford University Press, Oxford (1954).

A-12 Alfvén, H. and Wilcox, J. M., "On the Origin of the Satellites and the Planets," Astrophysical Journal, Vol. 136, pp. 1016-1022, (1962).

A-13 Patrick, R. M. and Schneiderman, A. M., "Performance Characteristics of a Magnetic Annular Arc," AIAA J, Vol. 4, No. 2, February 1966, pp. 283-290.

A-14 Malliaris, A. C. and Libby, D. R., "Velocities of Neutral and Ionic Species in an MPD Flow," AIAA Paper No. 69-109, 7th Aerospace Sciences Meeting, New York, N. Y., Jan. 20-22, 1969.

A-15 Eniger, J., "Experimental Investigation of an Ionizing Wave in Crossed Electric and Magnetic Fields," in Phenomena in Ionized Gases, Beograd, 22-27 August 1965, Vol. 1, Gradevinska Knjiga Publishing House, 1966, pp. 520-527.

A-16 Byers, D. C., "Performance of Various Oxide Magazine Cathodes in Kaufman Thrusters," NASA TN D-5074 (1968).

A-17 Nakanishi, S., "Durability Tests of a Five-Centimeter Diameter Ion Thruster System," NASA TM X-68132.

A-18 Lidsky, L. M., Rothleder, S. D., Rose, D. J., Yoshikawa, A., Michelson, C. and Mackin, Jr., R. J., "Highly Ionized Hollow Cathode Discharge," J. of Appl. Phys., Vol. 33, No. 8, 1962.

A-19 Samson, J. A., Techniques of Vacuum Ultraviolet Spectroscopy, J. Wiley and Sons, 1967.

Appendix A: Semi-annual Statement of Expenditures

PULSED ELECTROMAGNETIC GAS ACCELERATION
NASA NGL 31-001-005
1 January 1973 thru 30 June 1973

Direct Costs

I.	Salaries and Wages		
	A. Professional	$17,250	
	B. Technicians	11,201	
	C. Students	3,000	
	D. Supporting Staff	3,644	
			$ 35,095
II.	Employee Benefits (21% of IA,IB,ID)		6,750
III.	Materials and Services		9,612
IV.	Travel		75
V.	Tuition		2,200
	Total Direct Costs		$ 53,732
VI.	Overhead (75% of I)		26,358
	Total		$ 80,090